Spring 3-21-2013

Use of Self-Assembled Monolayers to Tailor Surface Properties: From Lubrication to Neuronal Development

Natalie Ann LaFranzo
Washington University in St. Louis

WASHINGTON UNIVERSITY IN ST. LOUIS

Department of Chemistry

Dissertation Examination Committee:

Dr. Joshua A. Maurer, Chair
Dr. Michael L. Gross
Dr. Robert O. Heuckeroth
Dr. Garland R. Marshall
Dr. Kevin D. Moeller
Dr. John-Stephen A. Taylor

Use of Self-Assembled Monolayers to Tailor Surface Properties:

From Lubrication to Neuronal Development

by

Natalie A. LaFranzo

A dissertation presented to the
Graduate School of Arts and Sciences
of Washington University in
partial fulfillment of the
requirements for the degree
of Doctor of Philosophy

May 2013

St. Louis, Missouri

TABLE OF CONTENTS

LIST OF FIGURES

LIST OF ABBREVIATIONS AND SYMBOLS

%	percent
%R	percent reflectance
%T	percent transmission
(g)	gas
°	degrees
µ	micro
50:50	equimolar mixture
Å	angstroms
AFM	atomic force microscopy
Alexa	AlexaFluor protein label
B27	cell culture supplement
BDCA	bis(diethylamine)chloroarsine
C	Celcius or carbon
c	centi
CA	contact angle
CCD	charge-coupled device
CD-1	mouse strain
$CDCl_3$	chloroform
cDNA	complementary DNA from mRNA
cGMP	cyclic guanosine monophosphate
CH_2Cl_2	methylene chloride
CHO-K1	Chinese Hamster Ovary cell line
CMOS	complementary metal-oxide semiconductor
CO_2	carbon dioxide
CT	C-terminal cystein knot
Cu	copper
$Cu(MeCN)_4PF_6$	tetrakis(acetonitrile)copper(I) hexafluorophosphate
CuAAC	copper-catalyzed azide-alkyne cycloaddition
DAPI	4',6-diamidino-2-phenylindole
DI	deionized

DIPEA	diisopropylethylamine
DMEM	Dulbecco's modified Eagle's medium
DMF	dimethylformamide
DMSO	dimethylsulfoxide
DNA	deoxyribonucleic acid
DPBS	Dulbecco's phosphate buffered saline
E17	embryonic day 17
E18	embryonic day 18
EA	elemental analysis
ECM	extracellular matrix
EDTA	ethylenediaminetetraacetic acid
EGF	epidermal-growth factor like
ENS	enteric nervous system
eq	equivalents
ESI	electrospray ionization
Et_2O	diethyl ether
FA	focal adhesion
FBS	fetal bovine serum
Fc	Fc domain of an immunoglobulin protein
FT-IR	fourier transform infrared spectroscopy
g	gram or gravity
G418	geneticin
GDNF	glial derived neurotrophic factor
GFP	green fluorescent protein
H	proton or hydrogen
h	hours
H_2O	water
HBTU	O-Benzotriazole-N,N,N’,N’-tetramethyl-uronium-hexafluoro-phosphate
HCl	hydrochloric acid
His-tag	affinity tag containing repeating histidines
HOPG	highly ordered pyrolytic graphite
HPLC	high performance liquid chromatography

HR	high resolution
HRP	horseradish peroxidase
HSV-tag	affinity tag derived from 11 amino acid sequence of herpes simplex virus (HSV) glycoprotein D
Hz	hertz
ICP	inductively-coupled plasma analysis
IgG	immunoglobulin G
IKVAV	laminin-derived peptide sequence
in	inch
IPTG	Isopropyl-β-D-thio-galactoside
IR	Infrared
k	kilo
kD	kilodalton
L	liters
LamG	laminin-G
LB	luria broth
LBP110	laminin-binding protein
LR	low resolution
LRR	leucine-rich repeats
m	milli, multiplet, or meter (as appropriate)
M	molar
M	mega
m/z	mass-to-charge ratio
MALDI-MS	matrix-assisted laser desorption/ionization mass spectrometry
MEMS	Microelectromechanical systems
mol	mole
MS	mass spectrometry
N	newton
N	nitrogen (atom)
N_2	nitrogen (diatomic)
NaCl	sodium chloride
NEMS	nanoelectromechanical systems

$NiCl_2$	nickel (ii) chloride
nm	nanometer
NMR	nuclear magnetic resonance
no.	number
OD_{600}	optical density at 600 nm
OTS	octadecyltrichlorosilane
p	pico
P	papain
PAGE	polyacrylamide gel electrophoresis
PBS	phosphate buffered saline
PCR	Polymerase chain reaction
PDMS	Polydimethylsiloxane
PHEM	PIPES, HEPES, EGTA, MgSO4
ppm	parts per million
QCM	quartz crystal microbalance
RGD	laminin and fibronectin derived peptide sequence
ROI	region of interest
rpm	revolutions per minute
s	singlet or second
SAGA	spectral apertured grazing angle
SAM	self-assembled monolayer
SDS	sodium dodecyl sulfate
SERS	surface enhanced Raman spectroscopy
SMART	Simple, Modular, Architecture, Research Tool
$SOCl_2$	thionyl chloride
SPM	Scanning probe microcopy
SPR	surface plasmon resonance
SPRi	surface plasmon resonance imaging
S-tag	affinity tag derived from 20 amino acid sequence of pancreatic ribonuclease A
STM	scanning tunneling microscopy
t	triplet

T7	T7 promoter sequence
TAE	Tris-acetate-EDTA
T-BAG	tethering by aggregation and growth
TBTA	tris-(benzyltriazolylmethyl)amine
TB	terrific broth
TFA	trifluoroacetic acid
THF	tetrahydrofuran
TOF	time-of-flight
TOF-SIMS	time-of-flight secondary ionization mass spectrometry
U	activity units
V	volts
XPS	X-ray photoelectron spectroscopy
YIGSR	laminin-derived peptide sequence
δ	chemical shift
Δ	heat/reflux or change

ACKNOWLEDGEMENTS

Graduate school has been an incredible journey with many amazing moments of success and all too many moments of failure. Without the support of my family and friends, I would not have persevered through those moments of failure and disappointment, nor would I have enjoyed the sweet moments of success quite as much.

The first and biggest thank you goes to my mom, Carol, who instilled in me a hard-working, driven attitude and the requirement that I always try my best. Throughout many years of school and life, these principles have guided me and ensured that I will always be proud of what I accomplish. Without the support that you have provided in so many ways, I would never have been able to arrive at where I am today. Your determination, strength, and generosity inspire me every day. Thank you to Marty, for becoming an integral part of our family and acting as an incredible, quiet supporter of both my mom and I. You have taught my mom patience and given her the opportunity to relax and unwind a little, and we are ALL grateful for that. Special thanks to my sister, Suzanne, who has always been there to put things into perspective, and offer her advice. And of course, thank you to the rest of my family, Grandma, Grandpa, Aunt Nancy, Uncle Randy, Melissa, Jonathon, Mark, and Thu, who have been so supportive of my goals and achievements along the way.

Thank you to Andrew, who has taught me that I can accomplish everything I want to, especially with a strong supporter like you. You continually awe me with how caring and patient you are, and I feel lucky to have you by my side. I promise that I will relax a little

now that this is over, and I am excited to put our home in order, spend time with the dogs, and for the many more adventures I am sure we will have. Most importantly, I look forward to beginning the next chapter in our lives and seeing what our future holds!

Thanks to the friends I've gained along this journey, both at Bradley and Washington U. Both my chemistry and cheerleading friends at Bradley helped to prepare me for graduate school - thanks to Jessica, Chris, Katie and Ryan, Phil, James, Jon, Jeff, and all of the faculty and scientists at Bradley and the USDA lab. Of course, without my friends here at WashU, I never would have survived - thank you to Jill, Alison, and Jessica for so much fun. Thanks in particular to my labmates Dawn Johnson, Matt Hynes, Hannah Malcolm and Matt Strulson. You have each been instrumental in helping me survive many, many moments of disappointment and more importantly, have helped me to celebrate and savor each of our successes. Thanks for all the crazy adventures and never-ending encouragement.

Special thanks to the Department of Athletics, who gave me the opportunity to grow as a person, coach, and leader. While coaching, I have gotten the opportunity to meet so many incredible student-athletes who have taught me many lessons I will never forget.

I feel lucky to have been a member of The BALSA Group, and look forward to watching the organization grow and prepare many more scientists for future success.

Finally, thank you to the Department of Chemistry at Washington University and my advisor, Dr. Joshua Maurer. I am grateful that I have been able to pursue many opportunities throughout my time here, and truly tailor my graduate career to prepare me for the future I envisioned. Thank you for challenging me and helping me to grow as a scientist. I am grateful for the financial support I received from the Department of Chemistry, the Graduate School, the GAANN program, and the NIH in support of my graduate career. I am also grateful for the opportunities to attend conferences thanks to funding from the American Chemical Society and the National Science Foundation. Thank you to my committee members Dr. John-Stephen Taylor, Dr. Michael Gross, and Dr. Robert Heuckeroth for your insightful discussions and helpful advice. Thank you also to Dr. Kevin Moeller and Dr. Garland Marshall for serving on my defense committee.

ABSTRACT OF THE DISSERTATION

Use of Self-Assembled Monolayers to Tailor Surface Properties:

From Lubrication to Neuronal Development

by

Natalie A. LaFranzo

Doctor of Philosophy in Chemistry

Washington University in St. Louis, 2013

Professor Joshua A. Maurer, Chairperson

The subsequent work describes advances in modifying the chemical properties of various substrates to tailor the surface properties for specific applications. This is achieved by making use of a molecular assembly known as self-assembled monolayers, or SAMs. SAMs are composed of tightly packed organic molecules that form a well-ordered structure on a substrate. Typically, the head group of the monomer is covalently anchored to the substrate, and monolayer order and self-assembly is achieved through van der Waals interactions between the long alkyl chains of the monomer's tail group. Monolayers containing head groups consisting of thiols, siloxanes, and phosphonates have been demonstrated on gold, glass, and metal oxides, respectively. We have expanded upon existing monolayer technology and designed monolayers with either new head group or new tail group functionalities. The resulting surfaces have been characterized by a variety of techniques including infrared spectroscopy, contact angle analysis, quartz crystal microbalance analysis, surface plasmon resonance imaging, and atomic force microscopy. We have also explored applications for these functionalized

surfaces in areas ranging from microelectromechanical systems (MEMS) lubrication to platforms for studying neuronal development *in vitro.*

In the area of MEMS lubrication, the development of new surface coatings is critical for combating wear and increasing the device lifetime. We reported a class of arsonic acid SAMs that form readily on oxide substrates including silicon oxide, borosilicate glass, and titanium oxide. The monolayers are easily prepared using a straightforward soaking technique, which is amenable to large-scale commercial applications. We have characterized monolayer formation on borosilicate glass and titanium oxide using infrared spectroscopy. Monolayers on borosilicate glass, native silicon oxide and titanium oxide were also evaluated with contact angle measurements, and as wear measurements using nanoscratching experiments. On titanium oxide and borosilicate glass, monolayers prepared from hexadecylarsonic acid provide significantly greater surface protection than surfaces reacted under similar conditions with hexadecylphosphonic acid, a common modifying agent for oxide substrates.

To develop a platform for *in vitro* studies of neuronal development, we have utilized mixed-monolayers incorporating low densities of cell-adhesive peptides. The monomers feature a tetraethylene glycol moiety in the tail group to prevent the non-specific adsorption of proteins, and a low density of monomers were terminated with an azide moiety to specifically attach a laminin-derived peptide (IKVAV) terminated with an alkyne group via the copper-mediated azide-alkyne cycloaddition (CuAAC) reaction. To achieve this, a pentynoic acid molecule was appended to the N-terminus of the peptide during solid phase synthesis. Surfaces containing 0.01% and 0.1% azide-coupled peptide

were determined to be resistant to the non-specific adsorption of proteins. Hippocampal neurons dissected from embryonic mice were cultured on these surfaces and the effects of the peptides on neurite outgrowth were observed. Similar neurite numbers per cell were observed on both substrates, but longer neurites were measured on the 0.1% azide-coupled peptide substrate. Unfortunately, further studies revealed that aldehyde fixation methods for immunohistochemistry did not successfully attach neuronal cells to the surface due to limited attachment points on the surface.

Many developmental cell biology experiments require downstream immunohistochemical analysis. As such, to overcome this limitation and to simplify the surface preparation, a protein-resistant intermolecular zwitterionic monolayer, which supports cell fixation, was utilized. We have shown that the intermolecular zwitterionic monolayer has well-defined, non-receptor mediated cellular attachment provided by cell-surface sugar interactions. Exploiting these properties, we have developed a monolayer stripe assay, where the interactions between neurons (cell bodies and neurites) and extracellular matrix (ECM) proteins or guidance cues can be observed and quantified. This system goes beyond current technologies and is capable of evaluating neuronal response to the extracellular matrix protein, laminin, which has previously been considered a control molecule in neuronal stripe assays.

Taken together, this work highlights advancements in the field of self-assembled monolayer chemistry with practical applications. In particular, we have focused on the functionalization of glass and oxides surfaces for applications in device lubrication. As

well, we have developed two alkanethiol self-assembled monolayer approaches for generating surfaces that are both protein resistant and cell permissive, advancing the tools available for studying neuronal development *in vitro.*

CHAPTER ONE

INTRODUCTION

1.1. Overview

Tailoring the surface chemistry of a material is of great interest in many fields from biotechnology to materials science. The chemical properties at the surface of a material can greatly affect its performance in both biological and non-biological applications. Furthermore, while the properties of a bulk material such as conductivity, optical transparency, or hardness may be necessary for a specific application, the surface properties may need to be tailored for optimal performance. Although approaches such as polymer and protein coatings, acid/base treatment, and heat treatment have been explored as methods to modify surface properties, these suffer from a number of limitations. Polymer and protein coatings are formed from large molecules with many reactive sites. It is difficult to introduce specific chemical groups on a surface, with well-defined concentration and spatial control. Treating a surface with an acid or a base, although an effective means of introducing a specific functional group on the surface, is limited to only a few chemical groups such as acid, basic, or hydroxyl groups. Heat treatment, such as flame annealing, affects the physical properties but not the chemical properties of a surface.[1]

Beginning with early reports of silane and alkane thiol monolayers, SAMs have been explored as a tool to tailor surface chemistry.[2-5] These molecular assemblies, which

covalently attach to a specific substrate in a well-defined manner, have exceptional flexibility and modularity, which can be exploited to present a number of chemical moieties on a surface.

1.2. Self-Assembled Monolayer (SAM) Chemistry

Self-assembled monolayers are formed from monomers with three specific features as shown in Figure 1.1. In the figure, the head group, which is specific to the substrate on which the monolayer assembles, is denoted as "X". In the middle of the monomer, alkane chains are most common, facilitating ordering during assembly achieved through van der Waals interactions and hydrophobic forces. In these alkane monomers, a long alkane chain is necessary to facilitate ordering during assembly.[6, 7] However, other functional groups in the middle of the monomer, including aromatic rings, have been shown to assemble with pi-electron interactions.[8] At the end of the monomer, a tail-group (noted as "Y" in the figure below) may be functionalized to present the desired chemical moiety on the surface. Self-assembled monolayers have been shown to form on a wide range of substrates including glass, metal oxides, and precious metals (gold, silver, and platinum).[9-21]

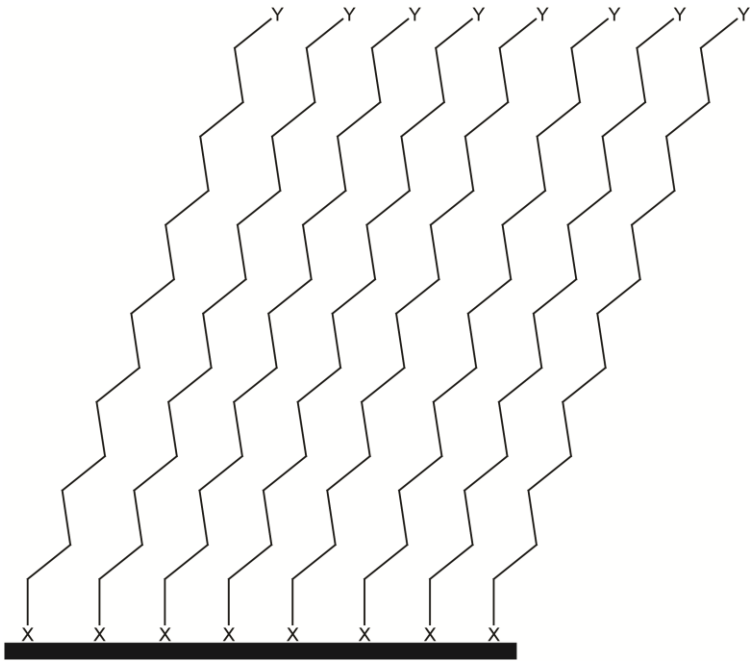

Figure 1.1. Alkane SAMs have 3 basic functionalities: a surface reactive head group, "X", an alkane chain which facilitates ordering, and a tail-group, "Y".

Self-assembled monolayers with a siloxane headgroup have been shown to form on glass.[6, 17] This is achieved through the reaction of either trichlorosilane monomers or alkoxysilane monomers. Trichlorosilane monomers, which are highly reactive towards glass substrates, are also highly reactive towards water, silica gel for flash chromatography, and other silane monomers in solution. As such, this class of monomers is problematic to synthesize and purify. The use of trialkoxylsilane monomers overcomes many of these issues, but requires more difficult assembly conditions including multiple soak and anneal steps. However, in either case, the resulting monolayer that forms from these silane monomers has a high degree of monomer crosslinking on the surface, as shown between the two center monomers circled in Figure 1.2. below. This crosslinking between monomers imparts a degree of instability to the monolayer, allowing for the monolayer to be peeled away from the surface. While these

monolayers have been shown to be useful in short-term applications,[15-17, 22, 23] the need for stable, glass reactive self-assembled monolayers is not met with silanes.

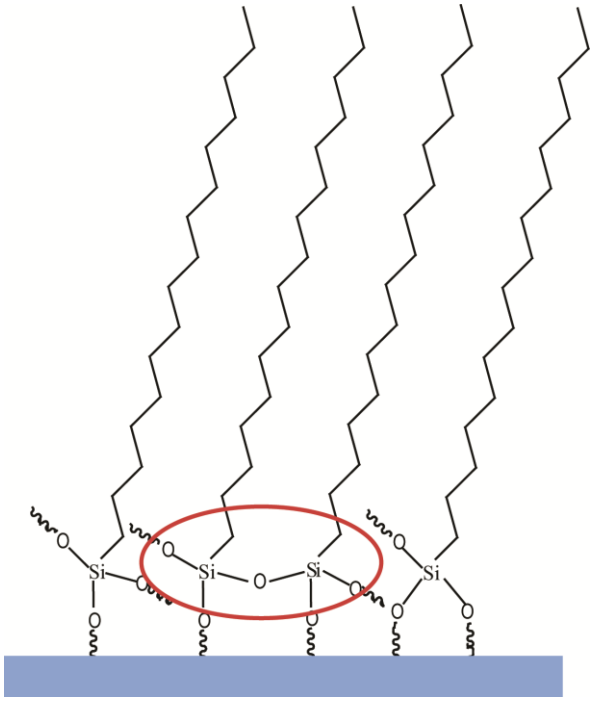

Figure 1.2. Self-assembled monolayers of trichloro- and trialkoxysilanes form on silicon oxide substrates including glass. Crosslinking occurs between silane monomers as shown circled above, resulting in decreased monolayer stability.

Another well-studied class of monomers are the phosphonic acids as shown in Figure 1.3. These monolayers assemble on many different substrates including metal oxides and silicon.[10-14, 24] Despite exhibiting polydentate binding to the substrate, which allows for high stability of the coating, their reactivity is slow, and assembly conditions for phosphonate monolayers are often difficult. Various methods for producing well-ordered monolayers have been reported, including aerosol coating, high-temperature annealing, tethering by aggregation and growth (T-BAG), and substrate pre-treating.[10-14, 24-26] These

methods are both time-intensive and resource-intensive, which limits the application of phosphonates for commercial products.

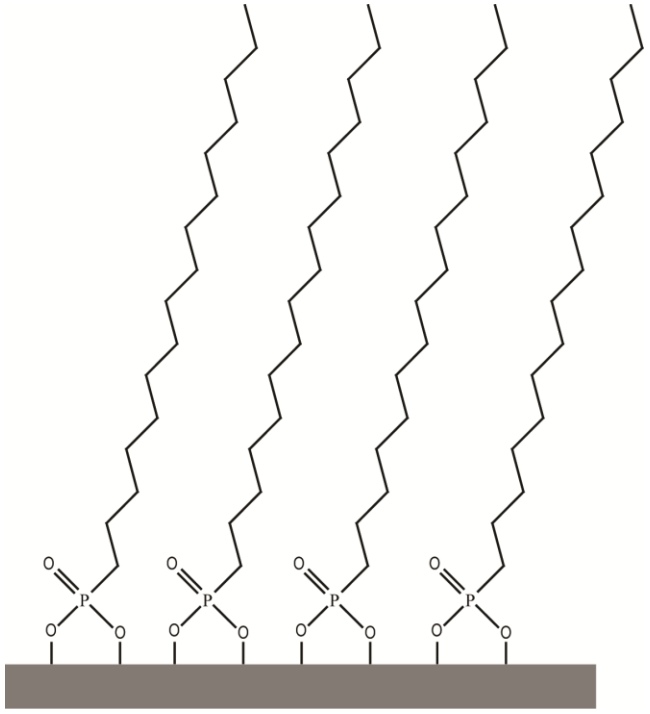

Figure 1.3. Phosphonate monolayers assemble on many different metal oxides with polydentate binding.

Finally, perhaps the most well-studied class of monolayers are thiol monomers assembled on precious metals such as gold and silver.[18] While thiols have been reported on other substrates such as palladium and platinum,[3, 27, 28] we have not found thiol assembly on these substrates to be as reproducible as on gold and silver. As demonstrated in Figure 1.4., thiol monolayers have a single attachment point to the substrate, which has high stability.

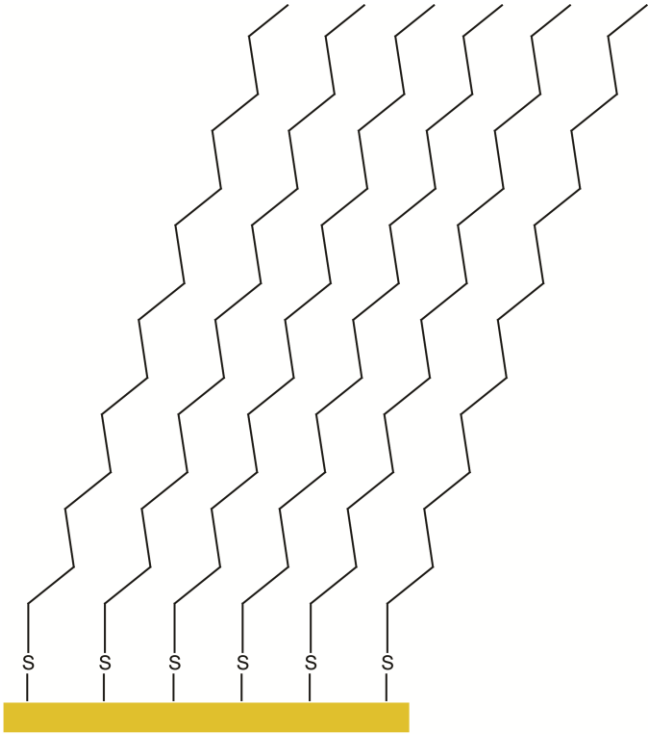

Figure 1.4. Thiol monomers assemble on precious metals including gold and silver with a single attachment point to the surface.

However, when the thiol-functionalized substrates are utilized in aqueous media, there are a number of places where instability is found in this system. First, the substrate must be very clean and flat, or disorder and defect sites may occur.[29-32] The defect site may allow reactive species such as oxygen to diffuse to the metal interface. This can affect the monolayer in two ways. On a silver substrate, this may cause the silver-silver bonds of the metal-coated substrate to break, displacing both the thiol molecule and the attached monomer. On either substrate, these defects sites can also allow for oxidation of the thiol head group, thereby displacing the thiol monomer from the substrate.[33] Advances made by our group and others demonstrate that by changing the functionality of the tail group, stability may be increased in the system.[34] As reported by Mrksich and Luk, this can be achieved by incorporating mannitol or D+L gulitol racemic sugars.[35, 36] As

reported by our group, incorporation of an amide linkage into the monolayer imparts stability of over five weeks in cell-culture conditions, which is unprecedented.[37] These advances, along with the non-toxic nature of gold, have allowed the thiol monolayer system to be viable for many applications in biotechnology.

1.3. Applications of Self-Assembled Monolayers (SAMs)

Each class of self-assembled monolayers covalently bonds to a specific type of substrate. Depending on the application and substrate utilized, various monolayer systems have been utilized for many applications as are described below.

1.3.1. Prevention of Biofouling

Biofouling is the undesired accumulation of biological species on a surface. Often, bacteria attach to the surface, and proliferate to form a biofilm. Then, organisms such as algae, barnacles, as well as other plants, animal species, or microorganisms may attach to and grow on exposed surfaces depending on the environment. When this occurs, the surface sterility and/or integrity may be compromised. Two major biofouling challenges, marine biofouling and medical device biofouling and the application of SAMs in combating these are described here.

1.3.1.1. Marine Fouling

Fouling caused by marine organisms on surfaces, such as ship hulls, is problematic owing to costs associated with maintenance and fuel consumption, as well as corrosion.[38, 39] The traditional method to prevent biofouling on surfaces includes the use of organotin coatings, such as tributyltin oxide and tributyltin fluoride. Although these are effective compounds, with activity against a wide-range of fouling species, recent environmental studies led to a ban of these compounds owing to negative environmental impacts.[40] Therefore, new approaches to prevent biofouling are of urgent need. When developing new technologies to prevent marine biofouling, self-assembled monolayers have played two important roles. First, studies using SAM surfaces have helped to illuminate the mechanism of microorganism attachment.[41-44] Understanding how organisms attach and biofilms form is integral to the development of new surface coatings to combat biofouling. As well, SAMs terminated with various tail-groups including sugars and oligo ethylene glycol were studied as potential biofouling coatings themselves.[45-47]

1.3.1.2. Medical Device Fouling

Within the body, it is also important to prevent biofouling in the form of unintended protein adsorption, cellular attachment, and/or biofilm formation on implanted devices. Bacterial infection resulting from device implants is a major medical problem. Devices such as stents[48] and shunts[49] are examples that have surfaces requiring protection from biofouling that have been functionalized with SAM coatings. Taken further, SAM coatings were also explored as therapeutic agents – a means of introducing drugs into the

body.[50] In a less direct application, SAMs have also been utilized to better understand on a molecular level how biomaterials and surface properties affect protein and cellular adhesion, influencing the development of better materials and coatings for medical devices. In particular, because SAMs may be prepared on a variety of surfaces, this system is amenable to studying protein adsorption with techniques such as surface plasmon resonance imaging (SPRi) and quartz crystal microbalance (QCM) as described below.[51] As well, SAMs serve as excellent substrates for *in vitro* cellular studies of biofouling.[52, 53]

1.3.2. Biomolecule Patterning/Cell Studies

As described previously with regard to biofouling, studying complex biological systems is difficult and requires fundamental mechanistic studies. Model surfaces prepared from self-assembled monolayers have also made it possible to explore a myriad of biological processes involving cells and biomolecules (proteins, ligands, etc.) in a well-defined, simplified manner. SAMs are ideal because there is spatial and concentration control over the adsorption and attachment of proteins, peptides, and other biomolecules. To perform these studies, it is important to produce and characterize a well-defined patterned monolayer. The approaches used exclusively in this work involve patterning SAMs with soft-lithographic techniques and preparing mixed-monolayer systems.

1.3.2.1. Patterning SAMs with Soft-Lithography

As first reported by Kumar and Whitesides, self-assembled monolayers may be patterned on surfaces using a combination of lithography and stamping.[54-56] This process was coined soft-lithography or microcontact printing and has found widespread use in biotechnology.[17, 57-59] While multiple methods of generating lithographic masters are available[60-62], in this work the process begins by generating a patterned master using traditional positive photoresist lithography. A clean silicon wafer is coated with an even, thin film of positive photoresist polymer. In this work, the AZ 9200 series of positive photoresist was utilized. A direct-write laser write system is utilized to expose the resist to 325 nm light according to a pattern imported into the software.[63] At the exposure site, an acid catalyst is generated, breaking the bonds of the photoresist polymer. The regions in which this has occurred are then rinsed away and neutralized in a basic developing solution. This method is illustrated below in Figure 1.5.

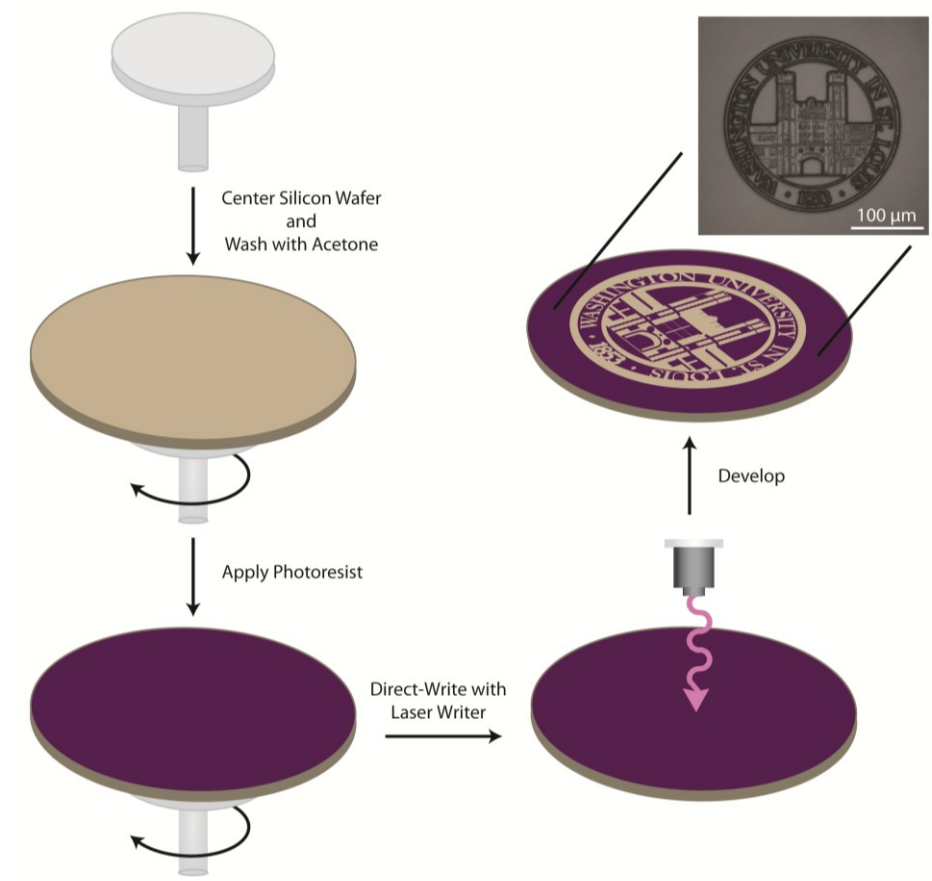

Figure 1.5. Preparation of lithographic master using a direct-write laser system and positive photoresist.

The lithographic master generated is the inverse of the desired pattern, and will be used to make an elastomeric stamp of the pattern. Polydimethylsiloxane (PDMS) polymer produced by Dow Corning and sold as Sylgard is most commonly used for stamp production. The pre-polymer and curing agent are mixed together, poured over the lithographic master and degassed to remove bubbles. After curing, the stamp is removed from the master. This is illustrated in Figure 1.6.[60]

Once the stamp is prepared, it may be inked by applying an ethanolic solution of hexadecane thiol monomer to the patterned surface. The ethanol is evaporated using inert nitrogen gas, and the stamp is applied using gentle pressure to a clean substrate. The remainder of the substrate may then be "backfilled" with a complementary monomer to generate a patterned substrate. In this work, alkanethiols exclusively are patterned on gold substrates. This technique will be further described in this dissertation, however, other SAMs have been patterned with similar approaches.[17]

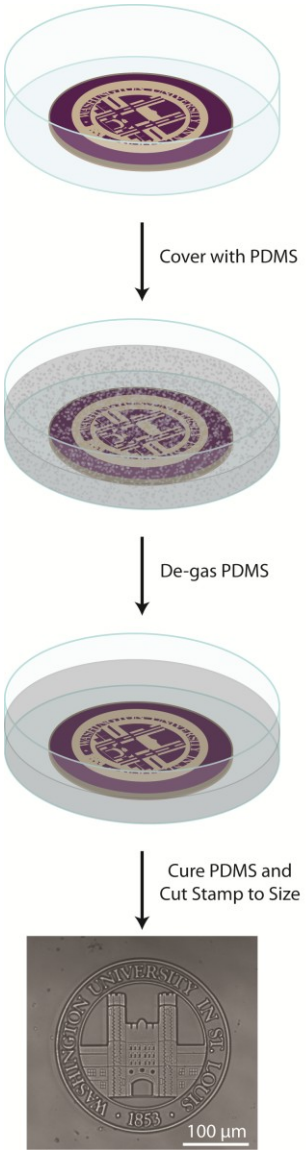

Figure 1.6. PDMS is poured over the lithographic master to generate an elastomeric stamp.

Building upon the discovery that oligo ethylene-glycol terminated monomers are capable of resisting protein adsorption, monomers with this tail group are often employed as "backfilling" monomers to generate patterned SAMs, which may be utilized to create protein patterns on a substrate. Once prepared as described above, and shown in Figure1.6., protein may be adsorbed simply by soaking the substrate in a protein solution. As illustrated in Figure 1.7., by fluorescently labeling the protein, the pattern may be visualized on the substrate using inverted fluorescence microscopy.[60] This is possible because of the minimal thickness of metal (50 Å titanium, 100 Å gold) on the surface, which is optically transparent.

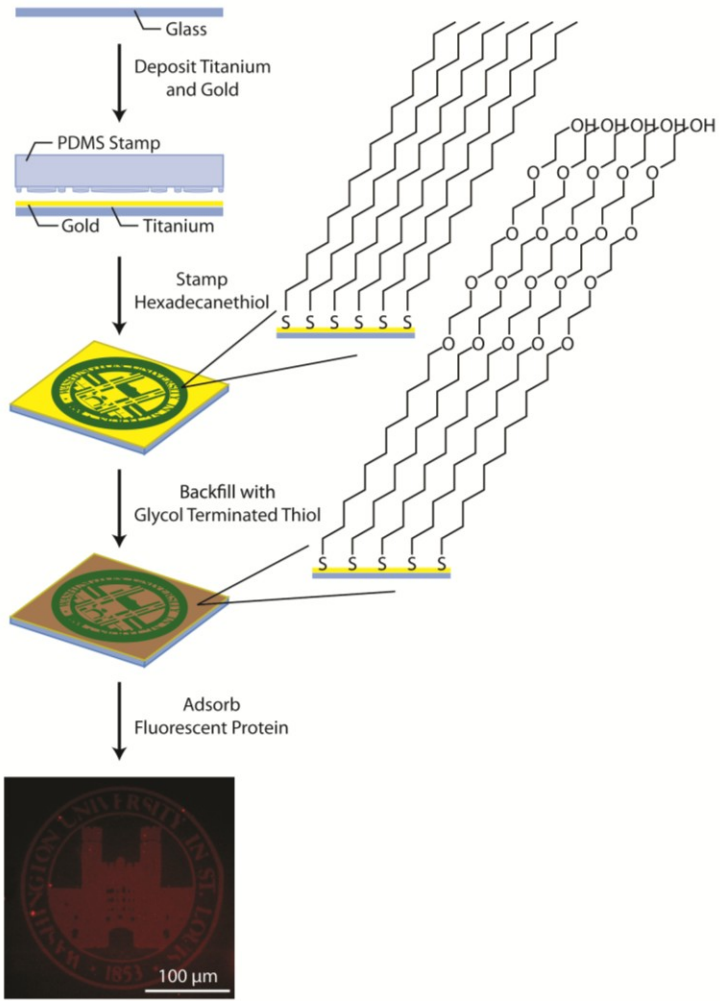

Figure 1.7. Scheme for microcontact printing alkanethiols on a gold substrate, followed by adsorption of a fluorescently labeled protein to the surface.

One of the major advantages of soft-lithography is the versatility in patterns that may be generated. This is limited only by (1) the technique by which one produces a lithographic master and (2) stamping technique. The major determinate in (1) is the wavelength of light used for patterning. To address (2), various research groups developed techniques such as submerged micro-contact printing that aids in shrinking pattern size and assists with patterning small features.[64, 65] Another advantage of this system is the wide-range of proteins that may be adsorbed to the monolayer. Proteins as small as 15 kD (glial derived

neurotrophic factor, GDNF) and as large as 900 kD (laminin-1) have been successfully adsorbed in this system in our hands.

Protein-patterned surfaces as described above are also excellent tools for patterning cells on a surface. For example, by adsorbing human plasma fibronectin to a simple geometric pattern, CHO-K1 cells grow selectively in the protein pattern, and not in the glycol-terminated monolayer in the background as shown in Figure 1.8.[60]

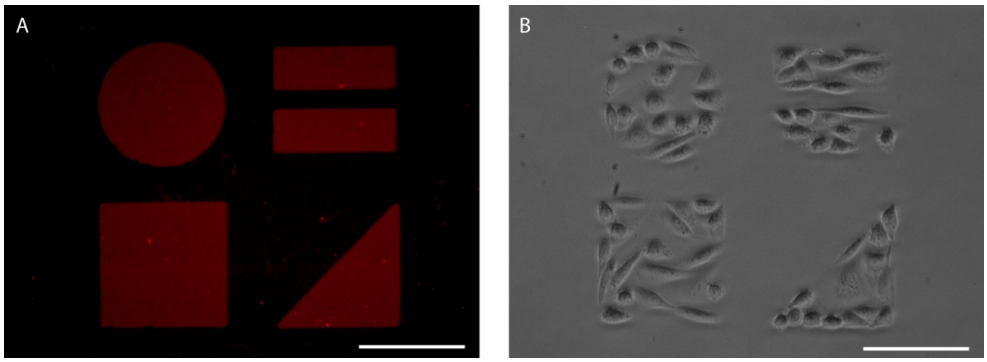

Figure 1.8. CHO-K1 cells seeded on a patterned alkanethiol SAM with fibronectin adsorbed preferentially grow on the protein regions. Fibronectin is labeled with Alexa647 and visualized with fluorescence microscopy in (A) and CHO-K1 cells are imaging using brightfield microscopy in (B).

However, for *in vitro* studies of protein guidance cues as described in Appendix Two, it is desirable to generate surfaces that are both protein-repulsive, but cell-permissive so that cells may adhere on the entire surface and sample the proteins patterns. To do this, new backfilling monomers must be developed that meet this need. In Chapters Three and Four of this work, we discuss two approaches for preparing protein-resistant, cell-permissive SAM substrates. Both of these approaches utilize two-component mixed-monolayer SAMs, one of which includes a reactive SAM to present biomolecules at well-defined spatial orientations.

1.3.2.2. Mixed-Monolayer Functionalized SAMs

Another technique to present biomolecules including peptides, carbohydrates, nucleotides, and proteins on a SAM surface in a well-defined manner involves the preparation of mixed-monolayer SAMs. Surfaces of two or more different monomers may be combined during solution-phase monolayer formation to afford a homogeneous surface that reflects the solution concentration of the monomers.[66] This homogeneity is present as long as the concentrations of the monomers fall within a certain regime (less than ten mole percent) to prevent clustering or "islanding" of monomers.[67] By incorporating specific moieties into the monomer, molecules may be covalently attached to the surface either before[68] or after SAM preparation with a variety of reactions including amide and ester-bond formation,[69-71] Diels-Alder,[72, 73] triazole ring formation,[66, 74, 75] and Michael addition.[76, 77] If a specific bioorthoganol point is introduced into the biomolecule for attachment to a reactive group on the surface, the orientation of the biomolecule can also be defined using this system.[66, 78] Furthermore, as described previously, monolayers with ethylene-glycol terminations resist non-specific protein adsorption. It has been shown that the introduction of low concentrations of monomers with covalently attached biomolecules in an ethylene-glycol terminated monolayer background retains protein resistance up to a specific concentration (less than 1 mole percent, depending on the system).[66, 79, 80] This technique is utilized in the work described in Chapter Three to develop a well-defined adhesive peptide substrate for neuron culture, but the technique has also been used for other applications.

1.3.3. Biosensors, Biochips, and Arrays

Substrates with immobilized biomolecules are important for the development of biosensors, biochips and bioarrays. As well, reproducible, molecular-level control over immobilization is ideal for these applications, which require high analytical sensitivity. As described previously, SAMs with ethylene glycol tail functionalities are capable of preventing non-specific protein adsorption and undesirable contamination and binding to the sensing surface.[81] Furthermore, monolayers may be prepared on a variety of surfaces such as gold, which can be studied by electrochemistry and surface plasmon resonance (SPR). Other techniques including quartz-crystal microbalance (QCM) and matrix-assisted laser desorption/ionization mass spectrometry (MALDI-MS) have also been used with SAMs for bioassays and biosensors.[81, 82] These techniques are described in detail below. Surfaces using SAM technology have been previously used to interrogate antigen-binding, protein-protein interactions, toxin and other molecular detection, and many other interactions.[83-87] Arrays of biomolecules prepared using SAM chemistry have also been shown to be useful for probing cellular interactions.[88]

1.3.4. Surface Protection in Materials Science Applications

In addition to the biological needs described above, self-assembled monolayers have potential for substrate protection in materials science applications. Two of these applications include protecting a surface from etchants in lithographic pattern generation, and from wear in tribological studies.

1.3.4.1 Etch Resists

Patterning thin films of metal, or directly patterning the microtopography of a substrate is required when generating devices such as microelectrode arrays[89], complementary metal-oxide semiconductor (CMOS) devices[90], and diffraction gratings[91]. Both patterns are achieved by using wet-etching techniques in which chemical etchants dissolve away the surface layers of a material. Traditional etching utilizes photoresist and lithography as described in Figure 1.5. or mask lithography[60] to generate the desired pattern on the surface. Following pattern development, the substrate is soaked in a chemical etchant that removes the exposed regions of the substrate not protected by the resist. While this technique is well-developed, it requires a time and resource intensive lithography step for each substrate that is etched.[92] Well-ordered SAMs have been shown to protect the surface from reactive species which compromise the stability of the monolayer as described in Section 1.2. above. As such, they are also ideal resists for etching. Furthermore, microcontact printing may be employed to pattern the monolayers on the surface. This minimizes the lithographic steps required – as one master and subsequent elastomeric stamps may be used to pattern multiple substrates. SAMs have been used as agents to protect surfaces such as palladium[90] and gold with both traditional[92] and specially developed[93] etchants[91]. Monolayers have also been shown to perform well in other etching conditions including plasma etching.[94]

1.3.4.2. Lubrication

Microelectromechanical (MEMS) and nanoelectromechanical (NEMS) systems have been established as central to the development of new technologies, particularly in the

areas of semiconductors and sensing devices.[95] As with any mechanical system, understanding the tribology, or science of interacting surfaces, with the goal of combating the negative effects of friction and adhesion between contact points is imperative. Tribological studies aimed at the prevention of wear and the development of materials for long-term lubrication are important for increasing device lifetime. However, these systems cannot make use of conventional mineral, vegetable, or synthetic oil lubricants owing to the nanometer-scale mechanical contacts of the devices.[96] As a result, new strategies must be developed for device protection that are applicable to large-scale manufacturing of MEMS and NEMS devices. SAMs formed from headgroups of silanes, phosphonates, and thiols with hydrophobic or fluorinated tail groups have all been explored as potential coatings for transistors and sensors, as well as lubricants for MEMS and NEMS devices.[97-104] However, those systems that have been reported thus far suffer from a number of limitations. In Chapter Two of this work, we discuss these limitations, and introduce a new class of monolayers which shows potential as a MEMS lubricant.[105]

1.4. Characterization

Characterization of self-assembled monolayers is approached using a variety of techniques that allow the properties of functionalized surfaces to be evaluated on the macroscale down to the nanoscale. Techniques used to characterize SAMs prepared in this work are described below. However, other methods including surface enhanced Raman spectroscopy (SERS)[106], ellipsometry[107-109], X-ray photoelectron spectroscopy (XPS)[108], scanning tunneling microscopy (STM)[29, 31], time-of-flight secondary ionization

mass spectrometry (TOF-SIMS)[110, 111], and electrochemical characterizations[112-114] have also been used by other groups to better understand the SAM surface.

1.4.1. Contact Angle

The ensemble hydrophobicity and hydrophilicity of a substrate is most easily evaluated by using contact angle measurements. A droplet (microliter volumes) of liquid is placed on the surface, and the angle (θ) between the surface and the line tangent to the drop edge (shown in Figure 1.9.) is measured. Water is the mostly commonly used hydrophilic liquid, and decane is often used as a hydrophobic liquid for measurements. This method provides a quick and easy means of confirming that surface functionalization has occurred.[105, 115]

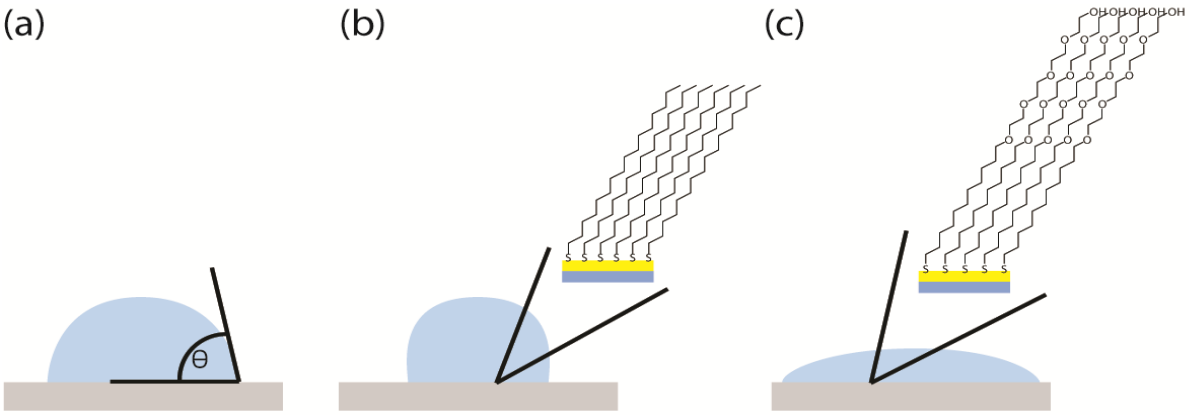

Figure 1.9. Water contact angle, θ is measured as shown in (a) and provides information about the hydrophobicity of the surface. A long-chain alkyl monolayer such as hexadecanethiol will give high values as shown in (b), whereas a glycol-terminated monolayer will give low values as shown in (c).

While sophisticated instrumentation that offers automated measurement and image analysis is available, a home-built substrate stage and digital camera, coupled with an ImageJ plugin[116], provides an inexpensive method of obtaining similar information. This

was recently described by Lamour, et al.[117] and our system, built in 2008 has a similar set-up as pictured in Figure 1.10.

Figure 1.10. Contact angle measurements are obtained on our home-built system and analyzed with an ImageJ plug-in.

1.4.2. Infrared Spectroscopy

Infrared (IR) spectroscopy is often used to obtain information about functional groups present in a molecule by identifying unique peaks corresponding to the stretching or bending of chemical bonds. This same technique can be applied to SAMs on both optically transparent (transmission mode) and reflective (grazing angle spectral reflectance mode) substrates. We and other groups have utilized this tool to evaluate successful monolayer preparation and/or degradation, as well as to monitor reactions on the monolayer surface.[66, 118-120] In addition to confirming the presence of specific functional groups, IR spectroscopy has also been extensively utilized to determine the degree of ordering in a SAM surface. This is done by looking specifically at the asymmetric and symmetric stretches of the methylene bonds in the alkyl chain of the

monolayer, as shown in Figure 1.11. For our analysis, we define "ordered" monolayers as having asymmetric methylene stretching frequencies below 2920 cm^{-1} and symmetric methylene stretching frequencies below 2850 cm^{-1}. These definitions are based on peak positions for crystalline alkane chains in the extended *trans* conformation.[121]

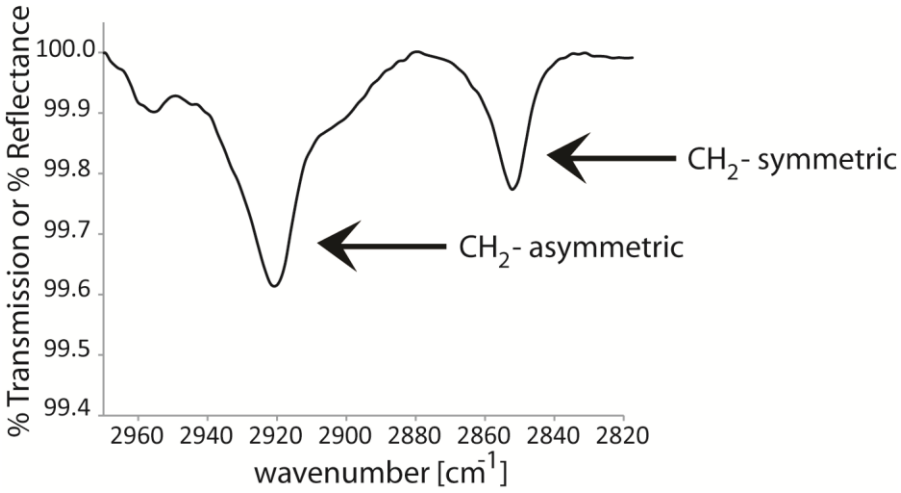

Figure 1.11. The asymmetric and symmetric methylene stretches are highlighted in this example IR spectrum.

Coupled with infrared spectroscopy of the methylene stretching region, a mechanical peel test may be performed to confirm covalent attachment of a monolayer to the substrate.[12, 105] The method uses common Scotch tape, which when adhered to the surface and then peeled off, exerts a defined force on the functionalized substrate.[122] The IR spectra before and after the peel test may be compared. If no significant changes between peak positions in the two spectra are observed, this indicates that a covalent linkage between the monomers and the substrates has been formed. Furthermore, if the peak intensity does not decrease, the surface is likely a monolayer and not a multilayer of adsorbed molecules.

1.4.3. Mass Spectrometry

Matrix-assisted laser desorption/ionization mass spectrometry, or MALDI-MS, is a technique that measures mass-to-charge ratios of ions ablated from a surface. It is considered a "softer" ionization technique, compared to ionization methods which vaporize and fragment molecules. MALDI allows large organic and biological molecules to be studied with less fragmentation than other mass spectral methods.[123] MALDI is another powerful tool which may be used to determine if a SAM has been successfully formed on a substrate[105], as well as monitor chemical reactions on a SAM surface.[119]

1.4.4. Quartz Crystal Microbalance

Quartz crystal microbalance (QCM) is a technique that has been developed to measure very small changes in mass. This is achieved by oscillating a quartz crystal at a defined frequency. When mass is added to the crystal, this oscillation frequency is dampened. According to Sauerbrey, a change in resonance frequency is proportional to a change in mass adsorbed on the surface.[124] Therefore, when a protein solution is flowed over a SAM surface, the change in frequency observed is a measurement of protein mass adsorbed to the surface. Therefore, this technique can be utilized to compare the protein resistance of SAM surfaces.[125, 126]

1.4.5. Surface Plasmon Resonance Imaging

Surface plasmon resonance (SPR) is a technique to measure changes in refractive index at a metal interface. Surface plasmons generated by near IR light undergo attenuated

total reflectance on a metal substrate and propagate along the surface. SPR is capable of measuring molecules that adsorb at this interface within a few nanometers of the surface.[127] This technique has found utility as a label-free detection method to measure adsorption and binding, and is ideal for studying alkanethiol monolayers as the metal substrate is most often gold.[128] In a traditional SPR experiment, the detector makes a bulk measurement of the substrate being probed. By utilizing a CCD camera as the detector as shown in Figure 1.12., the technique has been extended to include micron-scale spatial resolution, and is known as surface plasmon resonance imaging or SPRi.[129] SPRi allows for the visualization and quantification of protein adsorption to patterned substrates, as our group recently described.[118]

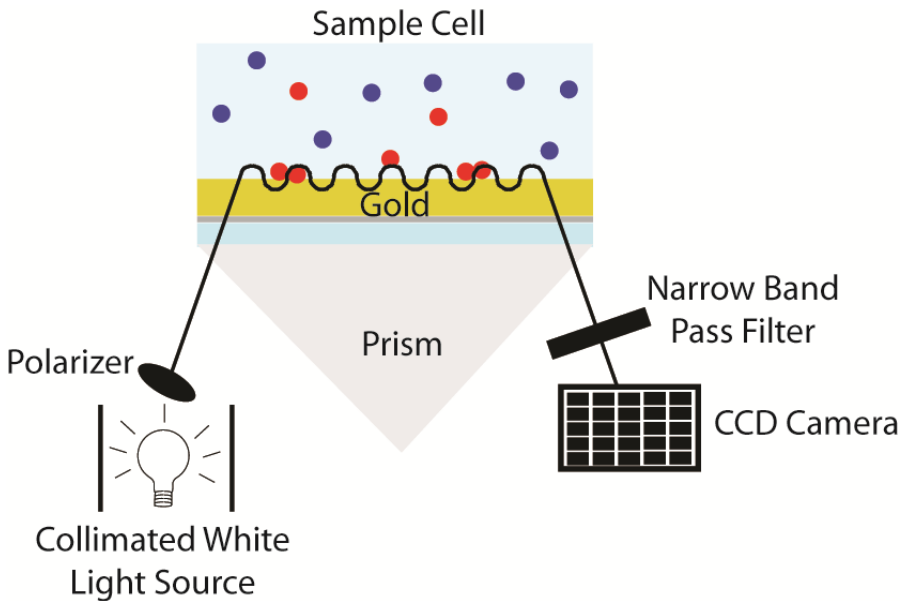

Figure 1.12. Surface plasmon resonance imaging (SPRi) is capable of measuring biomolecules (red/blue dots) absorbed at the interface of a metal substrate such as gold, and is ideal for evaluating the protein resistance of patterned SAM substrates.

1.4.6. Scanning Probe Microscopy

Scanning probe microcopy (SPM) is a multifaceted technique that provides information about the properties of a substrate. Most commonly, the technique has been used to image surface topography by measuring the height of small features on the surface. However, the chemical and physical properties of a surface may also be evaluated by measuring interactions of the SPM probe with a substrate. Surface properties such as electrostatic potential[130-132], nanomechanical properties[118, 133], and surface roughness[134-136] may all be evaluated using various experimental set-ups. The resolution of this technique is limited by the size of the probe, and the sensitivity of the detection system, which can be affected by thermal drift, as well as vibrations and other environmental influences. Multiple SPM techniques have been used to study the structure and properties of monolayers on the nanoscale and below.[32, 137-141] The term SPM includes both contact and non-contact interactions of the probe with the surface.

1.4.6.1. Nanoscratching

To examine the tribological properties of SAM-modified substrates, we utilized a SPM-based nanoscratching approach in this work. This method is an excellent tool for evaluating nanotribological properties or performing nanolithography in a versatile system with the NanoMan software package developed by Veeco/Bruker.[105, 142] While other instrumentation is available that measures nanotribology exclusively, these systems do not provide information about the other surface properties of the substrate, as is possible using a multifunctional SPM system. A diamond-tipped cantilever with a nm –

scale nominal tip radius may be used to scratch the surface of the substrate at defined forces. This stainless-steel cantilever and diamond tip are much more robust than conventional silicon cantilevers and tips, allowing micronewton forces to be evaluated. Following this wear simulation, the same probe may be used to image the scratches on the surface in tapping mode, allowing for measurement of the wear scars as shown in Figure 1.13.

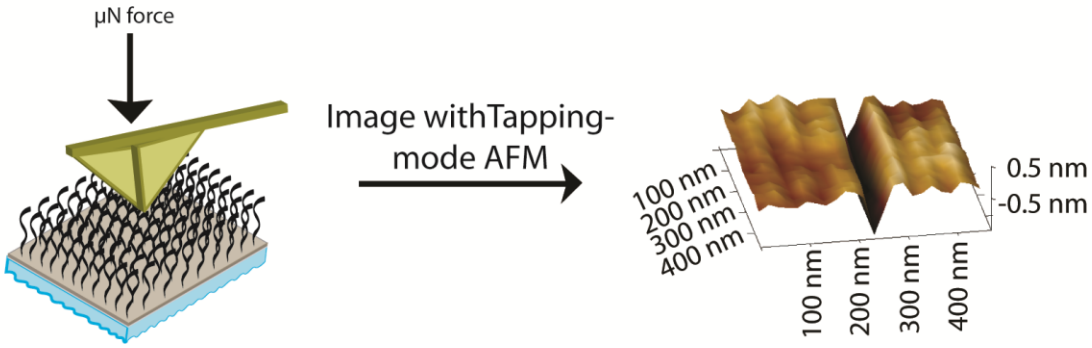

Figure 1.13. Nanoscratches made by dragging a 40 nm diamond-tipped cantilever across a surface with a well-defined force are imaged using tapping-mode atomic force microscopy (AFM).

By comparing the wear scars obtained from scratches made on substrates functionalized with different monolayer systems and on unfunctionalized substrates, the wear protection ability of a monolayer may be evaluated.

1.4.7. Fluorescence and Brightfield Microscopy

Inverted fluorescence microscopy can be used to visualize patterned monolayers with adsorbed proteins containing fluorescent tags.[60] The resolution of this technique is limited by both the numerical aperture of the objective used and the wavelength of light

detected. When characterizing protein patterns created with thiol SAMs on gold, another limitation is fluorescence quenching from the gold substrate.[143] Cells may also be seeded on the substrate and imaged live or following fixation with brightfield microscopy.[60] Furthermore, because the cell and protein resistant properties of the surface are related to the ordering and stability of the monolayer, the ability of the surface to confine protein and cell growth is an indication of the quality and stability of the monolayer. This was previously utilized by our group to compare the effect of intermolecular hydrogen bonding on monolayer stability.[37]

1.5. Summary

Self-assembled monolayers well-studied, and have the ability to generate well-defined surfaces that can be characterized by a number of experimental techniques. SAM surfaces have been explored previously for various applications, and in this work we built upon this in two major areas, surface coatings for MEMS lubrication and *in vitro* cell culture. We accomplished this by utilizing the modularity of self-assembled monolayers to tailor both the surface reactive group of the monomers and the chemical functionality presented on the surface.

We demonstrated that alkyl arsonate monolayers, a previously unexplored class of monomers, assemble on substrates such as glass, silicon, and metal oxides. These substrates are ideal materials for MEMS and NEMS devices which require non-conventional lubricants to prevent friction and wear. The arsonate monolayer system is effective at preventing wear within a micronewton force regime on each of these

substrates; with exceptional wear protection ability on titanium oxide. Previously studied monolayers for protein-patterned substrates have utilized protein-resistant and cell-resistant monolayers, which are unsuitable for studying neuronal guidance cues *in vitro*, as described in Chapters Three and Four. We have developed and characterized two thiol self-assembled monolayer systems that are protein-resistant but cell-permissive.

Our work in this area has advanced the growing field of self-assembled monolayer chemistry, introducing a new class of monomers and utilizing new characterization techniques. Perhaps more importantly, we also demonstrated viable applications for the monolayers we have explored, and provided new tools for scientists in other fields.

1.6. References

1. Maver, U.; Paninsek, O.; Jamnik, J.; Hassanien, A.; Gaberscek, M., Preparation of Atomically Flat Gold Substrates for AFM Measurements. *Acta Chimica Slovenica* 2012, 59, 212-219.
2. Nuzzo, R. G.; Allara, D. L., Adsorption of bifunctional organic disulfides on gold surfaces. *Journal of the American Chemical Society* 1983, 105, 4481-4483.
3. Ulman, A., Formation and structure of self-assembled monolayers. *Chemical Reviews* 1996, 96, 1533-1554.
4. Sagiv, J., Organized monolayers by adsorption. 1. Formation and structure of oleophobic mixed monolayers on solid surfaces. *Journal of the American Chemical Society* 1980, 102, 92-98.
5. Bigelow, W. C.; Pickett, D. L.; Zisman, W. A., Oleophobic monolayers: I. Films adsorbed from solution in non-polar liquids. *Journal of Colloid Science* 1946, 1, 513-538.
6. Schlecht, C. A.; Maurer, J. A., Functionalization of glass substrates: Mechanistic insights into the surface reaction of trialkoxysilanes. *RSC Advances* 2011, 1, 1446-1448.
7. Varatharajan, S.; Berchmans, S.; Yegnaraman, V., Tailoring self-assembled monolayers at the electrochemical interface. *Journal of Chemical Sciences* 2009, 121, 665-674.
8. Chang, S.-C.; Chao, I.; Tao, Y.-T., Structure of Self-Assembled Monolayers of Aromatic-Derivatized Thiols on Evaporated Gold and Silver Surfaces: Implication on Packing Mechanism. *Journal of the American Chemical Society* 1994, 116, 6792-6805.
9. Quiñones, R.; Gawalt, E. S., Study of the formation of self-assembled monolayers on nitinol. *Langmuir* 2007, 23, 10123-30.

10. Raman, A.; Dubey, M.; Gouzman, I.; Gawalt, E. S., Formation of self-assembled monolayers of alkylphosphonic acid on the native oxide surface of SS316L. *Langmuir* 2006, 22, 6469-72.
11. Gao, W.; Dickinson, L.; Grozinger, C.; Morin, F. G.; Reven, L., Self-assembled monolayers of alkylphosphonic acids on metal oxides. *Langmuir* 1996, 12, 6429-6435.
12. Gawalt, E.; Avaltroni, M.; Koch, N.; Schwartz, J., Self-assembly and bonding of alkanephosphonic acids on the native oxide surface of titanium. *Langmuir* 2001, 17, 5736-5738.
13. Hanson, E. L.; Schwartz, J.; Nickel, B.; Koch, N.; Danisman, M. F., Bonding self-assembled, compact organophosphonate monolayers to the native oxide surface of silicon. *J Am Chem Soc* 2003, 125, 16074-80.
14. Woodward, J.; Ulman, A.; Schwartz, D., Self-assembled monolayer growth of octadecylphosphonic acid on mica. *Langmuir* 1996, 12, 3626-3629.
15. Kluth, G.; Sung, M.; Maboudian, R., Thermal behavior of alkylsiloxane self-assembled monolayers on the oxidized Si(100) surface. *Langmuir* 1997, 13, 3775-3780.
16. Mrksich, M.; Whitesides, G. M., Using self-assembled monolayers to understand the interactions of man-made surfaces with proteins and cells. *Annu Rev Biophys Biomol Struct* 1996, 25, 55-78.
17. Yanker, D.; Maurer, J., Direct printing of trichlorosilanes on glass for selective protein adsorption and cell growth. *Molecular Biosystems* 2008, 4, 502-504.
18. Prime, K. L.; Whitesides, G. M., Self-assembled organic monolayers: model systems for studying adsorption of proteins at surfaces. *Science* 1991, 252, 1164-7.
19. Bain, C. D.; Troughton, E. B.; Tao, Y. T.; Evall, J.; Whitesides, G. M.; Nuzzo, R. G., Formation of monolayer films by the spontaneous assembly of organic thiols from solution onto gold. *Journal of the American Chemical Society* 1989, 111, 321-335.
20. Dubois, L.; Zegarski, B.; Nuzzo, R., Molecular Ordering of Organosulfur Compounds on AU(111) and AU(100) -Adsorption from Solution and in Ultrahigh-Vacuum. *Journal of Chemical Physics* 1993, 98, 678-688.
21. Love, J. C.; Estroff, L. A.; Kriebel, J. K.; Nuzzo, R. G.; Whitesides, G. M., Self-assembled monolayers of thiolates on metals as a form of nanotechnology. *Chem Rev* 2005, 105, 1103-69.
22. Tizazu, G.; el Zubir, O.; Patole, S.; McLaren, A.; Vasilev, C.; Mothersole, D. J.; Adawi, A.; Hunter, C. N.; Lidzey, D. G.; Lopez, G. P.; Leggett, G. J., Micrometer and nanometer scale photopatterning of proteins on glass surfaces by photo-degradation of films formed from oligo(ethylene glycol) terminated silanes. *Biointerphases* 2012, 7, 54.
23. Chen, S.; Jiang, S.; Mo, Y.; Luo, J.; Tang, J.; Ge, Z., Study of zwitterionic sulfopropylbetaine containing reactive siloxanes for application in antibacterial materials. *Colloids Surf B Biointerfaces* 2011, 85, 323-9.
24. Dubey, M.; Weidner, T.; Gamble, L.; Castner, D., Structure and Order of Phosphonic Acid-Based Self-Assembled Monolayers on Si(100). *Langmuir* 2010, 26, 14747-14754.
25. Thissen, P.; Peixoto, T.; Longo, R.; Peng, W.; Schmidt, W.; Cho, K.; Chabal, Y., Activation of Surface Hydroxyl Groups by Modification of H-Terminated Si(111) Surfaces. *Journal of the American Chemical Society* 2012, 134, 8869-8874.

26. Hanson, E.; Guo, J.; Koch, N.; Schwartz, J.; Bernasek, S., Advanced surface modification of indium tin oxide for improved charge injection in organic devices. *Journal of the American Chemical Society* 2005, 127, 10058-10062.
27. Li, Z.; Chang, S.-C.; Williams, R. S., Self-Assembly of Alkanethiol Molecules onto Platinum and Platinum Oxide Surfaces. *Langmuir* 2003, 19, 6744-6749.
28. Carvalho, A.; Geissler, M.; Schmid, H.; Michel, B.; Delamarche, E., Self-Assembled Monolayers of Eicosanethiol on Palladium and Their Use in Microcontact Printing. *Langmuir* 2002, 18, 2406-2412.
29. O'Dwyer, C.; Gay, G.; de Lesegno, B. V.; Weiner, J., The nature of alkanethiol self-assembled monolayer adsorption on sputtered gold substrates. *Langmuir* 2004, 20, 8172-8182.
30. Poirier, G. E., Mechanism of formation of Au vacancy islands in alkanethiol monolayers on Au(111). *Langmuir* 1997, 13, 2019-2026.
31. Sun, L.; Crooks, R. M., Indirect visualization of defect structures contained within self-assembled organomercaptan monolayers - Combined use of electrochemistry and scanning tunneling microscopy. *Langmuir* 1993, 9, 1951-1954.
32. Poirier, G. E., Characterization of organosulfur molecular monolayers on Au(111) using scanning tunneling microscopy. *Chemical Reviews* 1997, 97, 1117-1127.
33. Willey, T. M.; Vance, A. L.; van Buuren, T.; Bostedt, C.; Terminello, L. J.; Fadley, C. S., Rapid degradation of alkanethiol-based self-assembled monolayers on gold in ambient laboratory conditions. *Surface Science* 2005, 576, 188-196.
34. Cooper, E.; Leggett, G. J., Influence of Tail-Group Hydrogen Bonding on the Stabilities of Self-Assembled Monolayers of Alkylthiols on Gold. *Langmuir* 1999, 15, 1024-1032.
35. Bandyopadhyay, D.; Prashar, D.; Luk, Y.-Y., Stereochemical effects of chiral monolayers on enhancing the resistance to mammalian cell adhesion. *Chemical Communications* 2011, 47, 6165-6167.
36. Luk, Y.-Y.; Kato, M.; Mrksich, M., Self-Assembled Monolayers of Alkanethiolates Presenting Mannitol Groups Are Inert to Protein Adsorption and Cell Attachment. *Langmuir* 2000, 16, 9604-9608.
37. Strulson, M. K.; Johnson, D. M.; Maurer, J. A., Increased stability of glycol-terminated self-assembled monolayers for long-term patterned cell culture. *Langmuir* 2012, 28, 4318-24.
38. Rosenhahn, A.; Schilp, S.; Kreuzer, H.; Grunze, M., The role of "inert" surface chemistry in marine biofouling prevention. *Physical Chemistry Chemical Physics* 2010, 12, 4275-4286.
39. Salta, M.; Wharton, J.; Stoodley, P.; Dennington, S.; Goodes, L.; Werwinski, S.; Mart, U.; Wood, R.; Stokes, K., Designing biomimetic antifouling surfaces. *Philosophical Transactions of the Royal Society a-Mathematical Physical and Engineering Sciences* 2010, 368, 4729-4754.
40. Cao, S.; Wang, J.; Chen, H.; Chen, D., Progress of marine biofouling and antifouling technologies. *Chinese Science Bulletin* 2011, 56, 598-612.
41. Ista, L. K.; Callow, M. E.; Finlay, J. A.; Coleman, S. E.; Nolasco, A. C.; Simons, R. H.; Callow, J. A.; Lopez, G. P., Effect of substratum surface chemistry and surface energy on attachment of marine bacteria and algal spores. *Appl Environ Microbiol* 2004, 70, 4151-7.

42. Pranzetti, A., Salaün, S., Mieszkin, S., Callow, M. E., Callow, J. A., Preece, J. A. and Mendes, P. M., Model Organic Surfaces to Probe Marine Bacterial Adhesion Kinetics by Surface Plasmon Resonance. *Advanced Functional Materials* 2012.
43. Callow, M. E.; Callow, J. A.; Ista, L. K.; Coleman, S. E.; Nolasco, A. C.; López, G. P., Use of self-assembled monolayers of different wettabilities to study surface selection and primary adhesion processes of green algal (Enteromorpha) zoospores. *Appl Environ Microbiol* 2000, 66, 3249-54.
44. Finlay, J. A.; Callow, M. E.; Ista, L. K.; Lopez, G. P.; Callow, J. A., The influence of surface wettability on the adhesion strength of settled spores of the green alga enteromorpha and the diatom amphora. *Integr Comp Biol* 2002, 42, 1116-22.
45. Ederth, T.; Ekblad, T.; Pettitt, M. E.; Conlan, S. L.; Du, C. X.; Callow, M. E.; Callow, J. A.; Mutton, R.; Clare, A. S.; D'Souza, F.; Donnelly, G.; Bruin, A.; Willemsen, P. R.; Su, X. J.; Wang, S.; Zhao, Q.; Hederos, M.; Konradsson, P.; Liedberg, B., Resistance of galactoside-terminated alkanethiol self-assembled monolayers to marine fouling organisms. *ACS Appl Mater Interfaces* 2011, 3, 3890-901.
46. Schilp, S.; Rosenhahn, A.; Pettitt, M. E.; Bowen, J.; Callow, M. E.; Callow, J. A.; Grunze, M., Physicochemical properties of (ethylene glycol)-containing self-assembled monolayers relevant for protein and algal cell resistance. *Langmuir* 2009, 25, 10077-82.
47. Fyrner, T. e. a., Saccharide-Functionalized Alkanethiols for Fouling-Resistant Self-Assembled Monolayers: Synthesis, Monolayer Properties, and Antifouling Behavior. *Langmuir* 2011, 27, 15034-15047.
48. Mahapatro, A.; Johnson, D. M.; Patel, D. N.; Feldman, M. D.; Ayon, A. A.; Agrawal, C. M., The use of alkanethiol self-assembled monolayers on 316L stainless steel for coronary artery stent nanomedicine applications: an oxidative and in vitro stability study. *Nanomedicine* 2006, 2, 182-90.
49. Patel, K. R.; Tang, H.; Grever, W. E.; Simon Ng, K. Y.; Xiang, J.; Keep, R. F.; Cao, T.; McAllister, J. P., Evaluation of polymer and self-assembled monolayer-coated silicone surfaces to reduce neural cell growth. *Biomaterials* 2006, 27, 1519-26.
50. Mahapatro, A.; Johnson, D. M.; Patel, D. N.; Feldman, M. D.; Ayon, A. A.; Agrawal, C. M., Drug delivery from therapeutic self-assembled monolayers (T-SAMs) on 316L stainless steel. *Curr Top Med Chem* 2008, 8, 281-9.
51. Senaratne, W.; Andruzzi, L.; Ober, C. K., Self-assembled monolayers and polymer brushes in biotechnology: current applications and future perspectives. *Biomacromolecules* 2005, 6, 2427-48.
52. Moore, N.; Lin, N.; Gallant, N.; Becker, M., The use of immobilized osteogenic growth peptide on gradient substrates synthesized via click chemistry to enhance MC3T3-E1 osteoblast proliferation. *Biomaterials* 2010, 31, 1604-11.
53. Nakaoka, R.; Yamakoshi, Y.; Isama, K.; Tsuchiya, T., Effects of surface chemistry prepared by self-assembled monolayers on osteoblast behavior. *J Biomed Mater Res A* 2010, 94, 524-32.
54. Kumar, A.; Whitesides, Patterning Self-Assembled Monolayers - Applications in Microelectronics and Biotechnology. *Abstracts of Papers of the American Chemical Society* 1993, 206, 172-COLL.
55. Kumar, A.; Whitesides, G., Features of Gold having Micrometer to Cenitimeter Dimensions can be Formed Through a Combination of Stamping with an Elastomeric

Stamp and an Alkanethiol Ink Followed by Chemical Etching. *Applied Physics Letters* 1993, 63, 2002-2004.
56. Lopez, G.; Biebuyck, H.; Harter, R.; Kumar, A.; Whitesides, G., Fabrication and Imaging of 2-Dimensional Patterns of Proteins Adsorbed on Self-Assembled Monolayers by Scanning Electron-Microscopy. *Journal of the American Chemical Society* 1993, 115, 10774-10781.
57. Mrksich, M.; Whitesides, G. M., Patterning self-assembled monolayers using microcontact printing: A new technology for biosensors? *Trends in Biotechnology* 1995, 13, 228-235.
58. Chen, C. S.; Mrksich, M.; Huang, S.; Whitesides, G. M.; Ingber, D. E., Micropatterned surfaces for control of cell shape, position, and function. *Biotechnol Prog* 1998, 14, 356-63.
59. Ruiz, S. A. a. C., Christopher S., Microcontact printing: A tool to pattern. *Soft Matter* 2007, 2007, 168-177.
60. Johnson, D. M.; LaFranzo, N. A.; Maurer, J. A., Creating two-dimensional patterned substrates for protein and cell confinement. *J Vis Exp* 2011, e3164.
61. Kawata, H.; Carter, J. M.; Yen, A.; Smith, H. I., Optical projection lithography using lenses with numerical apertures greater than unity. In *Microelectronic Engineering*, 1989; Vol. 9, pp 31-3636.
62. Brock, P. J.; Levenson, M. D.; Zavislan, J. M.; Lyerla, J. R.; Cheng, J. C.; Podlogar, C. V., Fabrication of grooved glass substrates by phase mask lithography. *Journal of Vacuum Science & Technology B* 1991, 9, 3155-3161.
63. Lullo, G.; Leto, R.; Oliva, M.; Arnone, C., Multilevel pattern generation by GaN laser lithography: an application to beam shaper fabrication. *Proceedings of the SPIE - The International Society for Optical Engineering* 2006, 6290.
64. Bessueille, F.; Pla-Roca, M.; Mills, C.; Martinez, E.; Samitier, J.; Errachid, A., Submerged microcontact printing (S mu CP): An unconventional printing technique of thiols using high aspect ratio, elastomeric stamps. *Langmuir* 2005, 21, 12060-12063.
65. Xia, Y.; Whitesides, G. M., Extending Microcontact Printing as a Microlithographic Technique. *Langmuir* 1997, 13, 2059-2067.
66. Hudalla, G. A.; Murphy, W. L., Using "click" chemistry to prepare SAM substrates to study stem cell adhesion. *Langmuir* 2009, 25, 5737-46.
67. Stranick, S. J.; Parikh, A. N.; Tao, Y. T.; Allara, D. L.; Weiss, P. S., Phase Separation of Mixed-Composition Self-Assembled Monolayers into Nanometer Scale Molecular Domains. *The Journal of Physical Chemistry* 1994, 98, 7636-7646.
68. Derda, R.; Wherritt, D. J.; Kiessling, L. L., Solid-Phase Synthesis of Alkanethiols for the Preparation of Self-Assembled Monolayers. *Langmuir* 2007, 23, 11164-11167.
69. Yang, M.; Tsang, E. M. W.; Wang, Y. A.; Peng, X.; Yu, H.-Z., Bioreactive Surfaces Prepared via the Self-Assembly of Dendron Thiols and Subsequent Dendrimer Bridging Reactions. *Langmuir* 2005, 21, 1858-1865.
70. Bertilsson, L.; Liedberg, B., Infrared study of thiol monolayer assemblies on gold: preparation, characterization, and functionalization of mixed monolayers. *Langmuir* 1993, 9, 141-149.
71. Herrwerth, S.; Rosendahl, T.; Feng, C.; Fick, J.; Eck, W.; Himmelhaus, M.; Dahint, R.; Grunze, M., Covalent Coupling of Antibodies to Self-Assembled Monolayers

of Carboxy-Functionalized Poly(ethylene glycol): Protein Resistance and Specific Binding of Biomolecules†. *Langmuir* 2003, 19, 1880-1887.
72. Su, J.; Mrksich, M., Using MALDI-TOF Mass Spectrometry to Characterize Interfacial Reactions on Self-Assembled Monolayers. *Langmuir* 2003, 19, 4867-4870.
73. Yousaf, M. N.; Mrksich, M., Diels−Alder Reaction for the Selective Immobilization of Protein to Electroactive Self-Assembled Monolayers. *Journal of the American Chemical Society* 1999, 121, 4286-4287.
74. Lee, J. K.; Chi, Y. S.; Choi, I. S., Reactivity of Acetylenyl-Terminated Self-Assembled Monolayers on Gold: Triazole Formation. *Langmuir* 2004, 20, 3844-3847.
75. Collman, J. P.; Devaraj, N. K.; Chidsey, C. E. D., "Clicking" Functionality onto Electrode Surfaces. *Langmuir* 2004, 20, 1051-1053.
76. Smith, E. A.; Wanat, M. J.; Cheng, Y.; Barreira, S. V. P.; Frutos, A. G.; Corn, R. M., Formation, Spectroscopic Characterization, and Application of Sulfhydryl-Terminated Alkanethiol Monolayers for the Chemical Attachment of DNA onto Gold Surfaces. *Langmuir* 2001, 17, 2502-2507.
77. Houseman, B. T.; Gawalt, E. S.; Mrksich, M., Maleimide-Functionalized Self-Assembled Monolayers for the Preparation of Peptide and Carbohydrate Biochips†. *Langmuir* 2002, 19, 1522-1531.
78. Peng Yang, S. M. M., and Ashutosh Chilkoti, Spatially Addressable Chemoselective C-Terminal Ligation of an Intein Fusion Protein from a Complex Mixture to a Hydrazine-Terminated Surface†.
79. Murphy, W. L.; Mercurius, K. O.; Koide, S.; Mrksich, M., Substrates for Cell Adhesion Prepared via Active Site-Directed Immobilization of a Protein Domain. *Langmuir* 2003, 20, 1026-1030.
80. Roberts, C.; Chen, C. S.; Mrksich, M.; Martichonok, V.; Ingber, D. E.; Whitesides, G. M., Using Mixed Self-Assembled Monolayers Presenting RGD and (EG)3OH Groups To Characterize Long-Term Attachment of Bovine Capillary Endothelial Cells to Surfaces. *Journal of the American Chemical Society* 1998, 120, 6548-6555.
81. Wink, T.; vanZuilen, S.; Bult, A.; vanBennekom, W., Self-assembled monolayers for biosensors. *Analyst* 1997, 122, R43-R50.
82. Gooding, J.; Darwish, N., The rise of self-assembled monolayers for fabricating electrochemical biosensors-An interfacial perspective. *Chemical Record* 2012, 12, 92-105.
83. Kyo, M.; Usui-Aoki, K.; Koga, H., Label-free detection of proteins in crude cell lysate with antibody arrays by a surface plasmon resonance imaging technique. *Analytical Chemistry* 2005, 77, 7115-7121.
84. Patrie, S.; Mrksich, M., Self-assembled monolayers for MALDI-TOF mass Spectrometry for Immunoassays of human protein antigens. *Analytical Chemistry* 2007, 79, 5878-5887.
85. Kwon, Y.; Han, Z.; Karatan, E.; Mrksich, M.; Kay, B., Antibody arrays prepared by cutinase-mediated immobilization on self-assembled monolayers. *Analytical Chemistry* 2004, 76, 5713-5720.
86. Frisk, M.; Tepp, W.; Johnson, E.; Beebe, D., Self-Assembled Peptide Monolayers as a Toxin Sensing Mechanism within Arrayed Microchannels. *Analytical Chemistry* 2009, 81, 2760-2767.

87. Laboria, N.; Fragoso, A.; Kemmner, W.; Latta, D.; Nilsson, O.; Botero, M.; Drese, K.; O'Sullivan, C., Amperometric Immunosensor for Carcinoembryonic Antigen in Colon Cancer Samples Based on Monolayers of Dendritic Bipodal Scaffolds. *Analytical Chemistry* 2010, 82, 1712-1719.
88. Orner, B. P.; Derda, R.; Lewis, R. L.; Thomson, J. A.; Kiessling, L. L., Arrays for the Combinatorial Exploration of Cell Adhesion. *Journal of the American Chemical Society* 2004, 126, 10808-10809.
89. Abbott, N.; Rolison, D.; Whitesides, G., Combining Micromachining and Molecular Self-Assembly to Fabricate Microelectrodes. *Langmuir* 1994, 10, 2672-2682.
90. Love, J.; Wolfe, D.; Chabinyc, M.; Paul, K.; Whitesides, G., Self-assembled monolayers of alkanethiolates on palladium are good etch resists. *Journal of the American Chemical Society* 2002, 124, 1576-1577.
91. Kumar, A.; Biebuyck, H.; Whitesides, G., Patterning Self-Assembled Monolayers - Applications in Materials Science. *Langmuir* 1994, 10, 1498-1511.
92. Kim, E.; Kumar, A.; Whitesides, G., Combining Patterned Self-Assembled Monolayers of Alkanethiolates on Gold with Anisotropic Etching of Silicon to Generate Controlled Surface Morphologies. *Journal of the Electrochemical Society* 1995, 142, 628-633.
93. Xia, Y.; Zhao, X.; Kim, E.; Whitesides, G., A selective etching solution for use with patterned self-assembled monolayers of alkanethiolates on gold. *Chemistry of Materials* 1995, 7, 2332-2337.
94. Lercel, M.; Craighead, H.; Parikh, A.; Seshadri, K.; Allara, D., Plasma etching with self-assembled monolayer masks for nanostructure fabrication. *Journal of Vacuum Science & Technology a-Vacuum Surfaces and Films* 1996, 14, 1844-1849.
95. Mahalik, N. P., Principle and applications of MEMS: a review. *International Journal of Manufacturing Technology and Management* 2008, 13, 324-342.
96. Bhushan, B., Nanotribology and nanomechanics in nano/biotechnology. *Philos Transact A Math Phys Eng Sci* 2008, 366, 1499-537.
97. de Boer, M.; Mayer, T., Tribology of MEMS. *MRS Bulletin* 2001, 26, 302-304.
98. Halik, M.; Klauk, H.; Zschieschang, U.; Schmid, G.; Dehm, C.; Schütz, M.; Maisch, S.; Effenberger, F.; Brunnbauer, M.; Stellacci, F., Low-voltage organic transistors with an amorphous molecular gate dielectric. *Nature* 2004, 431, 963-6.
99. Mottaghi, M.; Lang, P.; Rodriguez, F.; Rumyantseva, A.; Yassar, A.; Horowitz, G.; Lenfant, S.; Tondelier, D.; Vuillaume, D., Low-operating-voltage organic transistors made of bifunctional self-assembled monolayers. *Advanced Functional Materials* 2007, 17, 597-604.
100. Pranzetti, A.; Salaun, S.; Mieszkin, S.; Callow, M.; Callow, J.; Preece, J.; Mendes, P., Model Organic Surfaces to Probe Marine Bacterial Adhesion Kinetics by Surface Plasmon Resonance. *Advanced Functional Materials* 2012, 22, 3672-3681.
101. Tsukruk, V., Molecular lubricants and glues for micro- and nanodevices. *Advanced Materials* 2001, 13, 95-108.
102. Patton, S.; Eapen, K.; Zabinski, J.; Sanders, J.; Voevodin, A., Lubrication of microelectromechanical systems radio frequency switch contacts using self-assembled monolayers. *Journal of Applied Physics* 2007, 102.
103. Halik, M.; Hirsch, A., The Potential of Molecular Self-Assembled Monolayers in Organic Electronic Devices. *Advanced Materials* 2011, 23, 2689-2695.

104. DiBenedetto, S.; Facchetti, A.; Ratner, M.; Marks, T., Molecular Self-Assembled Monolayers and Multilayers for Organic and Unconventional Inorganic Thin-Film Transistor Applications. *Advanced Materials* 2009, 21, 1407-1433.
105. LaFranzo, N. A.; Maurer, J. A., Arsonic Acid Self-Assembled Monolayers Protect Oxide Surfaces from Micronewton Nanomechanical Forces. *Advanced Functional Materials* 2012, n/a-n/a.
106. Compagnini, G.; Galati, C.; Pignataro, S., Distance dependence of surface enhanced Raman scattering probed by alkanethiol self-assembled monolayers. *Physical Chemistry Chemical Physics* 1999, 1, 2351-2353.
107. Geer, R. E.; Stenger, D. A.; Chen, M. S.; Calvert, J. M.; Shashidhar, R.; Jeong, Y. H.; Pershan, P. S., X-ray and Ellipsometric Studies of Self-Assembled Monolayers of Fluorinated Chlorosilanes. *Langmuir* 1994, 10, 1171-1176.
108. Folkers, J. P.; Laibinis, P. E.; Whitesides, G. M., Self-assembled monolayers of alkanethiols on gold: comparisons of monolayers containing mixtures of short- and long-chain constituents with methyl and hydroxymethyl terminal groups. *Langmuir* 1992, 8, 1330-1341.
109. Sastry, M., A note on the use of ellipsometry for studying the kinetics of formation of self-assembled monolayers. *Bulletin of Materials Science* 2000, 23, 159-163.
110. Offord, D. A.; John, C. M.; Griffin, J. H., Contact Angle Goniometry, Ellipsometry, XPS, and TOF-SIMS Analysis of Gold-Supported, Mixed Self-Assembled Monolayers Formed from Mixed Dialkyl Disulfides. *Langmuir* 1994, 10, 761-766.
111. Wolf, K. V.; Cole, D. A.; Bernasek, S. L., High-Resolution TOF-SIMS Study of Varying Chain Length Self-Assembled Monolayer Surfaces. *Analytical Chemistry* 2002, 74, 5009-5016.
112. Ding, S.; Chang, B.; Wu, C.; Lai, M.; Chang, H., Impedance spectral studies of self-assembly of alkanethiols with different chain lengths using different immobilization strategies on Au electrodes. *Analytica Chimica Acta* 2005, 554, 43-51.
113. Berchmans, S.; Nirmal, R.; Prabaharan, G.; Mishra, A.; Yegnaraman, V., Solution phase electron transfer versus bridge mediated electron transfer across carboxylic acid terminated thiols. *Journal of Solid State Electrochemistry* 2006, 10, 439-446.
114. Walczak, M.; Popenoe, D.; Deinhammer, R.; Lamp, B.; Chung, C.; Porter, M., Reductive Desorption of Alkanethiolate Monolayers at Gold-A Measure of Surface Coverage. *Langmuir* 1991, 7, 2687-2693.
115. Laszlo, J.; Evans, K., Influence of self-assembled monolayer surface chemistry on Candida antarctica lipase B adsorption and specific activity. *Journal of Molecular Catalysis B-Enzymatic* 2007, 48, 84-89.
116. Stalder, A.; Kulik, G.; Sage, D.; Barbieri, L.; Hoffmann, P., A snake-based approach to accurate determination of both contact points and contact angles. *Colloids and Surfaces a-Physicochemical and Engineering Aspects* 2006, 286, 92-103.
117. Lamour, G.; Hamraoui, A.; Buvailo, A.; Xing, Y.; Keuleyan, S.; Prakash, V.; Eftekhari-Bafrooei, A.; Borguet, E., Contact Angle Measurements Using a Simplified Experimental Setup. *Journal of Chemical Education* 2010, 87, 1403-1407.
118. Hynes, M. J.; Maurer, J. A., Photoinduced monolayer patterning for the creation of complex protein patterns. *Langmuir* 2012, 28, 16237-42.

119. Hynes, M. J.; Maurer, J. A., Unmasking photolithography: a versatile way to site-selectively pattern gold substrates. *Angew Chem Int Ed Engl* 2012, 51, 2151-4.
120. Frey, B. L.; Corn, R. M., Covalent Attachment and Derivatization of Poly(l-lysine) Monolayers on Gold Surfaces As Characterized by Polarization−Modulation FT-IR Spectroscopy. *Analytical Chemistry* 1996, 68, 3187-3193.
121. Snyder, R. G.; Schachtschneider, J. H., Vibrational analysis of the n-paraffins—I: Assignments of infrared bands in the spectra of C3H8 through n-C19H40. *Spectrochimica Acta* 1963, 19, 85-116.
122. Adhesion Measurement of Thin Films, Thick Films, and Bulk Coatings. In *Adhesion Measurement of Thin Films, Thick Films, and Bulk Coatings*, Mittal, K. L., Ed. American Society for Testing and Materials: 1978.
123. Fukuzawa, S.; Asanuma, M.; Tachibana, K.; Hirota, H., Combination of Mixed Self-Assembled Monolayer and Matrix-Assisted Laser Desorption/Ionization Mass Spectrometry, a Simple Tip-Based Screening Method for Proteomics. *Journal of Mass Spectrometry Society of Japan* 2006, 54, 187-193.
124. Sauerbrey, G., Verwendung von Schwingquarzen zur Wägung dünner Schichten und zur Mikrowägung. *Zeitschrift für Physik* 1959, 155, 206-222.
125. Hayashi, T.; Tanaka, Y.; Koide, Y.; Tanakac, M.; Hara, M., Mechanism underlying bioinertness of self-assembled monolayers of oligo(ethyleneglycol)-terminated alkanethiols on gold: protein adsorption, platelet adhesion, and surface forces. *Physical Chemistry Chemical Physics* 2012, 14, 10196-10206.
126. Menz, B.; Knerr, R.; Gopferich, A.; Steinem, C., Impedance and QCM analysis of the protein resistance of self-assembled PEGylated alkanethiol layers on gold. *Biomaterials* 2005, 26, 4237-4243.
127. Steiner, G., Surface plasmon resonance imaging. *Analytical and Bioanalytical Chemistry* 2004, 379, 328-331.
128. Linman, M.; Abbas, A.; Cheng, Q., Interface design and multiplexed analysis with surface plasmon resonance (SPR) spectroscopy and SPR imaging. *Analyst* 2010, 135, 2759-2767.
129. Rothenhausler, B.; Knoll, W., Surface-Plasmon Microscopy. *Nature* 1988, 332, 615-617.
130. Nonnenmacher, M.; Oboyle, M.; Wickramasinghe, H., Kelvin Probe Force Microscopy. *Applied Physics Letters* 1991, 58, 2921-2923.
131. Saito, N.; Hayashi, K.; Sugimura, H.; Takai, O.; Nakagiri, N., Surface potentials of patterned organosilane self-assembled monolayers acquired by Kelvin probe force microscopy and ab initio molecular calculation. *Chemical Physics Letters* 2001, 349, 172-177.
132. Krok, F.; Sajewicz, K.; Konior, J.; Goryl, M.; Piatkowski, P.; Szymonski, M., Lateral resolution and potential sensitivity in Kelvin probe force microscopy: Towards understanding of the sub-nanometer resolution. *Physical Review B* 2008, 77.
133. Houston, J.; Kim, H., Adhesion, friction, and mechanical properties of functionalized alkanethiol self-assembled monolayers. *Accounts of Chemical Research* 2002, 35, 547-553.
134. Ivanova, E.; Truong, V.; Webb, H.; Baulin, V.; Wang, J.; Mohammodi, N.; Wang, F.; Fluke, C.; Crawford, R., Differential attraction and repulsion of Staphylococcus

aureus and Pseudomonas aeruginosa on molecularly smooth titanium films. *Scientific Reports* 2011, 1.
135. Miller, J.; Veeramasuneni, S.; Drelich, J.; Yalamanchili, M.; Yamauchi, G., Effect of roughness as determined by atomic force microscopy on the wetting properties of PTFE thin films. *Polymer Engineering and Science* 1996, 36, 1849-1855.
136. Chockalingam, M.; Darwish, N.; Le Saux, G.; Gooding, J., Importance of the Indium Tin Oxide Substrate on the Quality of Self-Assembled Monolayers Formed from Organophosphonic Acids. *Langmuir* 2011, 2545-2552.
137. Jandt, K., Atomic force microscopy of biomaterials surfaces and interfaces. *Surface Science* 2001, 491, 303-332.
138. Butt, H.; Seifert, K.; Bamberg E., Imaging Molecular Defects in Alkanethiol Monolayers with an Atomic-Force Microscope. *Journal of Physical Chemistry* 1993, 97, 7316-7320.
139. Xu, S.; Laibinis, P.; Liu, G., Accelerating the kinetics of thiol self-assembly on gold - A spatial confinement effect. *Journal of the American Chemical Society* 1998, 120, 9356-9361.
140. McDermott, C.; McDermott, M.; Green, J.; Porter, M., Structural Origins of the Surface Depressions at Alkanethioloate Monolayers on Au(111) - a Scanning Tunneling and Atomic Force Micrscopy Investigation. *Journal of Physical Chemistry* 1995, 99, 13257-13267.
141. Delamarche, E.; Michel, B.; Biebuyck, H.; Gerber, C., Golden interfaces: The surface of self-assembled monolayers. *Advanced Materials* 1996, 8, 719-&.
142. Yan, Y.; Sun, T.; Pan, B.; Zhao, J.; Dong, S., Controlled monolayer self-assembly process based on the atomic force microscopy nanoscratching method. *Journal of Vacuum Science & Technology B* 2009, 27, 1247-1250.
143. Tan, J.; Tien, J.; Chen, C., Microcontact printing of proteins on mixed self-assembled monolayers. *Langmuir* 2002, 18, 519-523.

CHAPTER TWO

HEXADECYLARSONIC ACID MONOLAYERS PROTECT SUBSTRATES FROM MICRONEWTON NANOMECHANICAL FORCES

2.1. Introduction

Microelectromechanical (MEMS) and nanoelectromechanical (NEMS) systems have been established as central to the development of new technologies, particularly in the areas of semiconductors and sensing devices.[1] As with any mechanical system, combating the negative effects of friction and adhesion between contact points is imperative. Prevention of wear, as well as provision of long-term lubrication, are important for increasing device lifetime. However, these systems cannot make use of conventional mineral, vegetable or synthetic oil lubricants owing to the nanometer-scale mechanical contacts of the devices, and the large film thickness of these lubricants. As a result, new strategies must be developed for device protection that are applicable to large-scale manufacturing of MEMS and NEMS devices. Self-assembled monolayers (SAMs) have been utilized extensively to tailor the surface properties of the substrates to which they are bonded, and have previously been explored as potential coatings for transistors and sensors, as well as lubricants for MEMS and NEMS devices.[2-9]

SAMs formed from alkanethiols on gold surfaces are well-studied and used in a variety of applications.[5, 10] However, this system requires that devices be coated with precious metals such as silver or gold, which are soft and conductive materials and are not amenable to mechanical or electronic applications. Phosphonate monolayers have been demonstrated to exhibit polydentate binding to metal oxides, but, their preparation is slow and special conditions are typically required to obtain complete substrate coverage. Methods for producing well-ordered phosphonate monolayers including aerosol coating, high-temperature annealing, T-BAG (tethering by aggregation and growth), and substrate pre-treating have been developed for stable, well-ordered monolayer formation.[11-18] Alternatively, trichlorosilane and triethoxysilane monomers react readily and quickly with a wide variety of substrates. However, these monomers can react with each other giving rise to cross-linking and leading to coating instability.[19, 20] This reduces the durability and utility of silane monolayers for device coatings. Furthermore, the high reactivity of trichlorosilanes with themselves and water, causes the synthesis, purification, and shelf-life of this class of monomers to be problematic.

To be useful in wide-spread commercial applications, a straight-forward coating methodology that generates robust, stable surface protection is necessary. We have chosen to exploit the chemical similarities between phosphorus and arsenic to demonstrate the first arsonic-acid-based self-assembled monolayer system. Prepared via a straightforward soaking method, arsonic acid monolayers are stable, non-toxic, and have some degree of ordering. Here, we show the formation of monolayers on titanium oxide, native silicon oxide, and borosilicate glass. The ability to form monolayers

directly on bare glass demonstrates the increased reactivity of the arsonate headgroup compared to the phosphonate headgroup, which is non-reactive towards glass. Using nanoscratching experiments, the surface coating was characterized as potential MEMS lubricants. The nanotribological properties of the hexadecylarsonic acid SAMs on glass, silicon, and titanium oxide substrates were compared to bare unfunctionalized substrates and hexadecylphosphonic acid functionalized substrates prepared under the same conditions (Figure 2.1.).

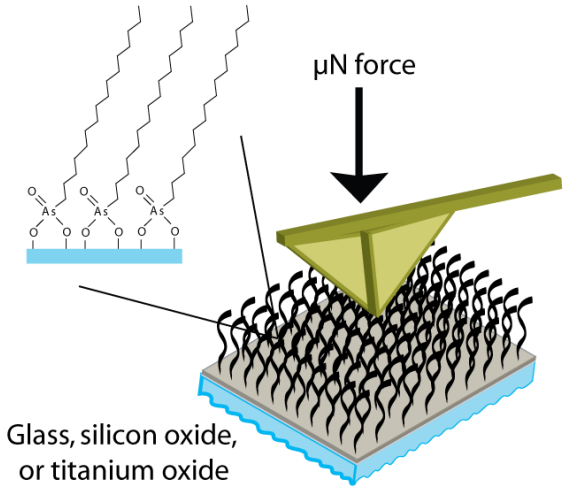

Figure 2.1. Hexadecylarsonic acid monolayers are assembled onto glass, silicon oxide and titanium oxide substrates and evaluated as potential MEMS lubricants using an SPM-based nanoscratching method.

2.2. Results and Discussion

2.2.1. Synthesis and Surface Coating

Many methods to synthesize alkyl arsonic acids have been developed; however, early methods were tedious and resulted in a complex mixture of products that were difficult to purify. In 1883, Meyer reported the first synthesis using alkyl halides.[21] This method has become the backbone for modern synthetic methods.[22, 23] In 1968, McBrearty and

coworkers revisited this work and reported a modified synthetic route that mirrored the synthesis of arsinic acids, using a bis(diethylamin)chloroarsine (BDCA) intermediate.[24, 25] This method is capable of accommodating longer-chain alkyl moieties, up to twenty carbons, with higher purity and yields than previously reported. Since that time, little information on organoarsenic species with high aliphatic character such as these has been reported. Organoarsenic species such as monomethyl and dimethyl arsonic acid, which result from the metabolism of inorganic species, have garnered much attention owing to their toxic nature. However, it is generally regarded that organoarsenic species with large organic groups (either hydrocarbon chains, cyclic moieties, or other functional groups) are excreted from the body, and are, therefore, less-toxic or non-toxic.[26, 27] By simplifying the reaction described by McBrearty to a one-pot synthesis (Figure 2.2.), we streamlined the route to hexadecylarsonic acid. Furthermore, we found that, both in solution and as monolayers, hexadecylarsonic acid is not toxic to mammalian cells in culture.

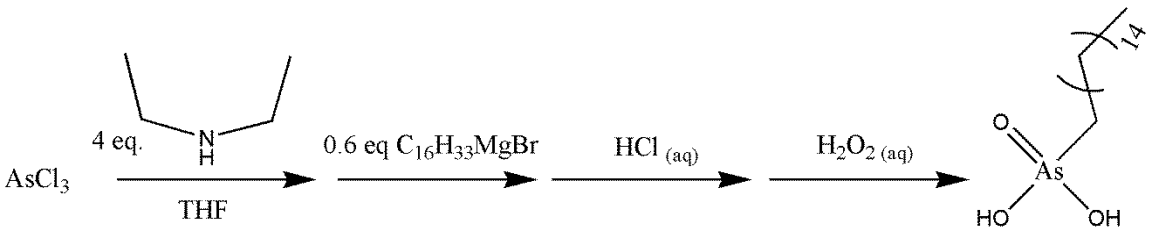

Figure 2.2. Scheme for 1-pot synthesis of hexadecylarsonic acid monomer.

Inspired by the use of phosphonates as coatings for a variety of oxide surfaces,[13, 15, 17, 28] we postulated that arsonic acid molecules would also have reactivity towards oxide substrates. Slow and limited reactivity is consistently described as a shortcoming of phosphonates, and limits their use as coatings for commercial applications. The chemical similarities between arsenic and phosphorus have been described previously,[29] and

periodic trends indicate that the arsonic acid headgroup should have higher reactivity. We observe an increased reactivity for hexadecylarsonic acid over hexadecylphosphonic acid that proves to be advantageous and allows for monolayers to be prepared by simpler methods, and on additional substrates.

To develop conditions for arsonate monolayer formation, we evaluated a variety of methods commonly used for phosphonate monolayer formation including T-BAG, slow evaporation, heated soaking, and thermal annealing. To screen these methods, water contact angles were measured following monolayer preparation. In our initial screen, the method that resulted in the highest water contact angle was the heated soaking method, and this method was further optimized as described below.

The simple soaking technique described in Figure 2.3. was chosen owing to ease and scalability, both of which are imperative for implementation in a commercial manufacturing process.

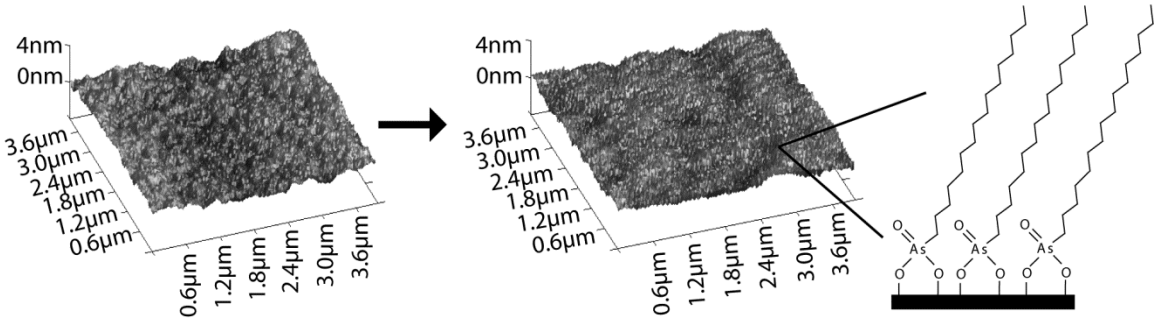

Figure 2.3. Borosilicate glass substrates are soaked in a 1 mM solution of hexadecylarsonic acid in tetrahydrofuran for 48 h at 40 ºC to achieve an arsonic acid self-assembled monolayer (SAM). Height images of functionalized substrates show decreased roughness when analyzed with a 40 nm diamond-tipped cantilever using tapping-mode scanning probe microscopy (SPM).

While the technique is time intensive, it does not require significant labor, hands-on processing, or specialized equipment. Furthermore, activated arsonate esters could potentially be employed to reduce the time required for monolayer setting. The substrates used for these experiments were cleaned and further oxidized by oxygen plasma. While this method does not provide a highly-uniform oxide layer, arsonate monolayers form on these substrates. Thus, these monolayers are highly versatile for surface functionalization.[30] As seen in Figure 2.3, the resulting surface after monolayer formation is uniform. There is no visible "islanding" present, indicating that the monolayer is formed homogenously on the surface. Markedly, the glass substrate as measured with a diamond-tipped cantilever (40 nm tip radius) using tapping mode atomic force microscopy (AFM), shows decreased roughness following SAM surface preparation (Figure 2.3). This change in surface roughness may be explained by a difference in nanomechanical properties between the clean, unfunctionalized substrate and the distinctly hydrophobic monolayer, which can affect the interaction of the tip with the surface. To confirm that the reaction of the molecule with the substrate is covalent and results in a well-defined SAM surface, we employed a variety of characterization methods.

2.2.2. Surface Characterization

2.2.2.1. Water Contact Angle

Measurement of water contact angle (CA) is one of the simplest methods for characterizing a surface functionalization that results in a change in hydrophobicity. As

demonstrated in Figure 2.4., the reaction of hexadecylarsonic acid with borosilicate glass, titanium oxide, and silicon oxide all result in water contact angles that, on average, are greater than 100°.

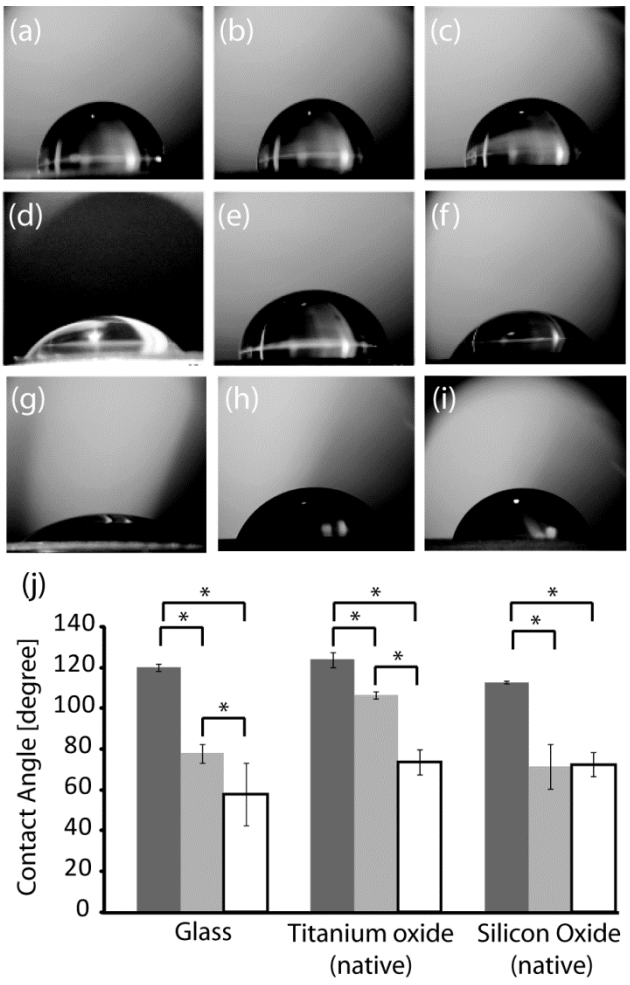

Figure 2.4. Representative images for water contact angle (CA) measurements for substrates functionalized with arsonic acid and phosphonic acid. Images are arsonate on (a) glass, (b) titanium oxide, and (c) silicon oxide; phosphonate on (d) glass, (e) titanium oxide, and (f) silicon oxide; and pentadecane on (g) glass, (h) titanium oxide, and (i) silicon oxide. Average values for each are summarized in (j). Arsonate monolayers are dark gray bars, phosphonate monolayers are light grey bars, and adsorbed pentadecane are white bars. Arsonic acid surfaces have CA values of greater than 100º for all substrates evaluated here, while only phosphonic acid on titanium oxide shows a comparable value. On glass and silicon oxide, the phosphonate surface more closely resembles physisorbed pentadecane. * indicates p value of less than 0.01, n = 6 for all measurements.

Alternatively, when identical conditions are used to react hexadecylphosphonic acid with these substrates, a water contact angle of greater than 100 ° is only seen on the titanium oxide substrate. This is not surprising, as phosphonates are known to assemble on titanium oxide, but have not been reported on glass.[13]

To evaluate the differences in CA between a covalently attached SAM and physically adsorbed molecules, arsonate and phosphonate reacted substrates were compared to substrates soaked in a 1 mM solution of pentadecane, which mirrors the hydrophobic nature of the monomers while lacking a surface reactive headgroup. When compared to these pentadecane-adsorbed substrates, the phosphonate substrates show similar CAs on both glass and silicon oxide. The plot in Figure 2.4. outlines these differences, and also exhibits that all three arsonic acid SAM substrates are visually and statistically different from pentadecane adsorbed on each.

2.2.2.2. Infrared Spectroscopy

FT-IR measurements of the arsonate-functionalized titanium oxide and glass substrates were obtained in grazing angle spectral reflectance mode and transmission mode, respectively. Figure 2.5. shows representative spectra for each of these samples, and data including errors is contained in Figure 2.6. For our analysis, we define "ordered" monolayers as having asymmetric methylene stretching frequencies below 2920 cm^{-1} and symmetric methylene stretching frequencies below 2850 cm^{-1}. These definitions are based on peak positions for crystalline alkane chains in the extended *trans* conformation.[31] For glass and titanium oxide, we observe that methylene stretching

frequencies for the arsonic acid monolayers are very close to those of ordered monolayers. On glass, the average asymmetric stretch is 2920 cm^{-1} and the average symmetric stretch is 2852 cm^{-1}. On titanium oxide, the average asymmetric stretch is 2921 cm^{-1} and the average symmetric stretch is 2852 cm^{-1}. The inability to form "ordered" monolayers based on the classical IR definition is likely due to the size of the arsenic atom in the headgroup of the monomer, which with an atomic radius of 115 pm is larger than the common headgroup atoms of phosphorus and silicon (100 and 110 pm, respectively).[32] This larger headgroup may not allow for tight packing of the monomers on the substrate, thereby introducing the slight disorder observed.

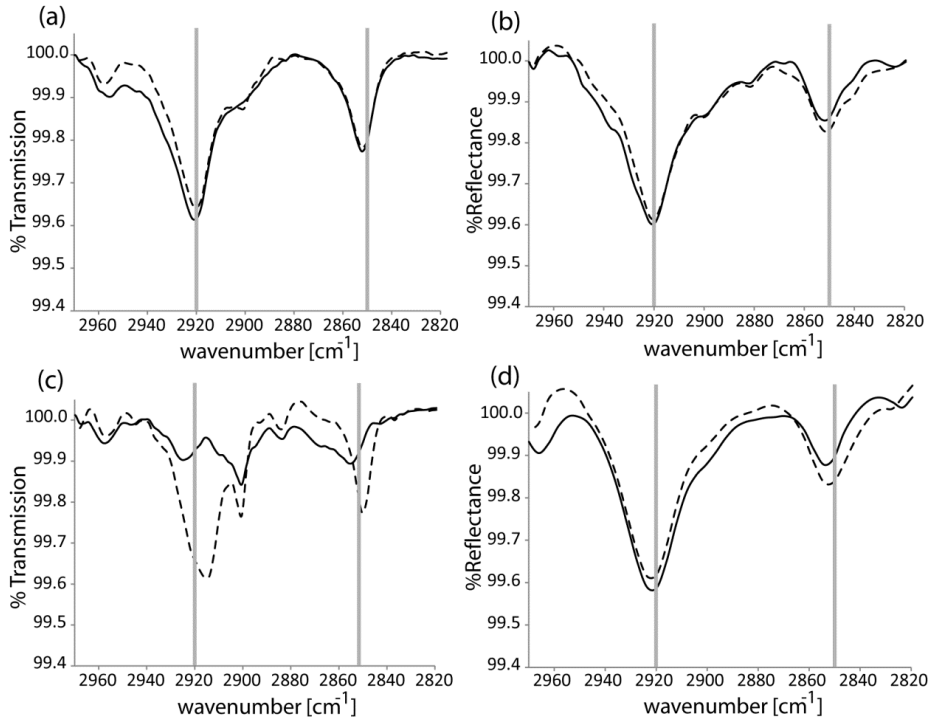

Figure 2.5. Covalent attachment of monolayers is evaluated using mechanical peel testing and infrared spectroscopy. Representative spectra are shown for (a) arsonic acid on glass substrate, (b) arsonic acid on titanium oxide substrate, (c) phosphonic acid on glass substrate, and (d) phosphonic acid on titanium oxide substrate before (dash) and after (solid) the peel test. Grey lines at 2920 and 2850 cm^{-1} indicate asymmetric and symmetric methylene stretches for "ordered" monolayers.

As demonstrated in Figure 2.5., this method also produces disordered phosphonate monolayers on titanium oxide substrates, with methylene stretching frequencies of 2921 cm^{-1} and 2852 cm^{-1}. This is in contrast to other methods that produce highly-ordered phosphonate monolayers. However, titanium oxide substrates prepared by electron beam deposition are rough on the nanometer scale, which may also affect monolayer order and packing. Phosphonate monolayers have not been reported to form on glass substrates, due to a lack of covalent attachment to the surface as we found and described below.

To ensure that the monomers were indeed covalently attached to the substrate, a mechanical peel test was performed.[13, 33] The representative FT-IR spectra for the substrates before (dashed lines) and after (solid lines) performing the peel test (Figure 2.5.) show no significant changes between the two spectra for the arsonic acid monolayers on either substrate or for the phosphonate monolayer on titanium oxide. This indicates that, on these substrates, a covalent linkage between the monomers and the substrates has been formed. Furthermore, because the intensity does not decrease, the surfaces are likely monolayers and not multilayers. The stark differences in peak positions before and after the peel test for the phosphonate monolayer on glass, as well as the significant decrease in transmission, indicates that the majority of the phosphonate on glass is physisorbed and not covalently attached to the substrate. This is not surprising, as phosphonates are generally regarded as being unreactive towards borosilicate glass.

(a)

		CH_2-asymmetry		CH_2-symmetric	
		Position, cm^{-1}	Intensity, %	Position, cm^{-1}	Intensity, %
Sample 1	Before	2921	99.61	2852	99.74
	After	2921	99.67	2852	99.82
Sample 2	Before	2920	99.62	2852	99.78
	After	2920	99.49	2852	99.65
Sample 3	Before	2919	99.55	2851	99.73
	After	2918	99.62	2850	99.81
Average	Before	2920 (0.5)	99.59 (0.02)	2852 (0.3)	99.75 (0.02)
	After	2920 (0.9)	99.59 (0.05)	2851 (0.7)	99.76 (0.06)

(b)

		CH_2-asymmetry		CH_2-symmetric	
		Position, cm^{-1}	Intensity, %	Position, cm^{-1}	Intensity, %
Sample 1	Before	2920	99.62	2851	99.83
	After	2920	99.59	2851	99.82
Sample 2	Before	2921	99.75	2852	99.81
	After	2921	99.47	2853	99.44
Sample 3	Before	2921	99.67	2852	99.80
	After	2921	99.54	2853	99.68
Average	Before	2921 (0.3)	99.68 (0.04)	2852 (0.3)	99.81 (0.01)
	After	2921 (0.3)	99.53 (0.03)	2852 (0.7)	99.64 (0.11)

Figure 2.6. FT-IR analysis of arsonic acid monolayers using the Scotch Tape Peel Test. Monolayers were evaluated by (a) transmission on glass substrates and (b) grazing angle reflectance on titanium oxide substrates. These measurements demonstrate that peak position and intensity do not change significantly following the adhesion test for both substrates evaluated, indicating covalent attachment of the monolayer to the substrate.

2.2.2.3. Mass Spectrometry

Matrix-assisted laser desorption/ionization mass spectrometry (MALDI-MS) was previously been utilized to confirm or identify monolayers assembled on a substrate.[34, 35] However, the hydrophobic nature of the arsonic acid substrate is not amenable to consistent, crystalline matrix application for this analysis. Furthermore, the molecular weight of the alkylarsonic acid is in the same mass range as typical MALDI matrices.

Despite these difficulties, MALDI-MS spectra of the arsonate monolayer formed on glass show ions for the [M + H^+] and [M + Na^+] species as shown in Figure 2.7.

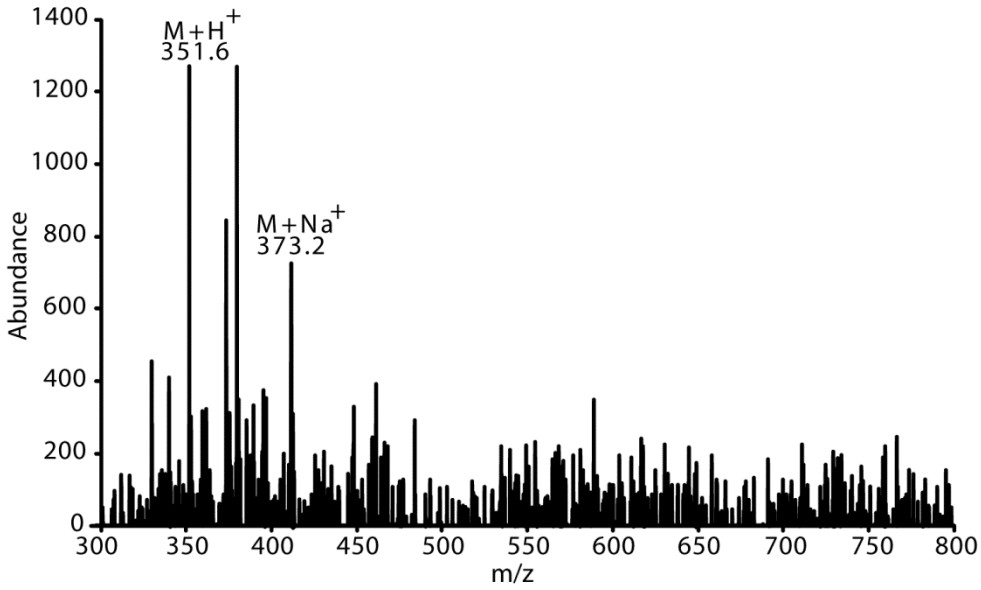

Figure 2.7. MALDI-MS for hexadecylarsonic acid on borosilicate glass.

2.2.3. Nanoscratching

To examine the tribological properties of modified substrates, we utilized a scanning probe microscopy (SPM) based nanoscratching approach. A diamond-tipped cantilever with a nominal tip radius of 40 nm was used to scratch the surface of the substrate at defined forces. Following this wear simulation, the same probe was used to image the scratches on the surface in tapping mode, allowing for measurement of the wear scars. Forces from 22 μN up to 105 μN were evaluated for all substrates.

SPM images and tabulated data of these experiments on all surfaces are provided in Figure 2.8. – Figure 2.20. below.

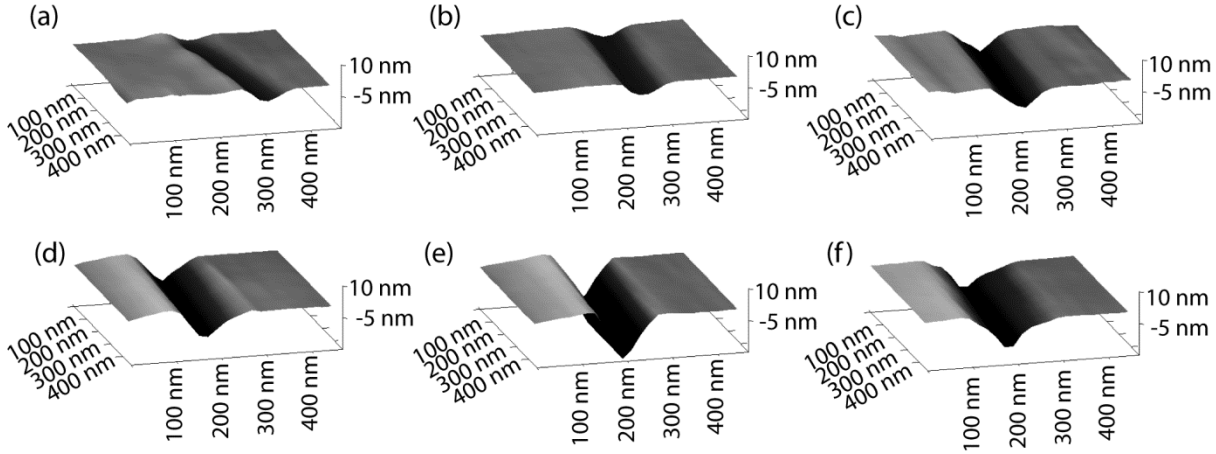

Figure 2.8. Representative wear scars on plasma-cleaned borosilicate glass nanoscratched at forces of: (a) 22 μN, (b) 35 μN, (c) 53 μN, (d) 70 μN, (e) 88 μN, and (f) 105 μN.

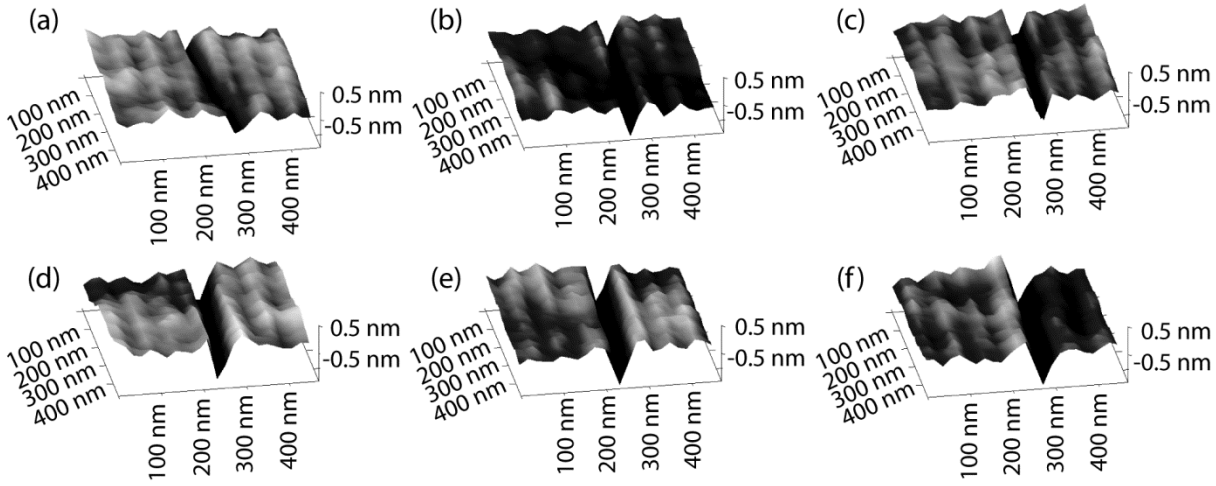

Figure 2.9. Representative wear scars on plasma-cleaned borosilicate glass functionalized with hexadecylphosphonic acid and nanoscratched at forces of: (a) 22 μN, (b) 35 μN, (c) 53 μN, (d) 70 μN, (e) 88 μN, and (f) 105 μN.

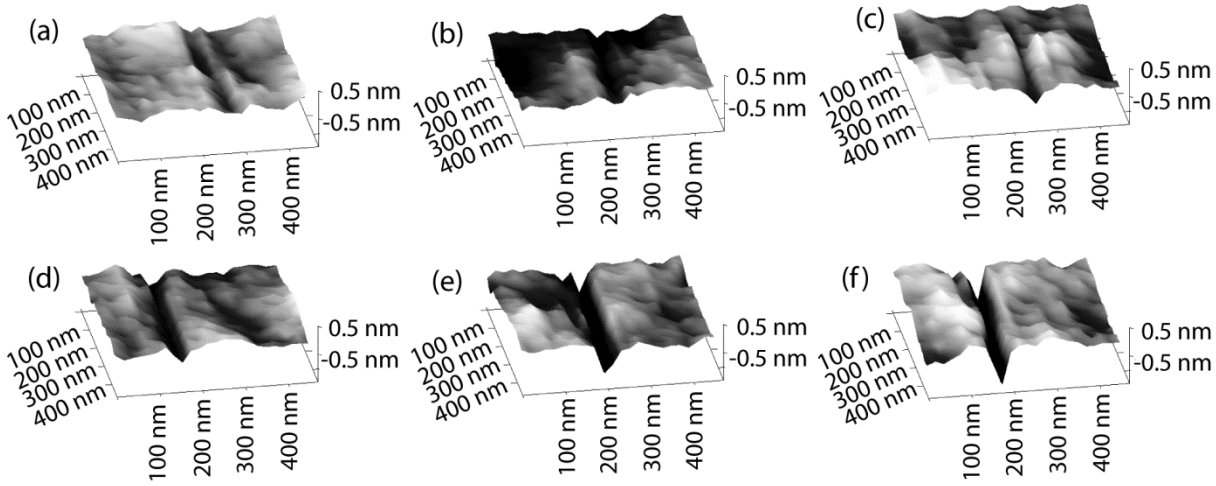

Figure 2.10. Representative wear scars on plasma-cleaned borosilicate glass functionalized with hexadecylarsonic acid and nanoscratched at forces of: (a) 22 μN, (b) 35 μN, (c) 53 μN, (d) 70 μN, (e) 88 μN, and (f) 105 μN.

(a)

Sample	#	Force, μ N	Depth, nm	Standard Deviation
Clean	1-1	22	4.2	1.0
		35	5.1	0.3
		53	8.5	1.4
		70	9.5	1.1
		88	19.3	1.5
		105	10.4	1.9
	1-2	22	3.3	0.8
		35	5.1	0.7
		53	16.9	6.0
		70	17.9	1.9
		88	27.5	2.7
		105	20.7	2.0
	2-1	22	2.7	0.4
		35	3.6	1.5
		53	4.0	0.2
		70	10.8	0.6
		88	13.1	0.7
		105	15.5	0.6
	2-2	22	4.9	0.8
		35	7.8	0.9
		53	9.3	1.6
		70	13.7	2.2
		88	20.4	1.7
		105	20.1	2.2

Figure 2.11. (a) Raw nanoscratching data for unfunctionalized borosilicate glass.

(b)

Sample	#	Force μ N	Depth, nm	Standard Deviation
Phosphonate	1-1	22	0.7	0.2
		35	1.0	0.3
		53	1.0	0.2
		70	1.3	0.2
		88	1.5	0.3
		105	1.6	0.3
	1-2	22	0.6	0.1
		35	0.8	0.2
		53	1.0	0.3
		70	1.1	0.4
		88	1.4	0.4
		105	1.5	0.4
	2-1	22	0.8	0.3
		35	1.1	0.3
		53	1.4	0.3
		70	1.5	0.3
		88	1.7	0.1
		105	2.1	0.3
	2-2	22	1.1	0.2
		35	1.4	0.2
		53	1.4	0.3
		70	1.5	0.2
		88	1.8	0.2
		105	2.0	0.4

Figure 2.11. (b) Raw nanoscratching data for borosilicate glass functionalized with hexadecylphosphonic acid.

(c)

Sample	#	Force, μ N	Depth, nm	Standard Deviation
Arsonate	1-2	22	0.5	0.1
		35	0.4	0.1
		53	0.4	0.2
		70	0.7	0.3
		88	0.9	0.2
		105	1.1	0.2
	1-3	22	0.4	0.1
		35	0.5	0.2
		53	0.7	0.1
		70	0.6	0.2
		88	0.8	0.2
		105	1.0	0.2
	2-1	22	0.6	0.2
		35	0.7	0.2
		53	0.8	0.2
		70	0.6	0.2
		88	1.2	0.2
		105	1.2	0.3
	2-3	22	0.0	0.0
		35	0.4	0.1
		53	0.4	0.1
		70	0.5	0.2
		88	0.7	0.2
		105	0.9	0.1

Figure 2.11. (c) Raw nanoscratching data for borosilicate glass functionalized with hexadecylarsonic acid.

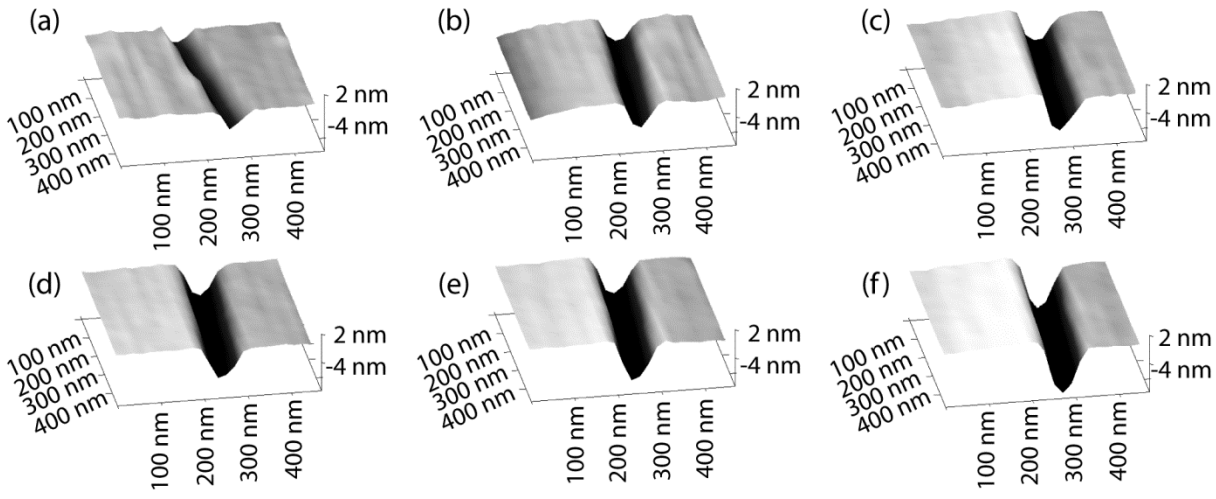

Figure 2.12. Representative wear scars on plasma-cleaned silicon oxide nanoscratched at forces of: (a) 22 μN, (b) 35 μN, (c) 53 μN, (d) 70 μN, (e) 88 μN, and (f) 105 μN.

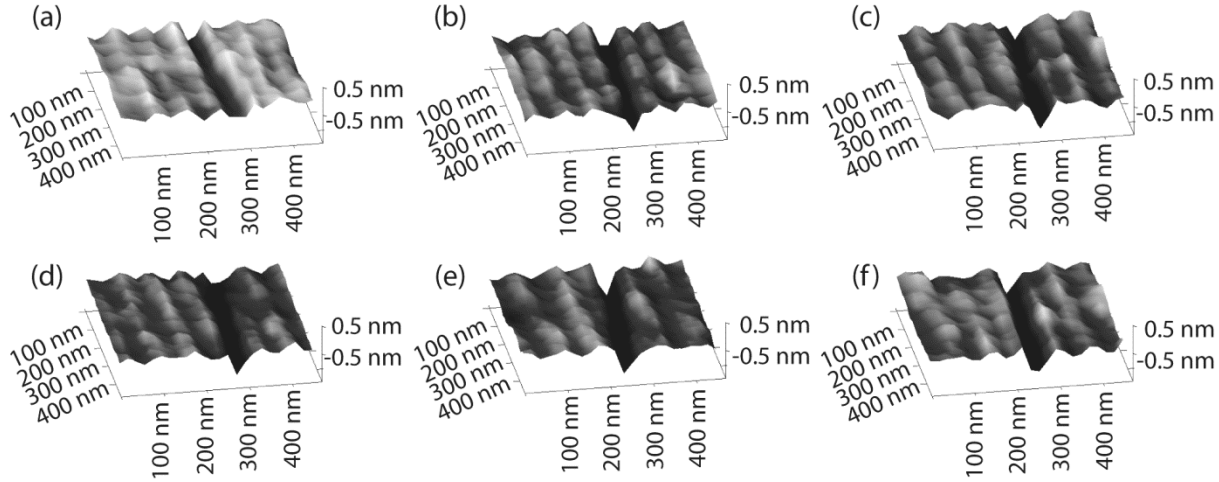

Figure 2.13. Representative wear scars on plasma-cleaned silicon oxide functionalized with hexadecylphosphonic acid and nanoscratched at forces of: (a) 22 μN, (b) 35 μN, (c) 53 μN, (d) 70 μN, (e) 88 μN, and (f) 105 μN.

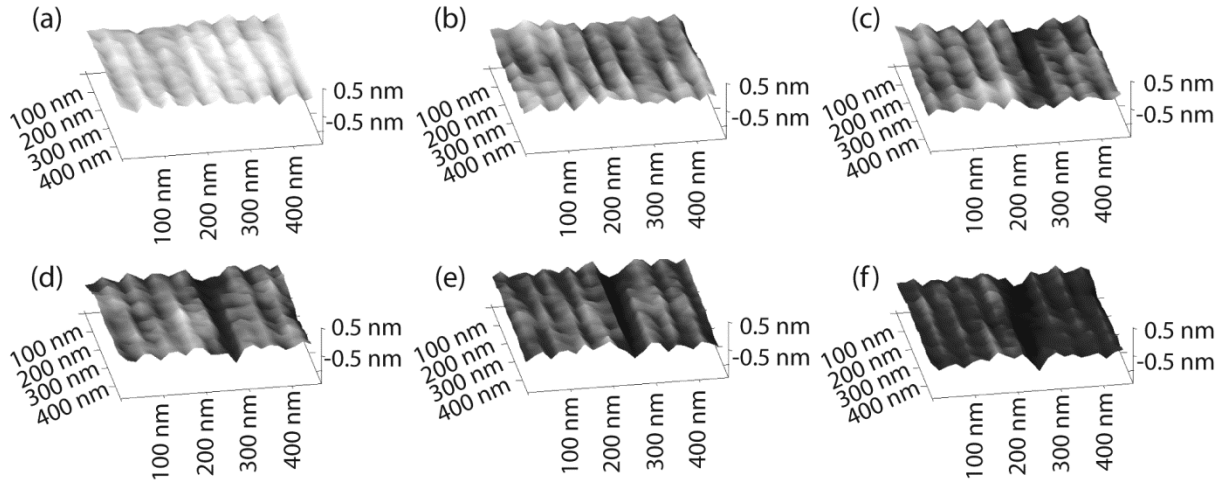

Figure 2.14. Representative wear scars on plasma-cleaned silicon oxide functionalized with hexadecylarsonic acid and nanoscratched at forces of: (a) 22 μN, (b) 35 μN, (c) 53 μN, (d) 70 μN, (e) 88 μN, and (f) 105 μN.

(a)

Sample	#	Force, μ N	Depth, nm	Standard Deviation
Clean	1-1	22	3.1	0.4
		35	4.4	0.5
		53	5.8	0.8
		70	6.1	0.3
		88	6.9	0.3
		105	8.8	0.3
	1-2	22	0.4	0.3
		35	1.5	0.2
		53	2.2	0.2
		70	4.0	0.8
		88	5.0	0.6
		105	4.0	0.3
	2-1	22	4.8	0.2
		35	4.7	0.3
		53	4.3	0.3
		70	6.1	0.4
		88	4.4	0.2
		105	3.9	0.5
	2-2	22	2.0	0.2
		35	3.1	0.5
		53	2.3	0.2
		70	3.5	0.3
		88	4.2	0.3
		105	3.2	0.2

Figure 2.15. (a) Raw nanoscratching data for unfunctionalized silicon oxide.

(b)

Sample	#	Force, μ N	Depth, nm	Standard Deviation
Phosphonate	1-1	22	0.5	0.2
		35	0.6	0.1
		53	0.7	0.2
		70	0.9	0.1
		88	1.0	0.2
		105	0.8	0.2
	1-2	22	0.6	0.1
		35	0.8	0.1
		53	0.8	0.1
		70	0.8	0.1
		88	1.0	0.1
		105	1.0	0.1
	2-1	22	0.9	0.2
		35	0.9	0.1
		53	0.9	0.1
		70	1.0	0.1
		88	1.2	0.2
		105	1.2	0.3
	2-2	22	0.8	0.1
		35	0.8	0.1
		53	0.9	0.2
		70	0.9	0.1
		88	1.1	0.2
		105	1.1	0.2

Figure 2.15. (b) Raw nanoscratching data for silicon oxide functionalized with hexadecylphosphonic acid.

(c)

Sample	#	Force, μ N	Depth, nm	Standard Deviation
Arsonate	1-2	22	0.8	0.2
		35	0.6	0.2
		53	0.9	0.2
		70	1.1	0.3
		88	0.9	0.2
		105	1.5	0.3
	1-3	22	0.0	0.0
		35	0.0	0.0
		53	0.4	0.1
		70	0.4	0.1
		88	0.6	0.1
		105	0.5	0.1
	2-1	22	0.0	0.0
		35	0.0	0.0
		53	0.7	0.2
		70	0.3	0.1
		88	1.0	0.4
		105	1.7	0.2
	2-2	22	0.6	0.1
		35	0.7	0.2
		53	0.8	0.2
		70	0.9	0.3
		88	0.9	0.2
		105	1.0	0.2

Figure 2.15. (c) Raw nanoscratching data for silicon oxide functionalized with hexadecylarsonic acid.

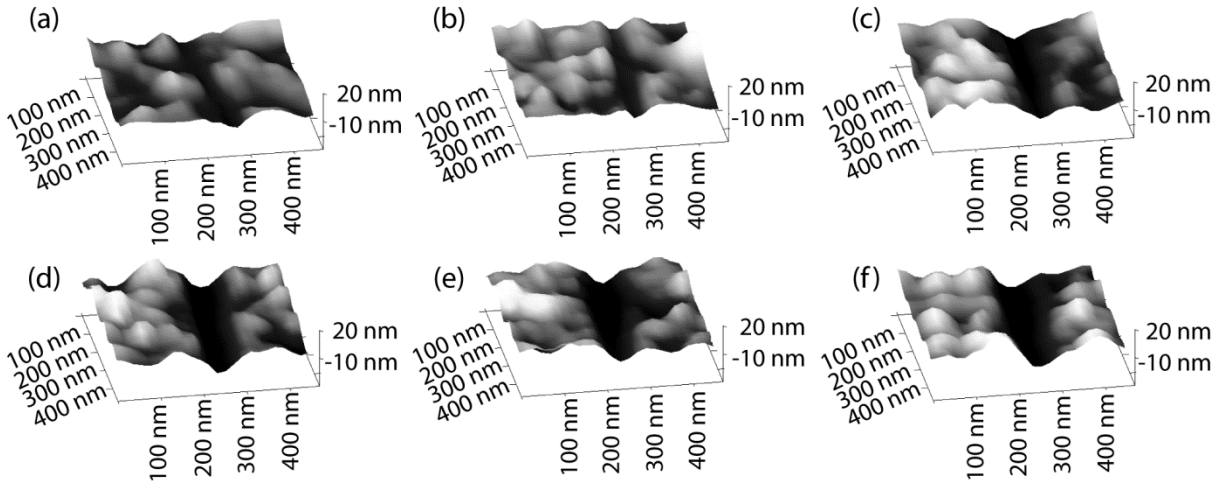

Figure 2.16. Representative wear scars on plasma-cleaned titanium oxide nanoscratched at forces of: (a) 22 μN, (b) 35 μN, (c) 53 μN, (d) 70 μN, (e) 88 μN, and (f) 105 μN.

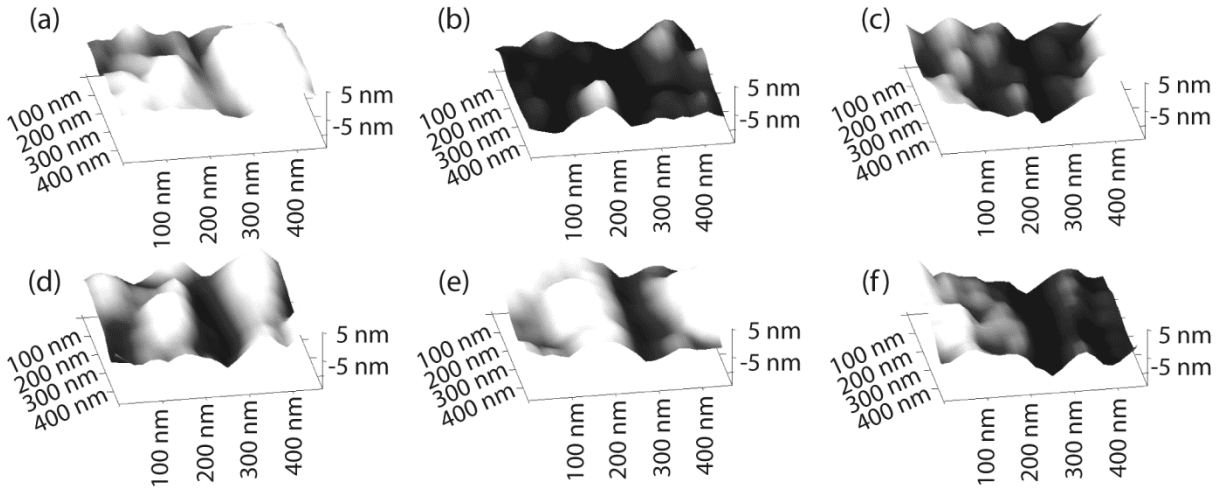

Figure 2.17. Representative wear scars on plasma-cleaned titanium oxide functionalized with hexadecylphosphonic acid and nanoscratched at forces of: (a) 22 μN, (b) 35 μN, (c) 53 μN, (d) 70 μN, (e) 88 μN, and (f) 105 μN.

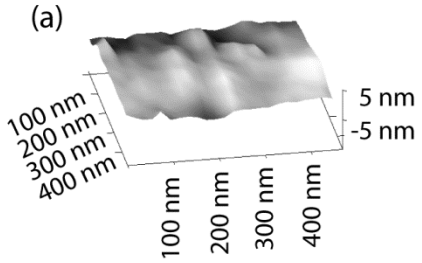

Figure 2.18. Representative wear scar on plasma-cleaned titanium oxide functionalized with hexadecylarsonic acid are not visible when nanoscratched at forces of: 22 μN, 35 μN, 53 μN, 70 μN, 88 μN, or 105 μN. Image (a) above is a representative image of the surface after scratching.

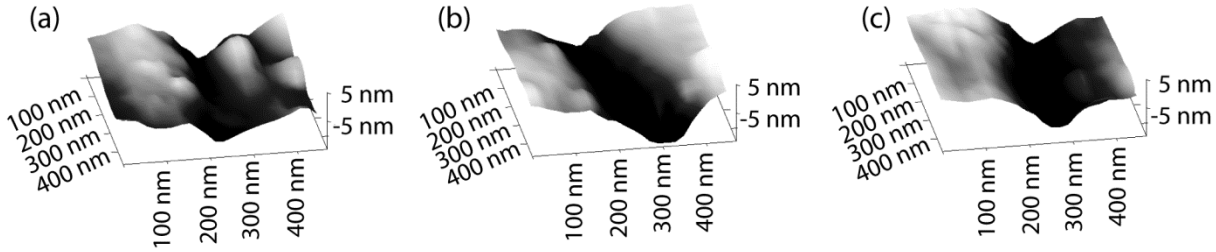

Figure 2.19. Representative wear scars on plasma-cleaned titanium oxide functionalized with hexadecylarsonic acid and nanoscratched at forces of: (a) 158 μN, (b) 175 μN, and (c) 263 μN.

(a)

Sample	#	Force, μ N	Depth, nm	Standard Deviation
Clean	1-1	22	11.6	2.7
		35	9.7	2.1
		53	11.9	1.8
		70	16.7	2.1
		88	16.6	4.0
		105	17.7	1.9
	1-2	22	11.3	1.7
		35	11.4	2.1
		53	12.5	1.4
		70	9.8	1.5
		88	10.7	2.5
		105	13.7	1.2
	2-1	22	9.5	2.2
		35	9.2	2.7
		53	9.0	2.1
		70	10.4	3.4
		88	10.7	2.9
		105	11.2	3.7
	2-2	22	10.0	1.2
		35	10.2	2.3
		53	11.1	2.1
		70	10.5	0.6
		88	13.8	1.4
		105	14.6	2.3

Figure 2.20. (a) Raw nanoscratching data for unfunctionalized titanium oxide.

(b)

Sample	#	Force, μ N	Depth, nm	Standard Deviation
Phosphonate	1-1	22	0.0	0.0
		35	0.0	0.0
		53	0.0	0.0
		70	7.0	1.4
		88	6.4	1.2
		105	7.6	1.2
	1-2	22	4.4	1.2
		35	3.8	1.4
		53	4.8	1.5
		70	6.0	1.3
		88	6.5	0.7
		105	6.3	2.0
	2-1	22	0.0	0.0
		35	0.0	0.0
		53	4.7	2.0
		70	5.9	1.4
		88	5.4	1.7
		105	6.0	1.2
	2-2	22	6.0	1.1
		35	6.0	2.0
		53	6.0	1.7
		70	7.4	1.5
		88	7.1	1.5
		105	4.8	0.3

Figure 2.20. (b) Raw nanoscratching data for titanium oxide functionalized with hexadecylphosphonic acid.

(c)

Sample	#	Force, μ N	Depth, nm	Standard Deviation
Arsonate	1-1	22	0.0	0.0
		35	0.0	0.0
		53	0.0	0.0
		70	0.0	0.0
		88	0.0	0.0
		105	0.0	0.0
	1-2	22	0.0	0.0
		35	0.0	0.0
		53	0.0	0.0
		70	0.0	0.0
		88	0.0	0.0
		105	0.0	0.0
	2-1	22	0.0	0.0
		35	0.0	0.0
		53	0.0	0.0
		70	0.0	0.0
		88	0.0	0.0
		105	0.0	0.0
	2-2	22	0.0	0.0
		35	0.0	0.0
		53	0.0	0.0
		70	0.0	0.0
		88	0.0	0.0
		105	0.0	0.0
Sample	#	Force, μ N	Depth, nm	Standard Deviation
Arsonate Additional Scratches	1-4	140	0.0	0.0
		158	9.6	1.9
		176	10.3	2.5
		263	12.5	2.6
	2-3	140	8.7	1.6
		158	9.9	1.8
		176	11.7	2.3
		263	11.9	2.3

Figure 2.20. (c) Raw nanoscratching data for titanium oxide functionalized with hexadecylarsonic acid.

SPM images with 3-D renderings of wear scars resulting from application of 88 μN force to the tip during the nanoscratching are shown in Figure 2.21. Bare substrates cleaned by oxygen plasma are compared to those functionalized with hexadecylphosphonic acid and hexadecylarsonic acid. Wear scars on the arsonic acid functionalized substrates are the

smallest on all of the substrates. In fact, on titanium oxide there is no visible scarring at these forces.

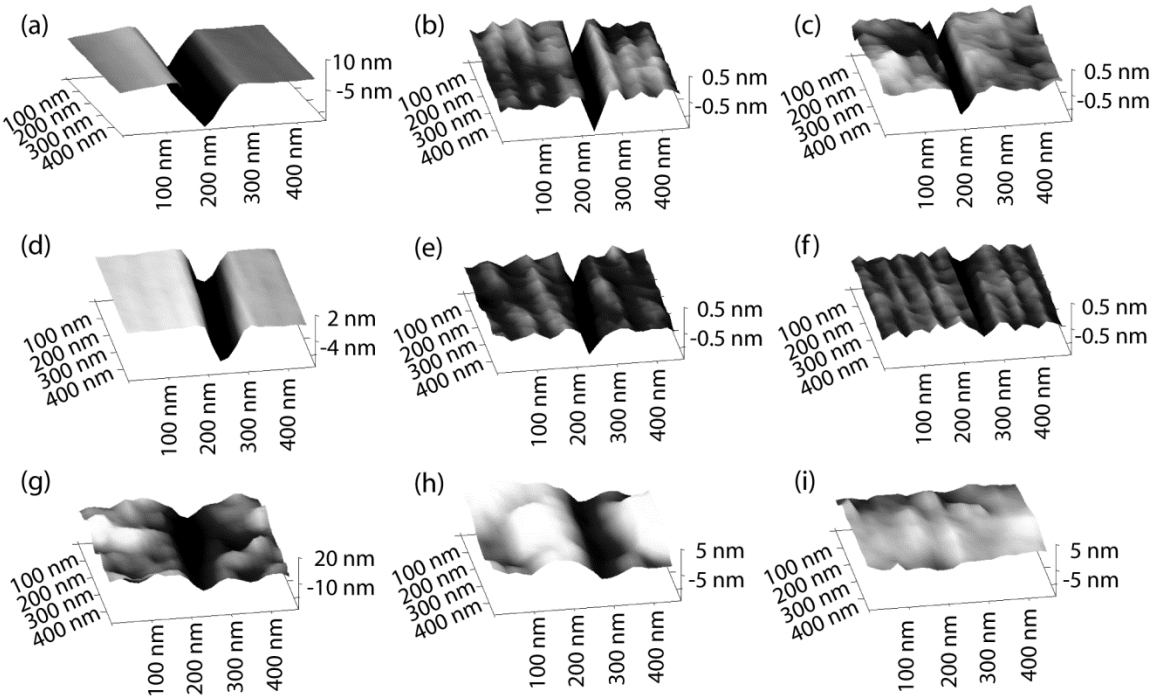

Figure 2.21. Nanoscratching experiments were used to compare the surface protection abilities of hexadecylarsonic acid to hexadecylphosphonic acid functionalized substrates prepared under identical conditions. The height scale for the images varies to accommodate the scratch depth for each sample. When scratched at a force of 88 μN, clear differences between the wear scars are seen. Images (a), (d), and (g) are representative of unfunctionalized borosilicate glass, silicon and titanium oxide substrates, respectively. Images (b), (e), and (h) show the same classes of substrates modified with hexadecylphosphonic acid, and images (c), (f) and (i) are of these substrates modified with hexadecylarsonic acid. Notably, no wear scar is visible on the titanium substrate functionalized with the arsonic acid monolayer (i), while on (g) and (h) these scars are clearly visible despite the increased roughness of the deposited metal oxide.

The depths of the wear scars/scratches resulting from these measurements were collected, and the "Percent Protection" was calculated by normalizing the depth of the wear scar on the functionalized substrates by the depth of the wear scar on the corresponding unfunctionalized substrate (Figure 2.22.).

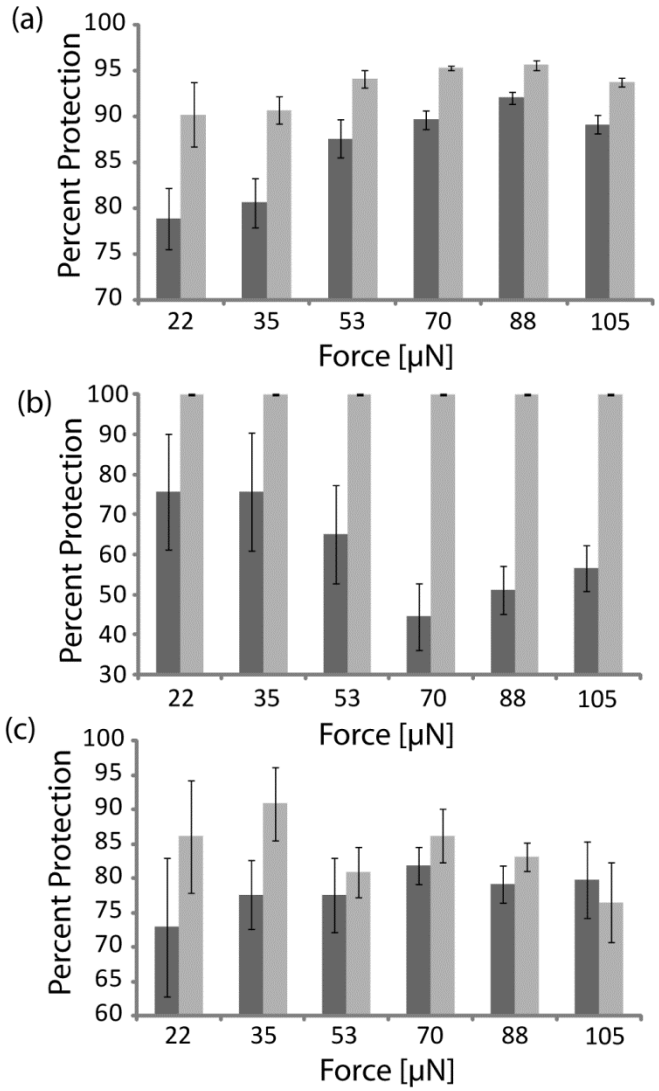

Figure 2.22. Normalized percent protection compares the wear scars of phosphonate (dark grey bars) and arsonate (light grey bars) functionalized substrates. On glass (a), at all forces, the arsonic acid monolayer protects the substrate from wear better than the phosphonic acid. For titanium oxide substrates (b), at the same forces, no wear scars are visible on the arsonic acid substrates, resulting in 100% protection. Finally, for silicon substrates (c), at lower forces the arsonic acid surface coating performs better than the phosphonic acid. All measurements are an average of ten measurements from four different scratches.

The arsonic acid monolayers outperform the phosphonic acid coating on both the glass and titanium substrates, showing a greater percent protection at all forces. On the silicon substrates, the trend is less visible. At lower force regimes (22 μN and 35 μN), the arsonic acid SAM appears to provide greater protection than the phosphonate coating. However, at higher forces, 53 μN -105 μN, the two coatings appear to perform similarly. This may indicate that the monolayer is not as stable on this substrate as on the other oxide surfaces, and the monolayer is removed or damaged under the mechanical stress of the scratch. The phosphonic acid and the arsonic acid coating provide significant surface protection over unfunctionalized silicon at these forces. On the titanium oxide surface, the arsonate SAM provides full protection against forces up to 105 μN, which is in stark contrast to the phosphonate monolayer, which only shows moderate protection with significant wear scars above 70 μN.

To further investigate the performance of the arsonic acid SAM on titanium oxide, additional nanoscratches at increased forces ranging from approximately 158 μN to 263 μN were carried out. The scratch depth data for these measurements are presented, along with the scratch depths observed for lower forces for the unfunctionalized substrate and the arsonate and phosphonate monolayers, in Figure 2.23. Within this greater force regime, wear scars were indeed visible on the substrate; however, the resulting depths are still less than those observed on the unfunctionalized substrate at lower forces. These experiments demonstrate that the arsonic acid SAM coating provides exceptional wear protection on titanium oxide substrates.

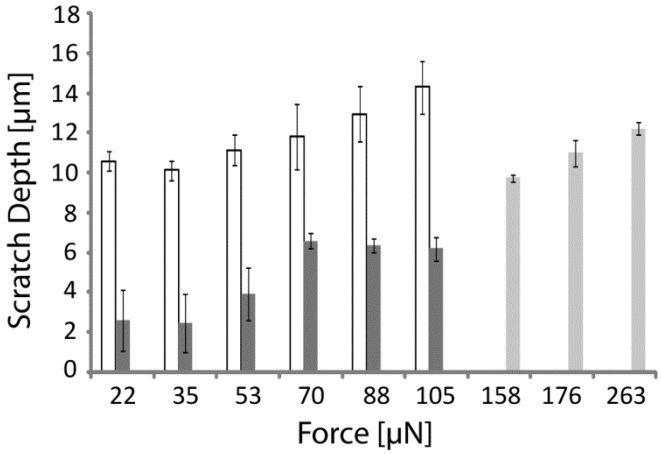

Figure 2.23. When additional force is applied during nanoscratching experiments on the hexadecylarsonic acid functionalized titanium oxide substrates, wear scars become visible. Unfunctionalized titanium oxide (white bars) are compared to phosphonate (dark grey bars) and arsonate (light grey bars) monolayers on titanium oxide. Arsonate data (light grey bars) from 22 µN to 105 µN is equal to zero, and is therefore not discernible on the graph. Notably, the scratch depths observed in the higher force regime are lower than those observed for unfunctionalized substrates (white bars) scratched at lower forces. Measurements are an average of ten measurements from four different scratches for all substrates from 22 µN to 105 µN, and 2 scratches for arsonate samples within high force regime (158 µN to 263 µN).

2.3. Conclusions

A one-pot synthesis of hexadecylarsonic acid and a simple method for the preparation of arsonate SAMs on multiple oxide surfaces has been achieved. The increased reactivity of arsonates over phosphonates allowed for the functionalization of ordinary glass substrates. A method for producing highly-ordered SAMs with this monomer has not been found; however, this may be possible with further optimization of the assembly method.

The arsonic acid monolayer provides surface protection against micronewton forces on a variety of substrates. As a wear-protection coating, the arsonate monolayer shows better performance on both titanium oxide and glass substrates compared to the corresponding

phosphonate analog. As mechanical properties are scale-dependent, the nanoscratching measurement utilized here is particularly relevant to the use of arsonate SAMs as coatings for MEMS devices, where the surface area of the device is large, but the volume is small.[36] The methodology described here is easy to implement and amenable to large-scale commercial applications for the functionalization of many oxide substrates, thus it has excellent potential for wear-protection applications within MEMS devices.

2.4. Materials and Methods

2.4.1. Materials and Instrumentation

Chemicals were obtained from the following manufacturers and used without further purification: diethyl amine, arsenic trichloride, 1-bromohexadecane, pentadecane and hexadecylphosphonic acid from Sigma-Aldrich; dry tetrahydrofuran (THF) from JT/Mallinckrodt Baker; Magnesium metal turnings from Fisher Sci.; hydrochloric acid (HCl), hydrogen peroxide, dimethylsulfoxide (DMSO) from VWR; diethyl ether from EMD Chemicals; ethanol (200 proof, absolute) from Pharmco-AAPER; 2,5-dihydroxybenzoic acid (DHB) from TCI America. All reactions were carried out under an argon atmosphere with dry solvents unless noted. Titanium metal and titanium dioxide were obtained from Kurt J. Lesker.

Borosilicate glass coverslips (25 mm, no. 1), were obtained from VWR, International; borosilicate glass slides from SPI Supplies; silicon wafers (2 in) from University Wafer. Substrates were treated with plasma oxidation before use with a Femto plasma oxidizer

(Diener Electronic). Titanium metal and titanium dioxide deposition was performed using a PVD-75 Electron-beam evaporator (Kurt J Lesker).

^{1}H NMR and ^{13}C NMR spectra were obtained on a 300 MHz Varian Innova instrument. Electrospray ionization mass spectrometry were obtained on a Thermo LCQ Deca Plus operating in positive mode (ThermoFisher Scientific). Melting point measurements were completed with an Electrothermal Manual Mel-Temp apparatus (Barnstead Thermolyne Corp.). FT-IR spectra were collected on a 670 Nicolet Fourier-Transform Infrared Spectrometer with Smart SAGA (spectral apetured grazing angle) reflectance accessory (Thermo Scientific). Matrix-assisted laser desorption/ionization mass spectrometry (MALDI-MS) of the monolayer substrate was obtained on a Voyager-DE STR spectrometer (Applied Biosystems) with 50 shots at an accelerator voltage of 20000 V and a grid voltage of 96.5 %, in positive, linear mode. Contact angle (CA) measurements were made at room temperature using a home-built apparatus consisting of a stage, microscope objective and digital camera. Images were taken with a digital camera and analyzed using the BIGDrop Analysis plugin for ImageJ with the Low Bond Axisymmetric Drop Shape Analysis model.[37] Nanoscratching measurements were obtained on a Multimode VIII scanning probe microscope (SPM) with NanoMan software package (Bruker).

2.4.2. Hexadecylarsonic acid monomer synthesis

Synthesis of 1-hexadecylarsonic acid was based on the method of McBrearty, et al.[25] with modification to a one-pot synthesis as described below. Diethyl amine (3.49 g, 4 eq)

was dissolved in THF (20 mL), cooled in a dry ice/acetone bath and arsenic trichloride (1 mL, 1 eq) was added dropwise. The ice bath was removed and reaction was allowed to proceed at room temperature for 3 hours. The resulting white precipitate was removed by filtration under argon. Unreacted diethyl amine and solvent were removed from the mixture by distillation at 90 °C. The remaining mixture was added dropwise at 0 °C to a Grignard reagent, prepared from 1-bromohexadecane (2.186 g, 0.6 eq) and magnesium metal turnings (175 mg, 0.6 eq) in THF (20 mL). The reaction was refluxed for 15 hours and then cooled to room temperature. HCl (4 N, 12 mL) was added dropwise and the mixture was refluxed for an additional 1.5 hours. An additional aliquot of HCl (4 N, 10 mL) was added to the flask, and the reaction mixture was extracted with diethyl ether (40 mL) and washed twice with water (20 mL). Hydrogen peroxide (35%, 5.5 mL) was added to the organic layer and the mixture was allowed to stir for 1 hour at room temperature. A white solid precipitated, was filtered and washed twice with ether. The solid was recrystallized from 80% ethanol (200 mL). Yield: 0.860 g (20.4%).

^{1}H NMR (300 MHz, $CDCl_3$ δ): 0.88 (t, 3H); 1.28 (m, 12H); 1.91 (m, 16H); and 2.32 (t, 2H). ^{13}C NMR (300 MHz, $CDCl_3$ δ): 32.15; 29.92; 29.84; 29.74; 29.71; 29.66; 29.64; 29.58; 29.55; 29.41; 29.30; 28.91 22.92; and 14.36. HRMS (ESI, *m/z*): [$M + H^+$] calculated for $C_{16}H_{36}O_3As$, 351.375, found 350.93. Melting point 122-126 ºC.

2.4.3. Surface Preparation

To prepare glass substrates for transmission FT-IR, CA and SPM analysis: borosilicate glass slides and coverslips were cleaned by oxygen plasma at 100% power for 10 minutes

on each side. The slides were subsequently rinsed with ethanol, deionized water, and ethanol, drying with nitrogen gas following each rinse. To prepare titanium substrates for reflectance FT-IR, CA and SPM measurements: borosilicate glass slides and coverslips were cleaned by oxygen plasma at 100% power for 20 minutes. The slides were subsequently rinsed with ethanol, deionized water, and ethanol, drying with nitrogen gas following each rinse. Titanium (5000 Å) and titanium dioxide (150 Å) were deposited using an electron beam evaporator at a rate of 0.1 Å/s followed by treatment with oxygen plasma at 100% power for 20 minutes. The slides were subsequently rinsed with ethanol, deionized water, and ethanol, drying with nitrogen gas following each rinse. To prepare silicon substrates for CA and SPM measurements: silicon wafers were cut to size and cleaned by oxygen plasma using plasma oxidation at 100% power for 20 min. The wafers were subsequently rinsed with ethanol, deionized water, and ethanol, drying with nitrogen gas following each rinse.

Substrates were immersed in a 1 mM solution of either hexadecylarsonic acid, hexadecylphosphonic acid or pentadecane in THF and warmed to 40 ºC in a jar vented with a small needle to minimize evaporation. Substrates were allowed to soak for 48 h, then rinsed twice with fresh THF for 30 seconds each, followed by a 1 hour soak in THF before rinsing twice with ethanol and drying with nitrogen gas. Substrates were stored dry prior to analysis.

2.4.4. Surface Characterization/Analysis

For contact angle measurements, samples were placed on the stage and a single drop of 18.1 MΩ water was placed on the sample. Drop images were collected and analyzed using the BIGDrop Analysis plugin. For each set of samples, two locations on three different substrates were averaged. Transmission and spectral reflectance infrared spectra and backgrounds were collected as single beam measurements at a resolution of 4 cm^{-1}. Spectra were processed to give percent transmission (%T) or percent reflectance (%R), and baseline corrected. MALDI-MS of monolayer substrates were obtained using DHB matrix dissolved in diethyl ether at 10 mg/mL. MALDI-MS (MALDI-TOF+, *m/z*): [M+H^+] calculated for $C_{16}H_{36}O_3As$, 351.4, found 351.6. (MALDI-TOF+, *m/z*): [M+Na^+] calculated for $C_{16}H_{36}O_3As$, 373.4, found 373.2. Mechanical stability of the monolayer was evaluated by the Scotch tape peel test as previously described by Gawalt, et al.[13]

2.4.5. Nanoscratching/mechanical wear testing

Experiments were performed at a temperature of 24-26 ºC and a relative humidity of 38-39 %. Nanoscratching experiments were executed using a diamond probe on a stainless steel cantilever (MDNISP-HS, nominal tip radius = 40 nm, spring constant = 419 N/m, deflection sensitivity = 419 nm/V, resonant frequency = 66 kHz, Bruker Probes). Scratches were made using NanoMan software in contact mode with a z distance of -20nm, z-velocity = 50 nm/s, xy-velocity = 1 μm/s with proportional and integral gains of 1.04 and 0.521, respectively. Substrates were scratched with the probe at forces of 21.95 μN, 35.11 μN, 52.67 μN, 70.22 μN, and 105 μN for approximately 5 μm. Surfaces were

immediately imaged using tapping mode with the same probe tuned to a drive frequency of 66 kHz. To analyze wear scars, 10 depth slices were analyzed within the same 2 μm region across all samples and scratches. Scratches not visible within the roughness of the sample were considered to have a depth of zero. Samples were scratched in two locations on each sample, and two samples were scratched for each experiment, except for the increased force measurements for arsonate on titanium oxide where two locations on one surface were analyzed.

2.5. References

1. Mahalik, N. P., Principle and applications of MEMS: a review. *International Journal of Manufacturing Technology and Management* 2008, 13, 324-342.
2. de Boer, M.; Mayer, T., Tribology of MEMS. *Mrs Bulletin* 2001, 26, 302-304.
3. Halik, M.; Klauk, H.; Zschieschang, U.; Schmid, G.; Dehm, C.; Schütz, M.; Maisch, S.; Effenberger, F.; Brunnbauer, M.; Stellacci, F., Low-voltage organic transistors with an amorphous molecular gate dielectric. *Nature* 2004, 431, 963-6.
4. Mottaghi, M.; Lang, P.; Rodriguez, F.; Rumyantseva, A.; Yassar, A.; Horowitz, G.; Lenfant, S.; Tondelier, D.; Vuillaume, D., Low-operating-voltage organic transistors made of bifunctional self-assembled monolayers. *Advanced Functional Materials* 2007, 17, 597-604.
5. Pranzetti, A.; Salaun, S.; Mieszkin, S.; Callow, M.; Callow, J.; Preece, J.; Mendes, P., Model Organic Surfaces to Probe Marine Bacterial Adhesion Kinetics by Surface Plasmon Resonance. *Advanced Functional Materials* 2012, 22, 3672-3681.
6. Tsukruk, V., Molecular lubricants and glues for micro- and nanodevices. *Advanced Materials* 2001, 13, 95-108.
7. Patton, S.; Eapen, K.; Zabinski, J.; Sanders, J.; Voevodin, A., Lubrication of microelectromechanical systems radio frequency switch contacts using self-assembled monolayers. *Journal of Applied Physics* 2007, 102.
8. Halik, M.; Hirsch, A., The Potential of Molecular Self-Assembled Monolayers in Organic Electronic Devices. *Advanced Materials* 2011, 23, 2689-2695.
9. DiBenedetto, S.; Facchetti, A.; Ratner, M.; Marks, T., Molecular Self-Assembled Monolayers and Multilayers for Organic and Unconventional Inorganic Thin-Film Transistor Applications. *Advanced Materials* 2009, 21, 1407-1433.
10. Love, J.; Estroff, L.; Kriebel, J.; Nuzzo, R.; Whitesides, G., Self-assembled monolayers of thiolates on metals as a form of nanotechnology. *Chemical Reviews* 2005, 105, 1103-1169.

11. Woodward, J.; Ulman, A.; Schwartz, D., Self-assembled monolayer growth of octadecylphosphonic acid on mica. *Langmuir* 1996, 12, 3626-3629.
12. Gao, W.; Dickinson, L.; Grozinger, C.; Morin, F. G.; Reven, L., Self-assembled monolayers of alkylphosphonic acids on metal oxides. *Langmuir* 1996, 12, 6429-6435.
13. Gawalt, E.; Avaltroni, M.; Koch, N.; Schwartz, J., Self-assembly and bonding of alkanephosphonic acids on the native oxide surface of titanium. *Langmuir* 2001, 17, 5736-5738.
14. Thissen, P.; Peixoto, T.; Longo, R.; Peng, W.; Schmidt, W.; Cho, K.; Chabal, Y., Activation of Surface Hydroxyl Groups by Modification of H-Terminated Si(111) Surfaces. *Journal of the American Chemical Society* 2012, 134, 8869-8874.
15. Dubey, M.; Weidner, T.; Gamble, L.; Castner, D., Structure and Order of Phosphonic Acid-Based Self-Assembled Monolayers on Si(100). *Langmuir* 2010, 26, 14747-14754.
16. Hanson, E.; Guo, J.; Koch, N.; Schwartz, J.; Bernasek, S., Advanced surface modification of indium tin oxide for improved charge injection in organic devices. *Journal of the American Chemical Society* 2005, 127, 10058-10062.
17. Raman, A.; Dubey, M.; Gouzman, I.; Gawalt, E. S., Formation of self-assembled monolayers of alkylphosphonic acid on the native oxide surface of SS316L. *Langmuir* 2006, 22, 6469-72.
18. Hanson, E. L.; Schwartz, J.; Nickel, B.; Koch, N.; Danisman, M. F., Bonding self-assembled, compact organophosphonate monolayers to the native oxide surface of silicon. *J Am Chem Soc* 2003, 125, 16074-80.
19. Kluth, G.; Sung, M.; Maboudian, R., Thermal behavior of alkylsiloxane self-assembled monolayers on the oxidized Si(100) surface. *Langmuir* 1997, 13, 3775-3780.
20. Schlecht, C. A.; Maurer, J. A., Functionalization of glass substrates: Mechanistic insights into the surface reaction of trialkoxysilanes. *RSC Advances* 2011, 1, 1446-1448.
21. Meyer, G., Ueber einige anomale Reaktionen. *Ber. Dtsch. Chem. Ges.* 1883, 16, 1439-1443.
22. Quick, A. J.; Adams, R., Aliphatic Arsonic and Arsinic Acids, and Aliphatic-aromatic Arsinic Acids. *J. Am. Chem. Soc* 1922, 44, 805-816.
23. Banks, C. K. e. a., Aliphatic Chloroarsines. *J. Am. Chem. Soc.* 1947, 69.
24. Irgolic, K.; Zingaro, R. A.; Smith, M. R., Arsinic Acids. *Journal of Organometallic Chemistry* 1966, 6, 17-24.
25. McBrearty, C. F.; Irgolic, K.; Zingaro, R. A., Arsonic Acids. *Journal of Organometallic Chemistry* 1968, 12, 377-387.
26. Sakurai, T.; Kojima, C.; Ochiai, M.; Ohta, T.; Fujiwara, K., Evaluation of in vivo acute immunotoxicity of a major organic arsenic compound arsenobetaine in seafood. *Int Immunopharmacol* 2004, 4, 179-84.
27. Adler, S.; Haskelberg, L.; Bergmann, F., Synthesis of lipophilic chemotherapeuticals. Part II. 4-Alkylaminoazobenzene-4′-arsonic acids. *J. Chem. Soc.* 1940, 576-578.
28. Quiñones, R.; Gawalt, E. S., Study of the formation of self-assembled monolayers on nitinol. *Langmuir* 2007, 23, 10123-30.
29. Wolfe-Simon, F.; Switzer Blum, J.; Kulp, T. R.; Gordon, G. W.; Hoeft, S. E.; Pett-Ridge, J.; Stolz, J. F.; Webb, S. M.; Weber, P. K.; Davies, P. C.; Anbar, A. D.;

Oremland, R. S., A bacterium that can grow by using arsenic instead of phosphorus. *Science* 2011, 332, 1163-6.
30. Shinohara, M.; Katagiri, T.; Iwatsuji, K.; Matsuda, Y.; Fujiyama, H.; Kimura, Y.; Niwano, M., Oxidation of the hydrogen terminated silicon surfaces by oxygen plasma investigated by in-situ infrared spectroscopy. *Thin Solid Films* 2005, 475, 128-132.
31. Snyder, R. G.; Schachtschneider, J. H., Vibrational analysis of the *n*-paraffins—I Assignments of infrared bands in the spectra of C_3H_8 through *n*-$C_{19}H_{40}$ *Spectrochemica Acta* 1963, 19, 85-116.
32. Slater, J. C., Atomic Radii in Crystals. *The Journal of Chemical Physics* 1964, 41, 3199-3204.
33. Adhesion Measurement of Thin Films, Thick Films, and Bulk Coatings. In *Adhesion Measurement of Thin Films, Thick Films, and Bulk Coatings*, Mittal, K. L., Ed. American Society for Testing and Materials: 1978.
34. Hynes, M. J.; Maurer, J. A., Unmasking photolithography: a versatile way to site-selectively pattern gold substrates. *Angew Chem Int Ed Engl* 2012, 51, 2151-4.
35. Mrksich, M., Mass spectrometry of self-assembled monolayers: a new tool for molecular surface science. *ACS Nano* 2008, 2, 7-18.
36. Bhushan, B., Nanotribology and nanomechanics in nano/biotechnology. *Philos Transact A Math Phys Eng Sci* 2008, 366, 1499-537.
37. Stalder, A.; Kulik, G.; Sage, D.; Barbieri, L.; Hoffmann, P., A snake-based approach to accurate determination of both contact points and contact angles. *Colloids and Surfaces a-Physicochemical and Engineering Aspects* 2006, 286, 92-103.

CHAPTER THREE

PROTEIN RESISTIVE SUBSTRATES WITH LOW CONCENTRATIONS OF LAMININ-DERIVED PEPTIDES FOR NEURONAL CULTURE

3.1. Introduction

Protein patterning technologies are of great interest in a variety of fields, and they have many applications. One key application is in the essential studies of cellular interactions. For example, probing the activity of putative guidance cues thought to be involved in neuronal wiring during development is difficult to explore using *in vivo* techniques. An excellent example of this is described in Appendix Two, for the complex system of the Slit family of protein guidance cues. Chemically modifying a substrate to include well-defined regions of protein resistance and protein adsorption is an ideal method for generating patterned substrates for these studies. Patterned surfaces allow for the study intricate protein-cell interactions such as this, with superior control over the system, limiting the non-specific interactions of excreted extracellular matrix (ECM) proteins that could modulate the guidance cue being probed. This patterning is achieved by utilizing self-assembled monolayer (SAM) chemistry in combination with soft lithography or microcontact printing as described in Chapter One. The most commonly studied protein-resistant SAM system is the ethylene glycol terminated monolayer, which has also been shown to be cell-resistant.[1-5]

However, in the case of studying cellular interactions, this cell-resistant feature is problematic because it does not allow cells to survive and interact with cues presented in the protein pattern, limiting the information that can be obtained. This can be overcome by introducing a very low-concentration of adhesive cue to the background regions as demonstrated in Figure 3.1. Using SAMs to chemically modify the substrate allows us to introduce specific, bioorthoganol attachment points for molecules. This enables us to know the orientation of a biomolecule on the surface and the concentration of biomolecule on the surface, as well as prevent the non-specific adsorption of proteins and cells to the surface.

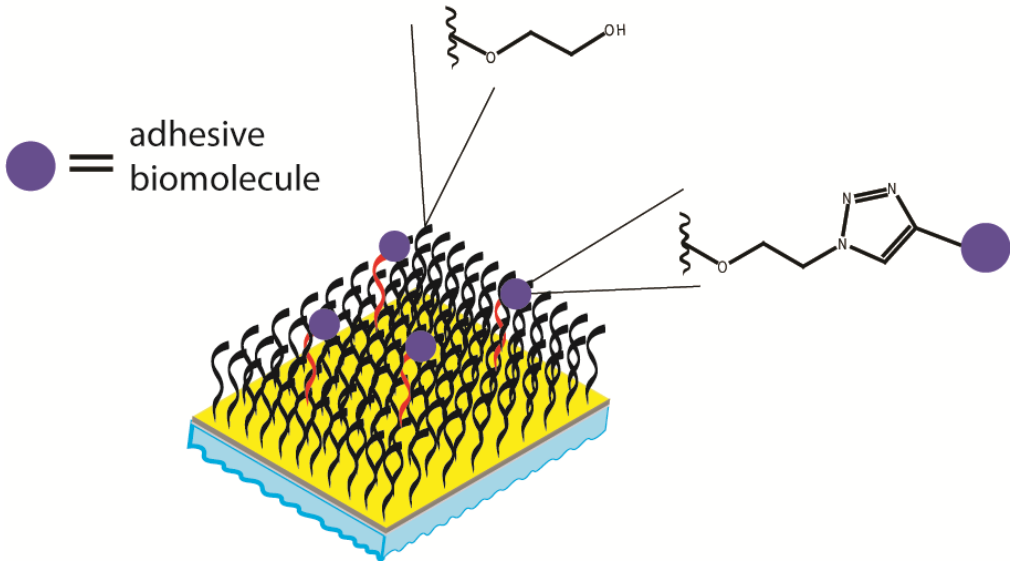

Figure 3.1. Using a mixed-monolayer system, we incorporated a low concentration of adhesive peptide into a protein-resistive background. The adhesive peptide is attached via triazole ring formation using the copper-catalyzed azide-alkyne cycloaddition (CuAAC) reaction.

This low concentration of adhesive cue allows receptor-mediated interaction with the cells while continuing to prevent non-specific protein adsorption of the ECM excreted by the cell. We utilized the copper-catalyzed azide-alkyne cycloaddition (CuAAC) reaction with a polytriazole copper-stabilizing ligand to attach, via a covalent linkage, our adhesive cue to the substrate. This reaction is well-studied and known to proceed rapidly and with high-yield.[6, 7]

When designing an appropriate adhesive cue, we were inspired by others who determined the active peptide sites on the laminin-1 protein. Laminin-1 is a 900 kD protein found abundantly in the ECM with both integrin and non-integrin receptor binding sites.[8, 9] The peptides IKVAV, YIGSR, and RGD, derived from domains in laminin-1, are the most well-studied of these peptides.[10-13] The location of these domains on the laminin protein structure are highlighted in Figure 3.2.

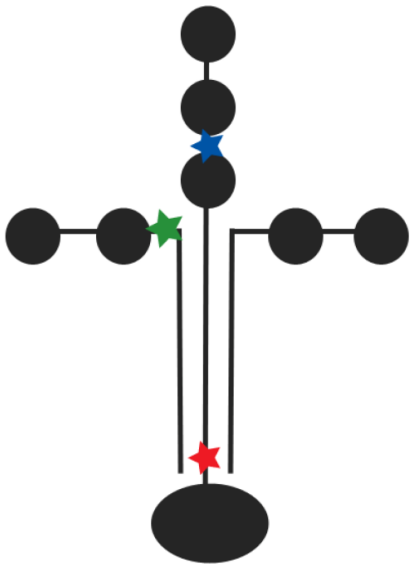

Figure 3.2. A cartoon representation of laminin-1 highlights the crucifix structure and globular nature (circles) of the protein. The IKVAV, YIGSR, and RGD sites are highlighted by blue, green, and red stars, respectively.

Interestingly, the IKVAV sequence has been found to be a non-integrin mediated cell attachment point. A 110-kDa membrane-associated protein which binds exclusively to this site on laminin was that identified by others, and is referred to as the laminin-binding protein or LBP110.[14-16] This receptor is found in multiple neuronal subpopulations

in the mouse brain, including the embryonic hippocampus.[14, 17] As such, this receptor is available on the embryonic hippocampal neurons utilized in these experiments. For this work, the IKVAV peptide was utilized exclusively.

In these experiments, we examined the adhesion of primary neuronal cells to surfaces functionalized with densities of IKVAV peptides ranging from 0.01% to 1% and compare these to a positive control (laminin adsorbed onto hexadecane thiol) and a negative control (100% glycol monolayer surface). The concentrations of peptide evaluated here are significantly lower than those previously utilized in cell-culture experiments.[12, 18] Analysis of the substrates with QCM experiments confirmed that the peptide substrates at 0.1% and below are protein resistive; however, the 1% peptide surface was not. This contradicts previous reports which assert that 100% IKVAV peptide substrates are protein resistive.[12] Furthermore, the interaction of the cells with the surfaces were analyzed by quantifying the neurite properties (number and length of longest neurite).

3.2. Results and Discussion

Mixed-monolayer substrates were previously explored to prepare substrates for cell-culture studies, probing the effect of low-concentrations of the RGD peptide.[7] However, there is limited information on how neurons respond to low-concentrations of the laminin-derived peptide, IKVAV. In this work, we follow a similar approach to these studies, utilizing the two thiol monomers shown in Figure 3.3. at specific mole percentages determined during monolayer setting. These solution mole percentages were

shown to mimic the SAM surface composition for mixed-monolayers below 10%, allowing the concentration of reactive sites available on the surface to be calculated.[7, 19]

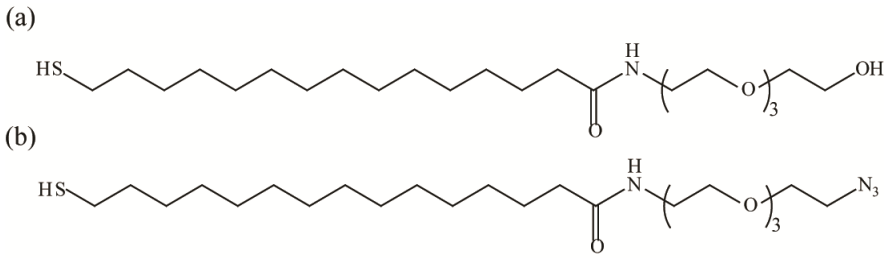

Figure 3.3. Two thiol monomers were utilized in this work to create a mixed-monolayer system. The monolayer consists primarily of glycol-terminated monomers (a), with a low-concentration of azide-terminated monomers (b).

During solid-phase peptide synthesis of the IKVAV peptide, an alkyne moiety was incorporated during the final coupling step at the N-terminus of the peptide as shown in Figure 3.4.

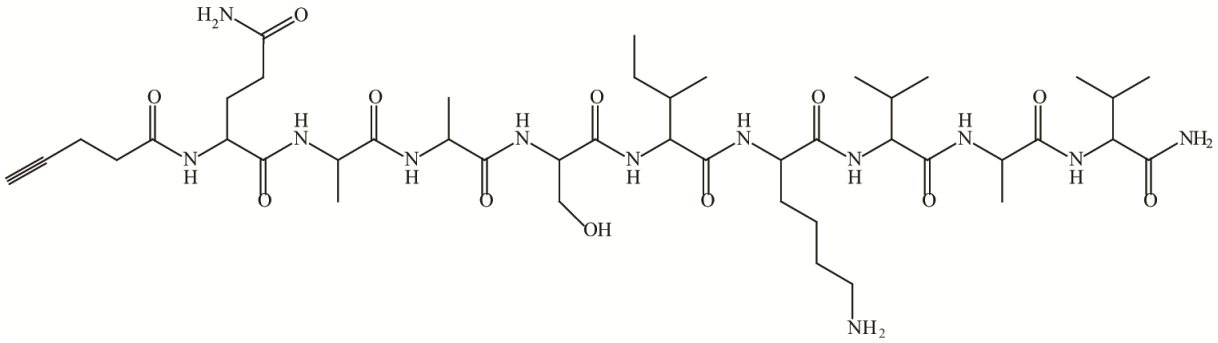

Figure 3.4. The structure for the laminin-derived peptide sequence, IKVAV, is shown including N-terminal alkyne moiety incorporated during synthesis. The peptide has previously been shown to promote cell attachment and neurite outgrowth at 100% concentration on the surface, but has not been explored at lower concentrations.[12]

ESI-MS indicates that following the final ether washes, the peptide product has few side products such as truncated sequences, and can therefore be used without purification (Figure 3.5.).

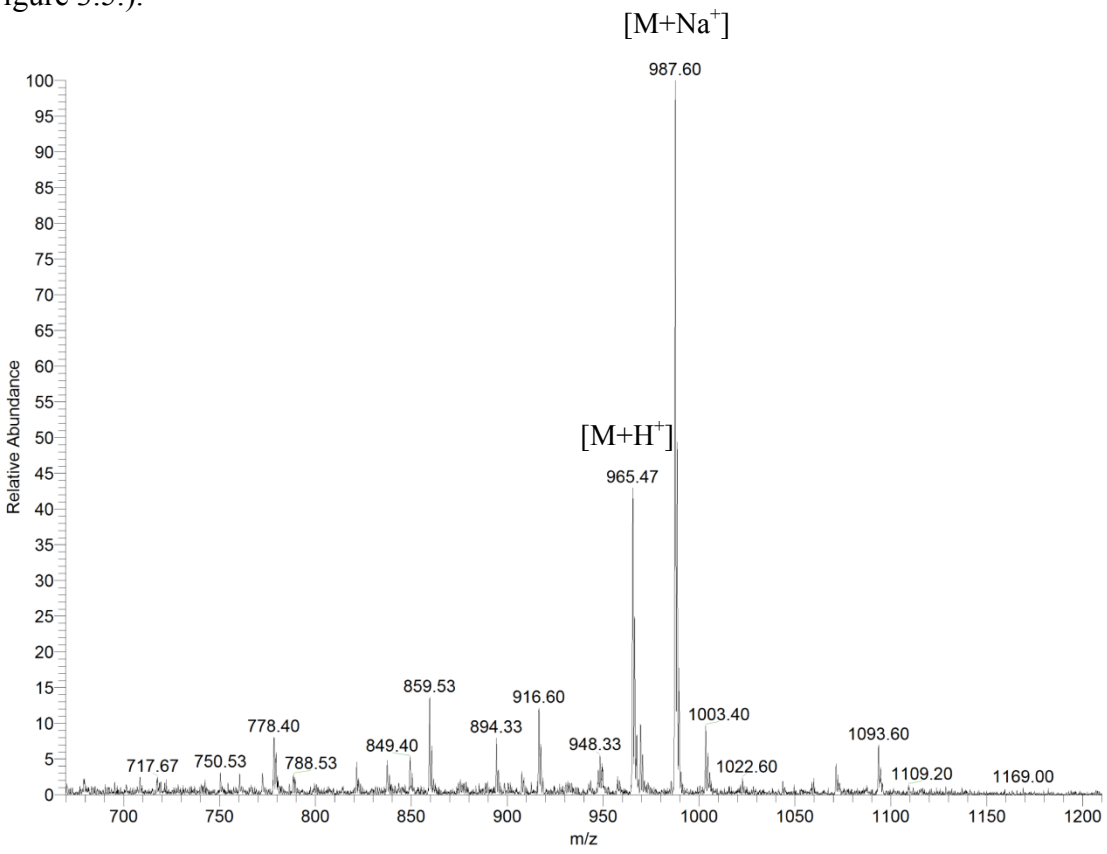

Figure 3.5. An ESI mass spectrum of IKVAV peptide, prepared via solid-phase peptide synthesis and precipitated from diethyl ether. The peptide is used without further purification. Peaks corresponding to a *m/z* of 965.47, [*M*+H^+] and a *m/z* of 987.60, [*M*+Na^+] are the primary peaks in the ESI-MS spectrum.

The copper-catalyzed azide-alkyne cycloaddition or "click" reaction has been demonstrated to extensively to quickly and efficiently form a bond between two molecules containing an azide and an alkyne moiety.[6, 20-26] In this work, we utilized this well-characterized reaction to covalently attach the adhesive peptide to the SAM substrate. The reaction utilizes a copper (I) catalyst that is stabilized by the *tris*-

(benzyltriazolylmethyl)amine (TBTA) reagent, as developed by the Sharpless laboratory.[6] A schematic for the reaction is shown below in Figure 3.6.

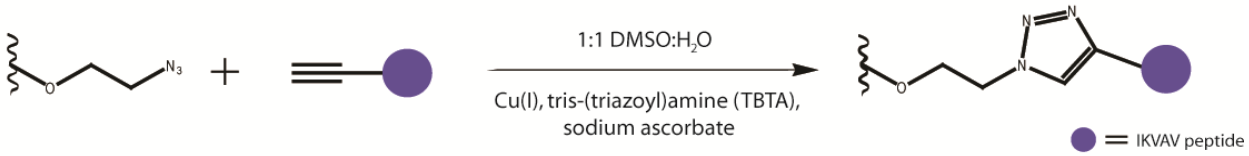

Figure 3.6. The copper-catalyzed azide-alkyne cycloaddition reaction was performed on the monolayer substrate, linking the azide-terminated thiol monomer to the alkyne terminated peptide. The reaction was performed in a DMSO/water solution containing TBTA (copper-stabilizing ligand) and sodium ascorbate to maintain the +1 oxidation state of the copper catalyst.

To measure whether the reaction proceeded efficiently on the surface, a 10% azide-terminated surface with IKVAV peptide coupled was analyzed by MALDI-MS. This 10% concentration was utilized to obtain sufficient signal-to-noise to discern the azide monomer and coupled product in the spectrum. In the resulting spectrum, peaks corresponding to the disulfide glycol molecule (*m/z* of 835.5) and the successfully coupled peptide on the surface (*m/z* of 1419.9) are seen in Figure 3.7. respectively. Notably absent from the spectrum is a peak corresponding to the [M+H^+] of the free azide monomer on the surface (or the disulfide), which would be found at (*m/z* = 432.6 or 455.6, [M+H^+] and [M+Na^+], respectively). This analysis, while not quantitative, qualitatively demonstrates the high coupling efficiency of this reaction.

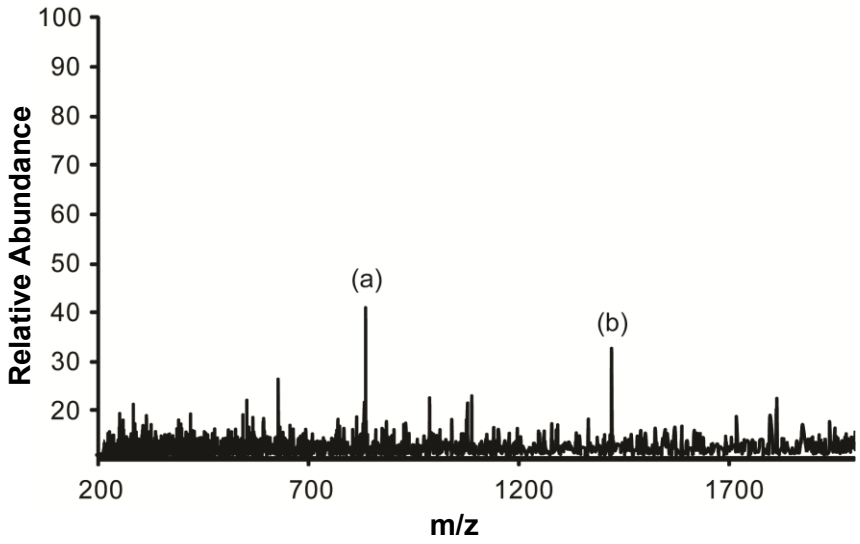

Figure 3.7. MALDI-MS analysis of a 10% azide-terminated substrate following CuAAC reaction with alkyne-IKVAV peptide shows no peaks for unreacted azide monomer. Primary peaks include the disulfide of the glycol monomer (a) as the [M+Na^+] of *m/z* 835.5 and the coupled product (b) as the [M+Na^+] of *m/z* 1419.9.

To assess the protein resistive quality of concentrations more relevant to our cell-culture studies, the following concentrations of substrates were prepared: 0% (glycol, negative control), 0.01% IKVAV peptide, 0.1% IKVAV peptide, 1.0% IKVAV peptide and a positive control of 100% hexadecane thiol on the surface. These surfaces were evaluated by quartz-crystal microbalance experiments with a 10% fetal bovine serum (FBS) solution in PBS as shown in Figure 3.8.

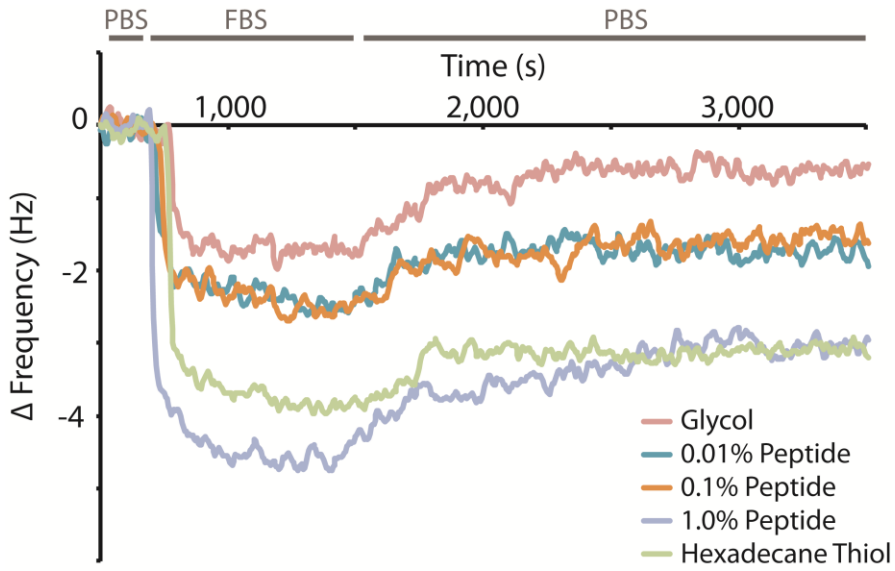

Figure 3.8. Using a quartz-crystal microbalance, we evaluated and compared the protein resistive qualities of the peptide substrates to a glycol-terminated substrate (resistive control) and hexadecane thiol (absorptive control). The change in frequency of the quartz substrate was measured, which is proportional to the amount of protein absorbed.

As described in Chapter One, a QCM experiment is a label-free means of evaluating the adsorption of proteins on a SAM surface. The SAM was prepared on the gold electrode of the QCM crystal, and protein was flowed over the substrate while the resonance frequency of the crystal was measured over time. According to Sauerbrey, a change in the resonance frequency is proportional to a change in mass adsorbed on the surface.[27] Therefore, the change in frequency observed in these experiments is a measure of the protein adsorbed on the surface and can be compared across substrates. A volume of 5 mL of FBS solution was flowed over the substrate, as labeled, and a sharp change in frequency was observed as seen in Figure 3.8. The complex mixture of proteins in FBS, including enzymes, albumins and globulins interacted with the surface and modulated the frequency.[28] Then, the substrate was rinsed extensively with PBS to remove any weakly

(reversibly) bound proteins, and the final change in frequency in Hz was compared across samples, with a higher Δ frequency indicating higher protein adsorption.

The substrate composed of 100% glycol-terminated monomers, is known to be protein resistive, and showed the lowest frequency change as expected. The lowest concentrations of peptides on the surface, 0.01% and 0.1%, show similar changes in frequency. These substrates have similar protein resistance, with only slightly more protein adsorbed than the glycol control. This additional adsorption was not unexpected, as the IKVAV peptide contains charged amino acids that likely allow electrostatically interact with the FBS proteins. These same electrostatic interactions are likely the reason that the substrate containing 1% peptide initially absorbs proteins to a higher degree than the hexadecane thiol control, which is known to be highly absorptive. However, after rinsing away reversibly bound proteins, the final measurement for the 1% peptide and hexadecanethiol substrates result in similar changes in frequency. This suggests these substrates have similar protein absorptivity. As a result of these experiments, we determined that at peptide concentrations of 1% and above, the proteins are non-specifically absorbed onto the surface. Therefore, cell-material interactions at peptide concentrations of 1% or above cannot be attributed only to receptor-peptide interactions.

E18 mouse hippocampal neurons were cultured on each of these substrates, including the positive (hexadecane thiol) and negative (100% glycol) controls (see Figure 3.9 for epresentative images of these cell cultures).

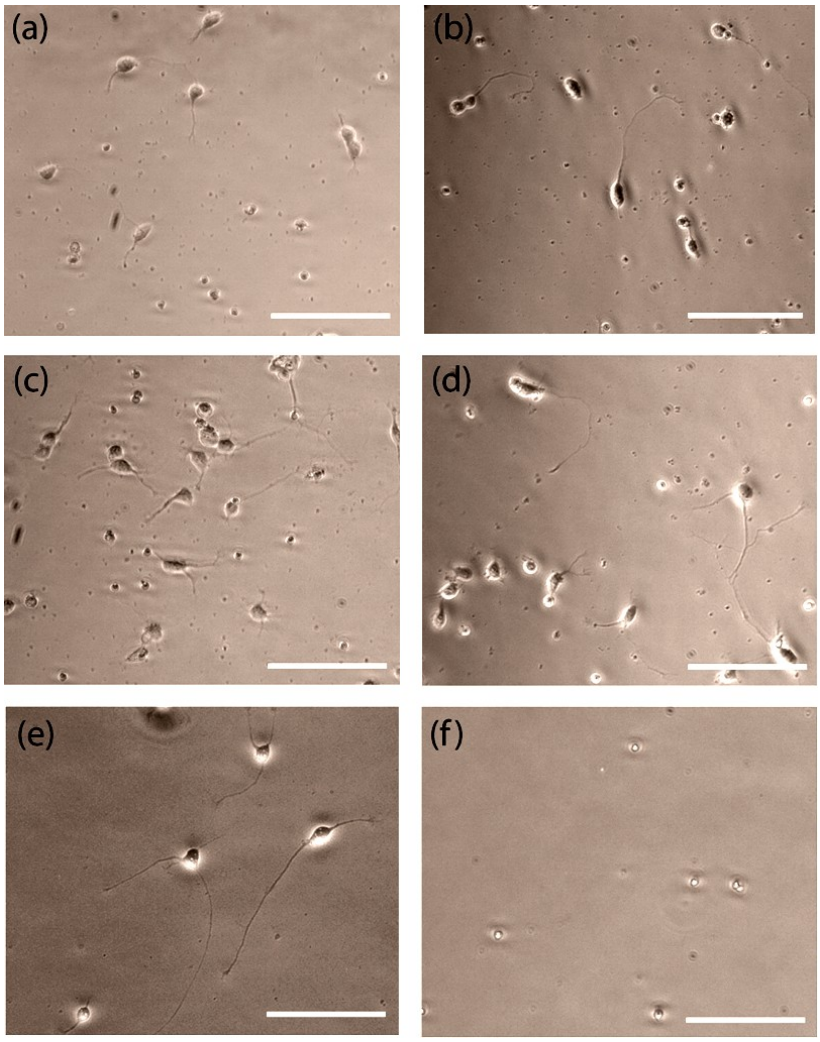

Figure 3.9. Representative images of E18 mouse hippocampal neuronal cells cultured on (a) 0.01% IKVAV, (b) 0.1% IKVAV, (c) 1% IKVAV, (d) 100% IKVAV, (e) laminin on hexadecane thiol (positive control), or (f) 100% glycol (negative control). Scale bar = 100 μm.

From these images, it is clear that there are some qualitative differences between the neurite outgrowths observed on each substrate. The 100% IKVAV substrate most closely resembles the positive control (hexadecane thiol with laminin absorbed). This was expected, as the 100% peptide substrate is protein absorptive based on QCM experiments. Furthermore, none of the peptide concentrations evaluated here resemble the 100% glycol negative control, where cell bodies are small, have no neurite outgrowths, and are likely dead. When images from one set of experiments were analyzed to compare the number of neurites and length of the longest neurite on a cell body, some trends were observed. Each peptide density examined in Figure 3.10. allows cells to grow similar numbers of neurites per cell body; however, longer neurite outgrowth occurred on the substrates with peptide concentrations above 0.01%. This indicates that the ideal surface for a patterned protein substrate designed to resist protein adsorption while still allowing neuron attachment and neurite outgrowth is approximately 0.1% IKVAV.

Unfortunately, during cell fixation for immunohistochemical analysis, the substrates with peptide concentrations at 1% or lower were unable to support cell fixation to the substrate. The amine-crosslinking reaction commonly utilized for cell fixation generally provides many anchorage points between the cell and the substrate. However, in this mixed-monolayer system, there are very few amines available on the substrate to anchor the cell. Therefore, we are unable to fix the neurons cultured on these substrates for downstream analysis using immunohistochemistry.

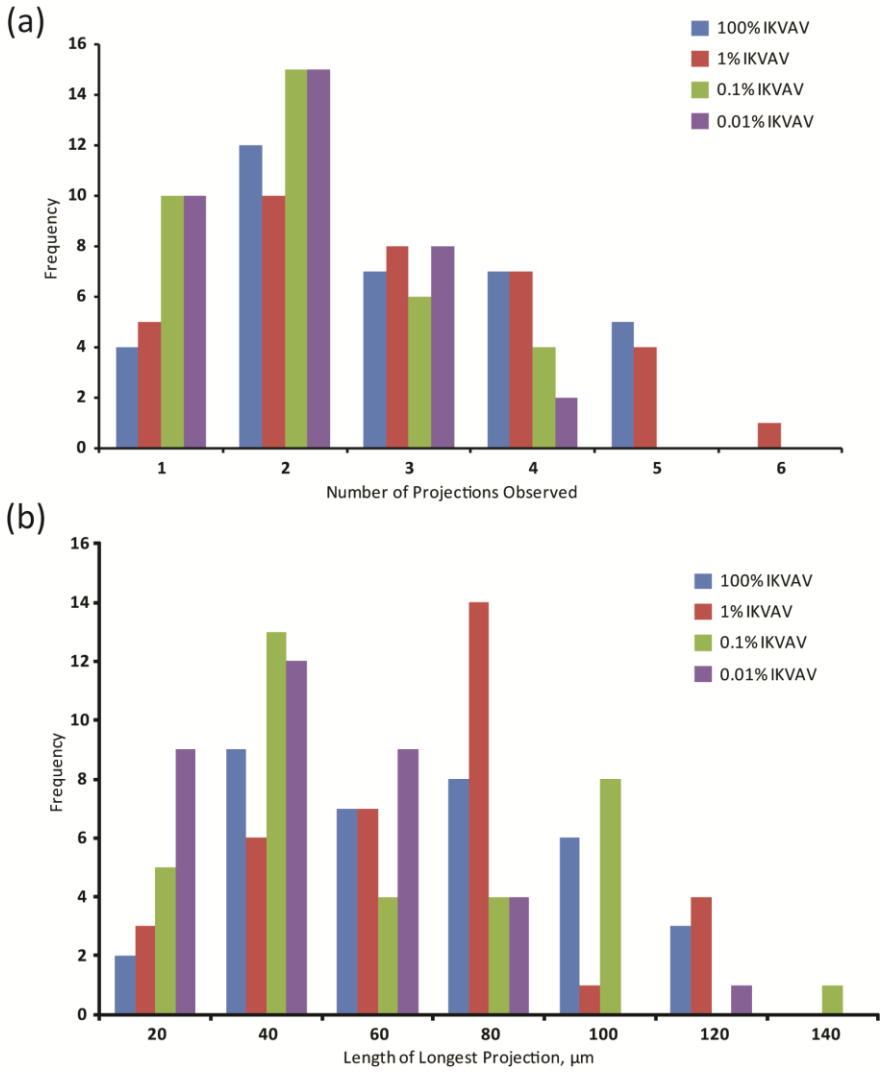

Figure 3.10. Bar graphs summarize data from one set of substrates with E18 mouse hippocampal neurons cultured on each concentration of peptide substrate. Graph (a) presents the number of projections per cell body observed and graph (b) presents the length of the longest neurite observed for each cell body.

3.3. Conclusions

Utilizing self-assembled monolayer chemistry, we developed a method for incorporating a low concentration of adhesive cue into a protein-resistant surface. This is facilitated by introducing a defined percentage of azide-terminated monomers into the glycol-

terminated monomer solution when setting the monolayer surface. The azide functional group presents a bio-orthogonal attachment point on the surface that can be reacted with an alkyne-terminated peptide. Successful peptide attachment was confirmed by MALDI-MS, and QCM was utilized to evaluate the protein-resistance of the substrates. Importantly, QCM characterization of the 1% peptide surface reveals this substrate is not protein resistive and therefore cellular interactions and phenotypes observed on this substrate are not solely due to peptide-mediated interactions. These experiments expand upon results presented in the literature where 100% peptide surfaces are incorrectly described as resistive.[12]

The long-term goal of research with these substrates is to provide a protein-resistive, cell-adhesive background for neuronal cell culture on patterned substrates. The ability of various concentrations of peptide to promote the attachment of neuronal cells and healthy growth of neurites was evaluated by analyzing brightfield microscopy images of live neuronal cells. Even at concentrations below 1% where the substrate has been determined to be protein resistive, the substrate continues to support neuronal attachment and neurite outgrowth. One limitation of this system is the inability to use standard fixation techniques to attach cells to the substrate for immunocytochemical analysis. Due to the low number of attachment points associated with the receptor-mediated interaction, amine-crosslinking reagents and organic fixing reagents do not support cell attachment.

3.4. Materials and Methods

3.4.1. Monomer Synthesis

Glycol-terminated and azide-terminated thiol monomers were synthesized by Matthew Hynes and Dr. David Fischer as previously reported by our laboratory.[29]

3.4. 2. Peptide Synthesis

IKVAV peptide was prepared by solid-phase peptide synthesis (CS136 Synthesizer, CS Bio, Co.). Fmoc-Rink Amide MBHA resin (Anaspec,) (0.1 mmol) was swelled in 5.0 mL dimethylformamide (DMF) (VWR). The resin was treated with 4.0 mL 20 % piperdine (Sigma-Aldrich) in DMF and mixed for 5 minutes. The resin was then treated with another 4.0 mL 20 % piperdine in DMF and mixed by inversion for 20 minutes. The resin was then washed with 2 x 4.0 mL DMF, 2 x 5.0 mL methylene chloride (CH_2Cl_2) (VWR), and 2 x 5.0 mL DMF. Then, a solution of 0.4 mmol (4 eq.) Fmoc-protected amino acid (Advanced ChemTech) and 0.4 mmol HBTU **(**Anaspec**)** in 5.0 mL DMF was mixed with 3.0 mL 0.16 M diisopropylethylamine (DIPEA) (Sigma-Aldrich) (8 eq.) in DMF. This solution was added to the resin and the resin was mixed by inversion for 45 minutes. The resin was then washed with 2 x 5.0 mL DMF, 5.0 mL CH_2Cl_2, and 5.0 mL DMF. The cycle was repeated for each amino acid coupling. In the final coupling step, 4-pentynoic acid (GFS Chemicals, Inc.) was coupled using the same conditions as above. Following the synthesis, the resin was collected and dried by vacuum filtration. The peptide was cleaved from the resin using 9.5 mL trifluoroacetic acid (TFA) (Sigma-Aldrich), 0.5 mL triisopropylsilane (Sigma-Aldrich), 0.4 mL DI water

in a 15 mL conical tube over 2 hours. The mixture was then vacuum filtered and the filtrated was collected in a 50mL conical tube. To the tube was added 40 mL ice cold diethyl ether (Et_2O) (EMD), yielding a yellow or white precipitate. The mixture was centrifuged at 10,000 rpm for 5 minutes and the liquid was decanted. The pellet was washed twice with 30 mL Et_2O, centrifuging each time as before. After the final centrifugation, the pellet (now predominately white) was dissolved in 5 mL DI water. If any insoluble material remained, it was filtered off and discarded. The aqueous solution was transferred to a 250 mL round bottom flask and lyophilized. Lyophilized peptide was dissolved in a minimal amount of sterile DI water, filter sterilized with 0.2 μm filters (Pall Corp.) and stored at -80 ˚C as a stock solution. Peptides were evaluated by electrospray ionization mass spectrometry (ESI-MS) on a Thermo LCQ Deca Plus operating in positive mode (ThermoFisher Scientific).

3.4.3. TBTA Synthesis

Synthesis for the polytriazole *tris*-(benzyltriazolylmethyl)amine, TBTA, was originally reported by Chan, et al.[6] The procedure was followed as reported with an extended reaction time. To a solution of tripropargylamine (660 mg; 5.03 mmol) in acetonitrile (15 mL) was added benzyl azide (2.33 g, 17.5 mmol), 2,6-lutidine (535 mg, 5.00 mmol), and $Cu(MeCN)_4PF_6$ (1.3 mol % with respect to total alkyne units). Following addition of the copper salt, the reaction was cooled in an ice bath, then allowed to warm to room temperature. The mixture was stirred at room temperature for 7 days. After 7 days, a white crystalline solid precipitated from the reaction. The solid was separated by filtration and washed with cold acetonitrile. The solid was recrystallized from 1:1 water :

t-butanol (70 mL) to afford fine, needle-like crystals (300 mg, 12.3% yield). ^{1}H NMR spectra was obtained on a 300 MHz Varian Innova instrument. ^{1}H NMR (300 MHz, $CDCl_3$ δ): 3.70 (s, 2H); 5.51 (s, 2H); 7.27 (m, 2H); 7.35 (m, 1H); 7.67 (s, 1H).

3.4.4. Substrate Preparation

Borosilicate glass coverslips (25mm, no. 1, VWR) were cleaned by oxygen plasma (Diener Electronic) at 100% power for 20 minutes. The slides were subsequently rinsed with ethanol, deionized water, and ethanol, drying with nitrogen gas following each rinse. Titanium, 50 Å and gold, 150 Å (Kurt J. Lesker) were deposited using a PVD-75 Electron-beam evaporator (Kurt J Lesker) at a rate of 0.1 Å/s.

3.4.5. Monolayer Preparation

Gold coverslips prepared as described above were immersed in a 1 mM absolute ethanolic solution of (a) glycol-terminated, (b) azide-terminated, or a defined mole-fraction mixture of both monomers for 12-14 hours in the dark. Substrates were rinsed twice with absolute ethanol and used as-is for control experiments, or further functionalized with the peptide CuAAC reaction. For control experiments, gold surfaces were soaked in 1 mM hexadecanethiol in absolute ethanol for 12-14 hours. Coverslips were rinsed and dried as described above. Coverslips were placed in a sterile teflon dish for cell-culture experiments. For hexadecanethiol control substrates, 12 µg of laminin protein (Cultrex) in Dulbecco's Phosphate Buffered Saline (DPBS) was adsorbed at 37˚C for 1 hour, then rinsed 3 times with DPBS before cell seeding.

3.4.6. Peptide-Surface CuAAC Reaction

To attach peptides by a copper-catalyzed azide-alkyne cycloaddition (CuAAC) or "click" reaction, the coupling solution was prepared as previously described.[7] Copper iodide (Sigma-Aldrich) and sodium ascorbate (Sigma-Aldrich) in dimethylsulfoxide (DMSO) (VWR) were dissolved at a concentration of 2 mM. To the solution containing copper iodide and sodium ascorbate in DMSO, TBTA (synthesized as described in **3.4.3.** above) was dissolved at a concentration of 2 mM. This coupling solution was mixed 1:1 with the aqueous peptides synthesized as described above in **3.4. 2.** Monolayer surfaces prepared as described above in **3.4.5.** were allowed to react in this solution (with shaking) for at least 2 hours in the dark. The coverslips were then rinsed sequentially with DI water, 0.1 % sodium dodecyl sulfate (Fisher Sci, Waltham, MA) in DI water, DI water, and finally absolute ethanol, followed by drying under a stream of $N_{2(g)}$.

3.4.7. MALDI-MS

Matrix-assisted laser desorption/ionization mass spectrometry (MALDI-MS) of a 10% azide-terminated substrate was performed on an Applied Biosystems 4700 MALDI TOF-TOF (Applied Biosystems)with a Nitrogen laser (337 nm) operating in reflectance mode as described previously.[29]

3.4.8. Quartz Crystal Microbalance

Quartz Crystal Microbalance (QCM) measurements were performed on a QCM 200 Digital Controller with a QCM 25 5 MHz crystal oscillator (Stanford Research Systems). Monolayers were assembled on QCM crystals, and peptides attached via the method

described above in **3.4.6.** Functionalized QCM substrates were mounted in the flow-cell chamber and connected to a standard high performance liquid chromatography (HPLC) pump system. A volume of 5 mL of 10% fetal bovine serum (FBS) in phosphate-buffered saline (PBS) was loaded into a PEEK loop by suction injection. PBS was flowed over the substrate at a fixed flow of 0.2 mL/min while the system equilibrated for approximately 30 minutes. Following equilibration, data collection began and PBS was allowed to flow for an additional 10 minutes before the 10% FBS solution was injected and allowed to flow over the substrate at the same flow rate of 0.2 mL/min. PBS was rinsed over the substrate for approximately 1 hour to remove weakly bound proteins.

3.4.9. E18 Hippocampal Neuron Culture

Time-pregnancy CD-1 outbred mice were obtained from Charles River Labs at E17 (embryonic day 17) for dissection on E18. Pregnant mice were euthanized with $CO_{2(g)}$ in a dessicator. Pups were removed from the uterus of the adult mouse, and separated from their membranes and yolk sacs. Pups were decapitated and the heads placed in ice cold Liebovitz's L-15 (Invitrogen Corp.). Brains were dissected and hippocampal tissues removed. Hippocampal tissue was placed in sterile ice-cold Hiberate E for storage at 4˚C until dissociation. Dissociation of the tissue was performed using a GentleMACS dissociator (Miltenyi Biotec) following the MACS protocol, "Preparation of single-cell suspensions from mouse neural tissue" using the Neural Tissue Dissociation Kit (P) (Miltenyi Biotec) and the mBrain programs. After dissociation, the cells were incubated with the Dead Cell Removal beads (Miltenyi Biotec, Gladbach, Germany) following the MACS Dead Cell Removal Kit protocol. Following the final centrifuge spin, buffer was

decanted and cells were re-suspended in fully-supplemented neurobasal media formulated containing Neurobasal medium, 2 mM Glutamax, 2% B27 Supplement, 1% penicillin/streptomycin (10,000 units/mL Penicillin G Sodium and 10,000 μg/mL Streptomycin Sulfate in 0.85% saline, Invitrogen, Corp.).

Cells were counted with a hemacytometer and 30,000 cells were seeded onto surfaces prepared as described above. Cells were grown at 37 °C and 5% CO_2 for 48 hours and visualized using phase-contrast live-cell inverted microscopy using a Nikon TE2000-PFS microscope running NIS-Elements imaging software and equipped with an incubator chamber at 37 ˚C, 5% CO_2 (In vivo Scientific), EXFO X-Cite UV illuminator and Photometrics CoolSNAP camera. For immunohistochemical analysis, cells were fixed with a solution of 3.7 % paraformaldehyde (Sigma-Aldrich) in PHEM (PIPES, HEPES, EGTA, $MgSO_4$) buffer. Solution was warmed to 37 ˚C and was added directly to the dish after media was removed. Cells were fixed for 20 minutes in a humidified incubator at 37 ˚C to help preserve morphology. Cells were rinsed 3 times with DPBS and mounted onto a clean glass slide with 1 drop ProLong Gold Antifade reagent with DAPI (Invitrogen, Corp.). Mounted coverslip was allowed to cure overnight in the dark before imaging.

3.5. References

1. Prime, K. L.; Whitesides, G. M., Self-assembled organic monolayers: model systems for studying adsorption of proteins at surfaces. *Science* 1991, 252, 1164-7.
2. Singhvi, R.; Kumar, A.; Lopez, G. P.; Stephanopoulos, G. N.; Wang, D. I.; Whitesides, G. M.; Ingber, D. E., Engineering cell shape and function. *Science* 1994, 264, 696-8.
3. Mrksich, M.; Whitesides, G. M., Using self-assembled monolayers to understand the interactions of man-made surfaces with proteins and cells. *Annu Rev Biophys Biomol Struct* 1996, 25, 55-78.
4. Chen, C. S.; Mrksich, M.; Huang, S.; Whitesides, G. M.; Ingber, D. E., Micropatterned surfaces for control of cell shape, position, and function. *Biotechnol Prog* 1998, 14, 356-63.
5. Strulson, M. K.; Johnson, D. M.; Maurer, J. A., Increased stability of glycol-terminated self-assembled monolayers for long-term patterned cell culture. *Langmuir* 2012, 28, 4318-24.
6. Chan, T.; Hilgraf, R.; Sharpless, K.; Fokin, V., Polytriazoles as copper(I)-stabilizing ligands in catalysis. *Organic Letters* 2004, 2853-2855.
7. Hudalla, G. A.; Murphy, W. L., Using "click" chemistry to prepare SAM substrates to study stem cell adhesion. *Langmuir* 2009, 25, 5737-46.
8. Mecham, R., Laminin Receptors. *Annual Review of Cell Biology* 1991, 7, 71-91.
9. Mecham, R., Receptors for Laminin on Mammalian Cells. *FASEB Journal* 1991, 5, 2538-2546.
10. Tashiro, K.; Sephel, G.; Weeks, B.; Sasaki, M.; Martin, G.; Kleinman, H.; Yamada, Y., A synthetic peptide containing the IKVAV sequence from the A chain of laminin mediates cell attachment, migration, and neurite outgrowth. *J Biol Chem* 1989, 264, 16174-82.
11. Graf, J.; Ogle, R.; Robey, F.; Sasaki, M.; Martin, G.; Yamada, Y.; Kleinman, H., A pentapeptide from the laminin B1 chain mediates cell adhesion and binds the 67,000 laminin receptor. *Biochemistry* 1987, 26, 6896-900.
12. Jans, K.; Van Meerbergen, B.; Reekmans, G.; Bonroy, K.; Annaert, W.; Maes, G.; Engelborghs, Y.; Borghs, G.; Bartic, C., Chemical and biological characterization of thiol SAMs for neuronal cell attachment. *Langmuir* 2009, 25, 4564-70.
13. Tashiro, K.; Sephel, G. C.; Greatorex, D.; Sasaki, M.; Shirashi, N.; Martin, G. R.; Kleinman, H. K.; Yamada, Y., The RGD containing site of the mouse laminin A chain is active for cell attachment, spreading, migration and neurite outgrowth. *J Cell Physiol* 1991, 146, 451-9.
14. Kibbey, M. C.; Jucker, M.; Weeks, B. S.; Neve, R. L.; Van Nostrand, W. E.; Kleinman, H. K., beta-Amyloid precursor protein binds to the neurite-promoting IKVAV site of laminin. *Proc Natl Acad Sci U S A* 1993, 90, 10150-3.
15. Kleinman, H. K.; Weeks, B. S.; Cannon, F. B.; Sweeney, T. M.; Sephel, G. C.; Clement, B.; Zain, M.; Olson, M. O.; Jucker, M.; Burrous, B. A., Identification of a 110-kDa nonintegrin cell surface laminin-binding protein which recognizes an A chain neurite-promoting peptide. *Arch Biochem Biophys* 1991, 290, 320-5.

16. Graf, J.; Iwamoto, Y.; Sasaki, M.; Martin, G.; Kleinman, H.; Robey, F.; Yamada, Y., Identification of an amino acid sequence in laminin mediating cell attachment, chemotaxis, and receptor binding. *Cell* 1987, 48, 989-96.
17. Luckenbill-Edds, L.; Kaiser, C. A.; Rodgers, T. R.; Powell, D. D., Localization of the 110 kDa receptor for laminin in brains of embryonic and postnatal mice. *Cell Tissue Res* 1995, 279, 371-7.
18. Heller, D. A.; Garga, V.; Kelleher, K. J.; Lee, T. C.; Mahbubani, S.; Sigworth, L. A.; Lee, T. R.; Rea, M. A., Patterned networks of mouse hippocampal neurons on peptide-coated gold surfaces. *Biomaterials* 2005, 26, 883-9.
19. Stranick, S. J.; Parikh, A. N.; Tao, Y. T.; Allara, D. L.; Weiss, P. S., Phase Separation of Mixed-Composition Self-Assembled Monolayers into Nanometer Scale Molecular Domains. *The Journal of Physical Chemistry* 1994, 98, 7636-7646.
20. Tornoe, C.; Christensen, C.; Meldal, M., Peptidotriazoles on solid phase: [1,2,3]-triazoles by regiospecific copper(I)-catalyzed 1,3-dipolar cycloadditions of terminal alkynes to azides. *Journal of Organic Chemistry* 2002, 67, 3057-3064.
21. Rostovtsev, V.; Green, L.; Fokin, V.; Sharpless, K., A stepwise Huisgen cycloaddition process: Copper(I)-catalyzed regioselective "ligation" of azides and terminal alkynes. *Angewandte Chemie-International Edition* 2002, 41, 2596-+.
22. Binder, W.; Kluger, C., Azide/alkyne-"click" reactions: Applications in material science and organic synthesis. *Current Organic Chemistry* 2006, 10, 1791-1815.
23. Evans, R., The rise of azide-alkyne 1,3-dipolar 'click' cycloaddition and its application to polymer science and surface modification. *Australian Journal of Chemistry* 2007, 60, 384-395.
24. Rodionov, V.; Presolski, S.; Diaz, D.; Fokin, V.; Finn, M., Ligand-accelerated Cu-catalyzed azide-alkyne cycloaddition: A mechanistic report. *Journal of the American Chemical Society* 2007, 129, 12705-12712.
25. Meldal, M.; Tornoe, C., Cu-catalyzed azide-alkyne cycloaddition. *Chemical Reviews* 2008, 108, 2952-3015.
26. Aragao-Leoneti, V.; Campo, V.; Gomes, A.; Field, R.; Carvalho, I., Application of copper(I)-catalysed azide/alkyne cycloaddition (CuAAC) 'click chemistry' in carbohydrate drug and neoglycopolymer synthesis. *Tetrahedron* 2010, 66, 9475-9492.
27. Sauerbrey, G., Verwendung von Schwingquarzen zur Wägung dünner Schichten und zur Mikrowägung. *Zeitschrift für Physik* 1959, 155, 206-222.
28. Menz, B.; Knerr, R.; Gopferich, A.; Steinem, C., Impedance and QCM analysis of the protein resistance of self-assembled PEGylated alkanethiol layers on gold. *Biomaterials* 2005, 26, 4237-4243.
29. Hynes, M. J.; Maurer, J. A., Unmasking photolithography: a versatile way to site-selectively pattern gold substrates. *Angew Chem Int Ed Engl* 2012, 51, 2151-4.

CHAPTER FOUR

DEVELOPMENT OF PATTERNED SUBSTRATES WITH INTERMOLECULAR ZWITTERIONIC MONOLAYERS TO INTERROGATE CELL-PROTEIN INTERACTIONS

4.1. Introduction

Improvement of existing *in vitro* platforms to probe cell-protein interactions is essential for the advancement of developmental studies, including mechanistic studies of axon/dendrite guidance and cell migration. For many applications, it is critical that proteins within the system be patterned on the micron scale, while maintaining the ability for cells to attach, spread, and proliferate over the entire cell culture substrate. Often, stripe assays, in which stripes of crude protein mixtures or purified proteins are patterned next to stripes of extracellular matrix (ECM) proteins, are used to investigate the effects of proteins or protein mixtures on cell adhesion, spreading, and migration.[1, 2] The major drawback of this approach is that ECM proteins have many integrin and non-integrin receptor-mediated binding sites that stimulate cell attachment, spreading, and migration, and are known to modulate the activity of other proteins.[3-5] Therefore, the background protein often acts as a cue itself, and while these proteins are found in the ECM, they are not typically found in isolation, or at the concentrations presented in these stripe assays. The consequence of using strong ECM cues for one of the stripes in this assay is that only

proteins exhibiting strong phenotypic responses can be differentiated from the background. Cell behavior in response to cues eliciting more subtle phenotypes, such as adhesion, weak attraction, or weak repulsion responses, would be masked by the strong response of cells to the ECM protein stripes. Using microcontact printing and intermolecular zwitterionic self-assembled monolayers (SAMs), we have developed a more sensitive stripe assay that can be used to understand the roles of proteins and polysaccharides in the ECM.

Microcontact printing of SAMs formed from alkanethiols on gold provides a robust method for creating protein patterns with well-defined features down to 200 nm.[6-9] This is most easily accomplished by stamping hexadecanethiol and backfilling with an ethylene glycol terminated alkanethiol monomer that is resistant to protein adsorption.[10, 11] The resulting substrates can be coated with ECM proteins to produce patterned cell culture substrates with a background region that is both protein and cell resistant. This approach is useful for studying cell confinement, and recently we have extended this method to allow confinement for up to 5 weeks,[12] and utilized this method to demonstrate that axon-dendrite differentiation is an environmentally determined process.[13] However, this approach is not useful for probing the effects of patterned cellular guidance cues or ECM proteins, because the patterned regions are the only regions of the substrate that support cell attachment and migration. To overcome this problem, low-concentrations of adhesive peptides were introduced into the background glycol-terminated monolayer. [14-16] Although this approach solves the adhesion problem, it still targets specific cellular receptors for attachment, and, in some cases, fixed cells do not remain robustly adhered to these substrates, restricting downstream analysis by immunohistochemical methods.

This is particularly problematic for primary culture neurons, which contain delicate neurite processes that must be preserved for downstream analysis. To maintain protein resistance in the monolayer background, peptides must be presented at densities of 0.1% or below, which hinders classical aldehyde fixation by limiting the sites available for substrate crosslinking.[17] Immunohistochemistry is critical for identifying cellular sub-populations, protein attachments, and protein localization, all of which are essential for most developmental studies. Therefore, low-density peptide surfaces severely restrict the types of analysis that can be performed. Moreover, because peptide-containing substrates target specific receptors on the cell surface, and the substrate prevents the cell from depositing its own ECM or carrying out ECM remodeling, the cellular attachments in these systems do not mimic attachments *in vivo*. Additionally, preparation of these peptide surfaces require on-surface coupling reactions, typically amide-bond formation or azide-alkyne cycloadditions. While these types of reactions are straightforward to carry out on the substrates, they require additional substrate preparation steps and do not always proceed in high yield.[18]

We developed a system that allows for robust protein patterning and background cellular attachment that is non-receptor mediated by replacing the classic glycol-terminated background in microcontact printed SAMs with an intermolecular zwitterionic monolayer (Figure 4.1). Both intramolecular and intermolecular zwitterionic terminated monolayers were previously examined and extensively employed as nanoparticle coatings for biological applications.[19-21] These monolayers are protein resistant to the same degree as the ethylene glycol terminated alkanethiol monolayers, and the resistance of mammalian cells to the intramolecular zwitterionic substrate was previously

described.[22, 23] Here, we show that intermolecular zwitterionic monolayers, although protein resistant, allow cell attachment of both cell lines and primary culture neurons. This attachment is facilitated by interaction between polysaccharides on the surface of the cell and the monolayer. These intermolecular zwitterionic surfaces can be regarded as a blank-slate, allowing for the evaluation of subtle protein guidance cues and ECM proteins.

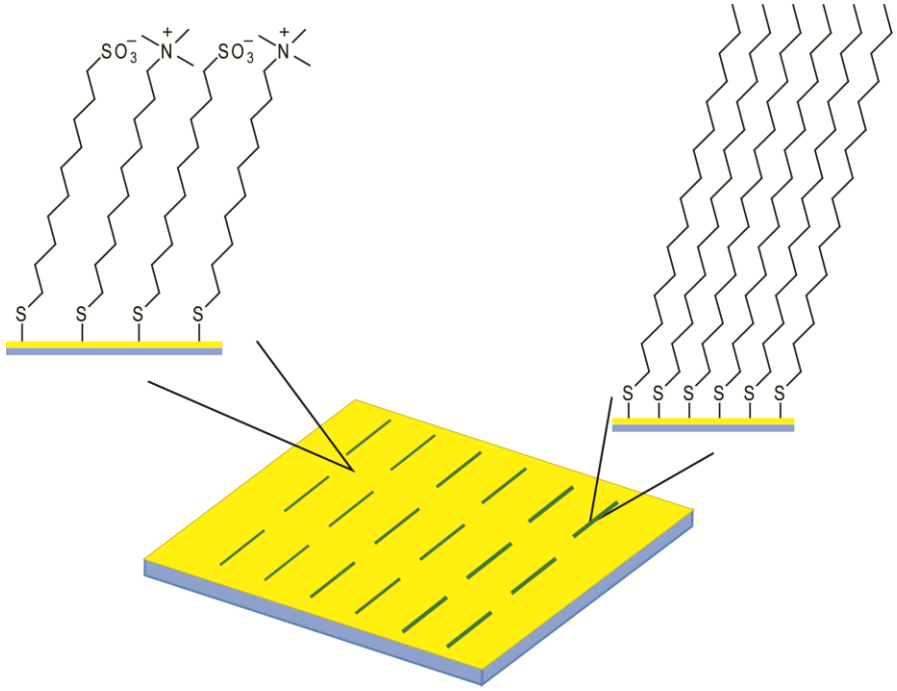

Figure 4.1. Schematic of a patterned surface, generated by microcontact printing, containing protein adsorptive (hexadecanethiol) and protein resistive (intermolecular zwitterionic monolayer) regions. The intermolecular zwitterionic monolayer is formed between sulfonate and quaternary amine terminated monomers.

4.2. Results and Discussion

The sulfonate and quaternary amine monomers were prepared as previously reported by Liu, et al.[19] and Holmlin, et al.,[23, 24] respectively. Patterned substrates were prepared by microcontact printing hexadecanethiol and backfilling with a 1 mM alkanethiol solution for 12 – 14 hours, as described previously.[6] Intermolecular zwitterionic backgrounds were prepared from 1 mM solutions containing equal molar concentrations of the sulfonate and quaternary amine monomers, and control substrates were prepared using 1 mM amide-linked glycol terminated monomers.[12]

Protein resistance of the intermolecular zwitterionic monolayer was evaluated by surface plasmon resonance imaging (SPRi) and compared to the amide-linked glycol-terminated alkanethiol monolayer. SPRi allows for the visualization and quantification of protein adsorption to patterned substrates.[25] To compare relative protein adsorption on a patterned substrate, the SPRi signals from the protein-resistant background regions of the monolayer were normalized to protein adsorption on the hexadecanethiol regions of the monolayer, which are highly adsorptive.[6, 12] Protein adsorption to the background regions of the pattern are reported as a fraction of the hexadecanethiol absorbance on the same substrate, with higher values indicating more protein adsorption. The resistance of the surfaces to absorption of fibronectin, a common extracellular matrix protein used in cell culture experiments, is shown in Figure 4.2. (average trace) and Figure 4.3. (normalized). The intermolecular zwitterionic monolayer and the glycol-terminated monolayers show similar resistance to fibronectin adsorption.

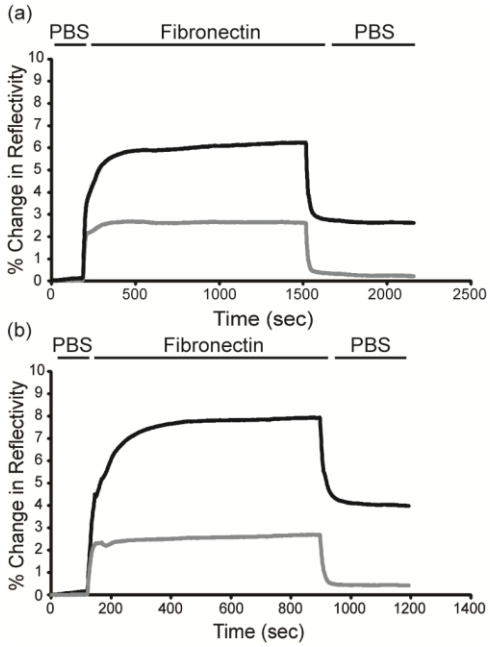

Figure 4.2. Average SPRi traces for fibronectin adsorbed onto patterned surfaces are shown above for (a) glycol-terminated alkanethiol and (b) intermolecular zwitterionic alkanethiol. Black trace represents the hexadecanethiol region of the pattern, grey traces correspond to the background region of the pattern.

When CHO-K1 cells were seeded at a low density (30,000 cells mL^{-1}) on the patterned substrate, the cells showed some preference for the fibronectin-coated region over the intermolecular zwitterionic background at 24 hours, Figure 3(b). However, spread cells were also observed outside of the patterned region, and at 48 hours, a confluent monolayer of cells was visible over the entire surface. Additionally, when cells were seeded at high densities (90,000 cells mL^{-1}), no preference was observed for the patterned region over the background. Since fibronectin is an extracellular matrix (ECM) protein and is known to contain cell-adhesive cues[26], it was anticipated that adhesion would occur first in the regions of the pattern containing fibronectin. Cellular attachment and spreading in the background is slower, as it requires cells to deposit their own ECM

proteins onto the substrate. This is similar to the process of cell attachment and spreading that occurs on a standard tissue culture dishes.

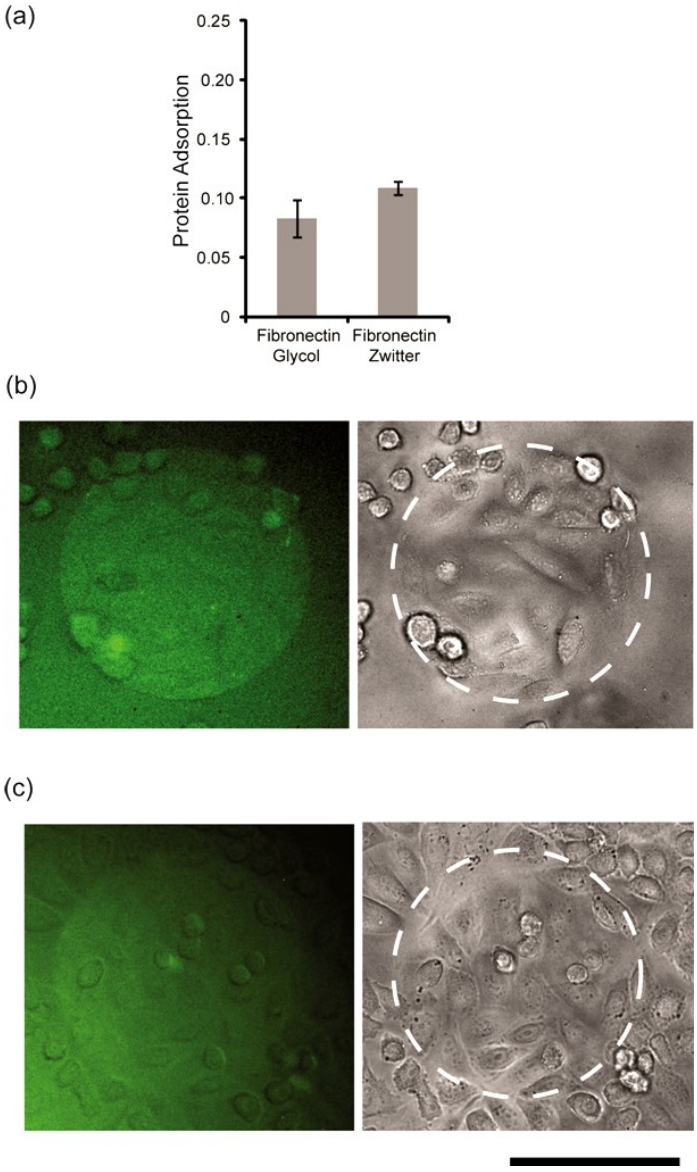

Figure 4.3. Fibronectin protein resistance of the intermolecular zwitterionic SAM is compared to a glycol-terminated SAM by SPRi (a). When CHO-K1 cells are cultured on this surface at low-densities, a preference for the fibronectin-coated region is initially observed at 24 hours (b), with some cells spread and growing in the intermolecular zwitterionic SAM background. After 48 hours, a confluent cell monolayer is observed, with little preference for the pattern (c). Scale bar is 100 μm.

Stripe assays are commonly employed to evaluate neuronal guidance and development.[1] In these assays, the preference of plated neuronal cell bodies or neurite outgrowths for the regions with and without a protein of interest, are compared. One of the major problems with this assay is preparing consistent, uniform substrates. There are currently two major methods of substrate preparation: direct protein printing, which typically results in highly denatured proteins[27], and microfluidic-based deposition methods, which require specific protein tags for attachment (typically FC-tags)[1]. Since intermolecular zwitterionic monolayers provide a rapid and straightforward method of patterning cells in a protein-resistant, cell-permissive background, this system is ideal for carrying out stripe analysis. As an initial test case, we evaluated the function of laminin, a large ECM protein, known to encourage neuronal cell attachment and neurite outgrowth.[28-33]

We confirmed resistance of the intermolecular zwitterionic SAM to laminin by SPRi, and compared this resistance to that observed for a glycol-terminated SAM, Figure 4.4. (average trace) and Figure 4.5. (normalized). The intermolecular zwitterionic SAM shows a significant improvement over the glycol-terminated monolayer in terms of laminin resistance. However, it should be noted that the glycol-terminated monolayer does provide both protein and cell-resistance upon laminin adsorption, as we have previously used this system to analyze the environmental effects of axon-dendrite differentiation. [13]

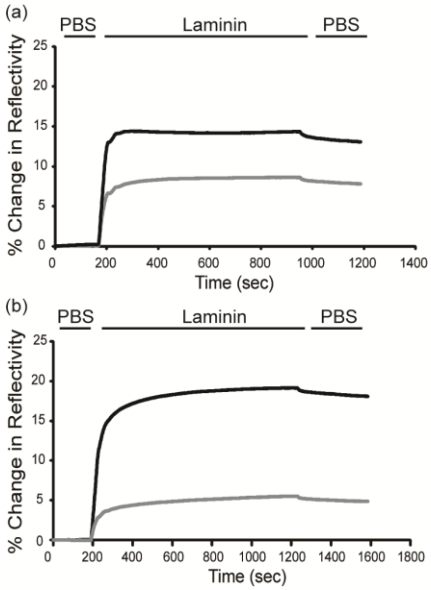

Figure 4.4. Average SPRi traces for laminin adsorbed onto patterned surfaces are shown above for (a) the glycol-terminated SAM and (b) the intermolecular zwitterionic SAM. Black trace represents the hexadecanethiol region of the pattern, grey traces correspond to the background region of the pattern.

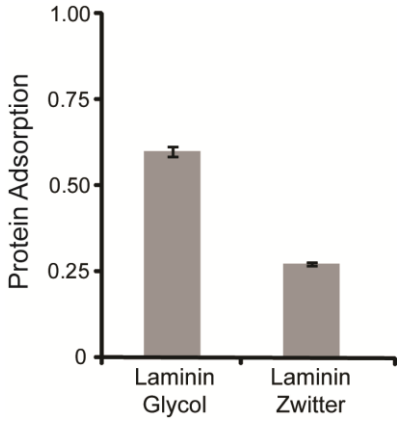

Figure 4.5. SPRi analysis of laminin protein adsorption shows the intermolecular zwitterionic alkanethiol monolayer has increased resistance to laminin adsorption over the glycol-terminated alkanethiol monolayer.

Fluorescently-labeled laminin was adsorbed onto patterned substrates containing a simple stripe pattern of hexadecanethiol backfilled with the intermolecular zwitterionic

monomer (Figure 4.1.). Following protein adsorption, dissociated embryonic day 18 (E18) mouse hippocampal neurons were plated onto the substrates. After 48 hours *in vitro*, the surface was rinsed with fresh media, and live-cell imaging was performed. In this assay, cell bodies can be either located on the zwitterionic background or the laminin stripe, and neurites could extend into either region, which gives rise to nine possible phenotypes (Figure 4.6.) All but phenotype (H) were observed in this experiment as shown in Figure 4.7.

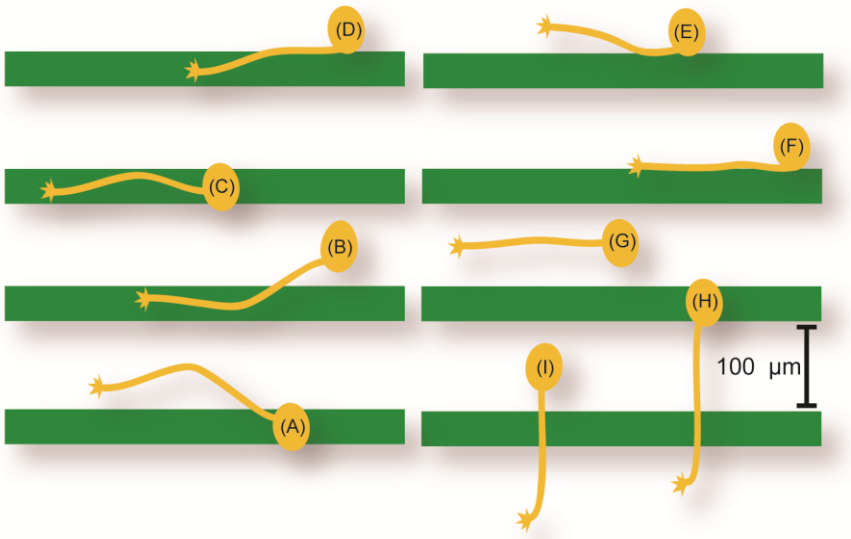

Figure 4.6. Multiple cell attachment and neurite outgrowth phenotypes on the patterned surface were predicted. Cells with neurites that follow different, heterogeneous paths are considered combination phenotypes and are denoted as (J). Laminin-coated hexadecanethiol stripes (green) are 12 µm, 15 µm, or 20 µm thick.

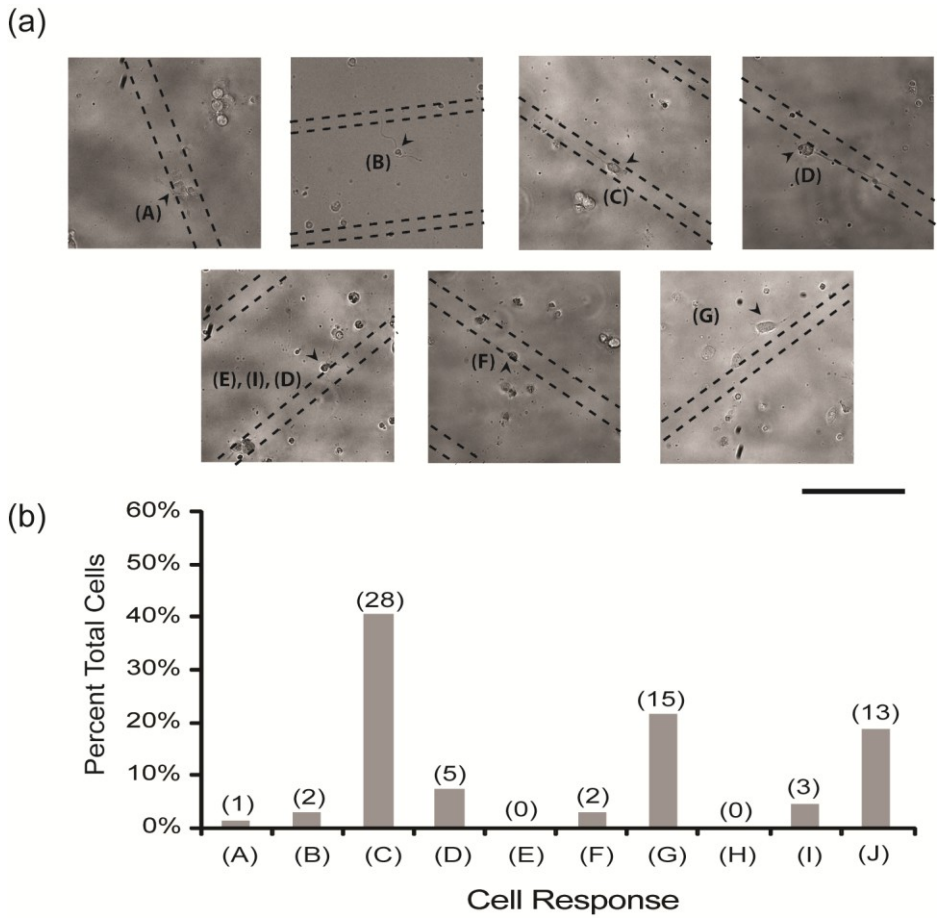

Figure 4.7. Representative images for neurons exhibiting cell attachment and neurite outgrowth phenotypes are shown in (a) with protein patterns outlined and cell bodies marked with arrows. The number of cells exhibiting each phenotype were counted, and summarized in (b). If different neurite outgrowths within a single cell exhibited a combination of phenotypes, they were denoted as (J). The number of cells observed for each phenotype is noted above the bar in parentheses. Scale bar = 100 µm.

We initially considered hexadecanethiol lines with widths of 12 µm, 15 µm, and 20 µm, spaced 100 µm apart. No significant difference was observed between line widths, Figure 4.8. This was not surprising, as all of the lines employed were large enough to support neuronal cell body attachment and were significantly greater than the width of a neurite outgrowth. If a neuron's ability to sense the surrounding environment did not play a role in its attachment, the percentage of the cell bodies located on the laminin

should correspond to the percentage of surface area occupied by laminin. For the 12 µm, 15 µm, and 20 µm lines this surface area probability is 11%, 13%, and 17%, respectively. However, the percentage of cell bodies attached to the laminin regions of the pattern are 20%, 39%, and 55%, respectively. This clearly indicates a strong preference for laminin over the zwitterionic background monolayer.

12 µm lines		**15 µm lines**		**20 µm lines**		**Total**		
Phenotype	**Number of Cells**	**Phenotype**	**Number of Cells**	**Phenotype**	**Number of Cells**	**Phenotype**	**Number of Cells**	**% total cells**
(A)	0	(A)	0	(A)	1	(A)	1	1%
(B)	0	(B)	1	(B)	1	(B)	2	3%
(C)	1	(C)	13	(C)	14	(C)	28	41%
(D)	0	(D)	4	(D)	1	(D)	5	7%
(E)	0	(E)	0	(E)	0	(E)	0	0%
(F)	0	(F)	2	(F)	0	(F)	2	3%
(G)	3	(G)	6	(G)	6	(G)	15	22%
(H)	0	(H)	0	(H)	0	(H)	0	0.0%
(I)	0	(I)	2	(I)	1	(I)	3	4%
(J)	1	(J)	5	(J)	7	(J)	13	19%
Total Cells	**5**	**Total Cells**	**33**	**Total Cells**	**31**	**Total Cells**	**69**	

Figure 4.8. Protein line widths do not affect phenotypes observed.

All neurites associated with a single cell body typically respond to the pattern in the same manner, with 81% of cells having all neurites exhibiting a single phenotype. Almost half of cell bodies were found on the laminin stripe (45%), which is consistent with the adhesive nature of laminin. Laminin is known to contain multiple integrin and non-integrin receptor binding sites, such as RGD, YIGSR, and IKVAV peptide sequences, that were previously demonstrated to enhance neuronal cell adhesion.[3, 4, 28-30] However, unlike traditional protein patterning using SAMs, the cells were not confined to the

protein pattern, and 55% of the cells adhered to the background intermolecular zwitterionic monolayer. Many of these cells, 39%, contained neurites that interacted solely with the zwitterionic monolayer, phenotype (G). Additionally, 35% of neurites explore regions of the pattern that are different than the cell body attachment region, including phenotypes (A), (B), (D), (I), and some cells included in (J). These experiments demonstrate the adhesive and attractive nature of laminin, with 45% of the cell bodies adhering to laminin, and 26% of the cells exhibiting a single phenotype having neurite outgrowths choosing to extend on laminin rather than zwitterionic monolayer. It is somewhat surprising that the majority of cells exhibit a single phenotype in this assay, and this suggests that even within the hippocampus, there are distinct subpopulations of neurons with differing laminin responses.

It is well-established that extracellular matrix proteins are required for normal cell-attachment and spreading; however, the intermolecular zwitterionic background is resistant to adhesion of most common extracellular matrix proteins, including fibronectin (Figures 4.2. and 4.3.) and laminin (Figures 4.4. and 4.5.). As a result, other biomolecules must mediate the interactions between the substrate, ECM proteins, and cells, to allow for proper cell attachment and spreading. Polysaccharides play critical roles within the extracellular matrix *in vivo,* and they were shown to specifically anchor proteins to the ECM,[34-38] and were implicated in other protein-cell interactions, especially in the case of neuronal pathfinding.[39-42] Moreover, many peripheral and integral membrane proteins found on mammalian cell surfaces are extensively glycosylated. One of the most common ECM polysaccharides is heparin, a member of the glycosaminoglycan family. To determine if polysaccharides could mediate interactions

between cells and the intermolecular zwitterionic SAM and allow cells to deposit their own ECM onto the SAM, we examined the binding of laminin to substrates that were first coated with heparin (Figure 4.9. and Figure 4.10.).

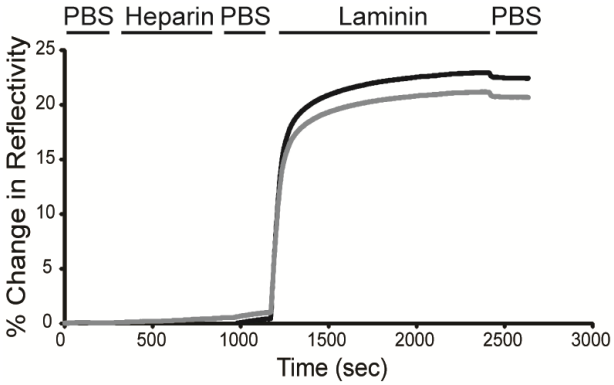

Figure 4.9. Average SPRi traces for laminin adsorbed onto a patterned substrate with intermolecular zwitterionic background. 10 μg mL^{-1} heparin is flowed over the substrate before the protein. Black trace is for the hexadecanethiol region of the pattern, grey trace corresponds to the background region of the pattern.

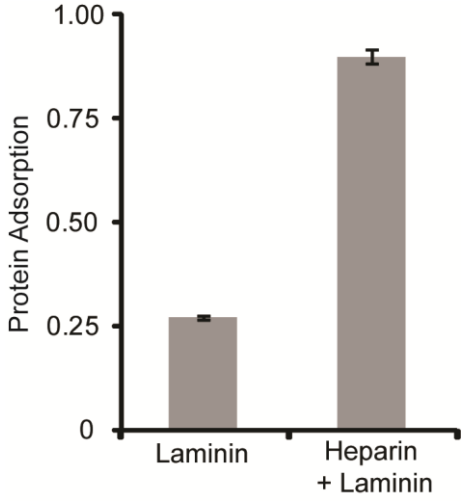

Figure 4.10. Heparin interacts with the intermolecular zwitterionic SAM surface, allowing much greater protein adsorption compared to the surface without heparin.

While the intermolecular zwitterionic monolayer provides resistance to laminin in the absence of heparin, if heparin is first allowed to bind to the zwitterionic surface, the subsequent laminin binding measured is similar to laminin binding to a hexadecanethiol monolayer. This demonstrates that while the intermolecular zwitterionic background is resistant to non-specific protein adhesion, it readily adsorbs polysaccharides. When cells are plated onto these SAMs, polysaccharides, which decorate the outer surface of the plasma membrane, can interact with the SAM, mediating cell adhesion. The substrate can then be remodeled by the binding of ECM proteins excreted by the cells to the polysaccharide-containing zwitterionic monolayer. This permits the cells to generate their own native ECM background. In the case of the stripe assays, this eliminates the influence of exogenous adhesive proteins or peptides on the proteins being studied.

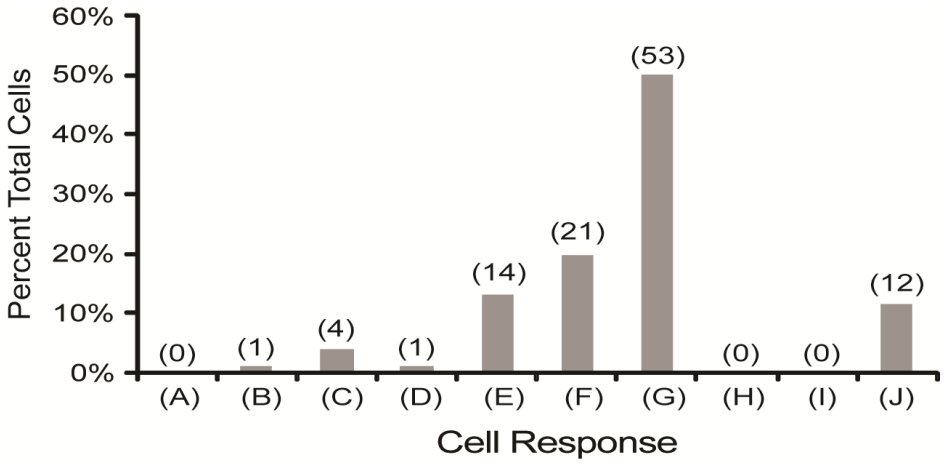

Figure 4.11. Addition of 2 μg of heparin in the media during E18 mouse hippocampal culture encourages greater attachment to the intermolecular zwitterionic surface over the patterned laminin regions. Illustrations for the phenotypes are shown in Figure 4 and the number of cells counted for each phenotype is noted above the bar in parentheses. No cells exhibiting phenotypes (A) or (H) were observed. Phenotype (I) was observed only in combination with other phenotypes and is counted in (J).

When hippocampal neurons were cultured on patterned intermolecular zwitterionic monolayers in media supplemented with heparin, we observed a very different distribution of neuronal phenotypes than was observed in the absence of heparin. As shown in Figure 4.11., in heparin-supplemented media, we observed a decrease in the preference for the protein pattern, with only 4% of cell bodies and neurites confined to the protein lines. Furthermore, there was a significant increase in the cell bodies that were found off of the pattern with phenotypes (E), (F), and (G) totaling 83%. We also observed an increase in the number of cell bodies that were found at the protein-zwitterionic monolayer interface, with phenotypes (D), (E), and (F) totaling 42% in the presence of heparin, as compared to only 14% in the absence of heparin. These phenotypes are interesting examples of guidance phenomena similar to those observed *in vivo*, such as in (F) where the neurite follows the protein interface and where high levels of laminin actually serve as a repulsive cue relative to native ECM proteins deposited by the cell. This further demonstrates the ability of heparin to modulate the cell's response to laminin. Once more, no significant differences between protein line widths were observed, Figure 4.12.

12 µm lines		15 µm lines		20 µm lines		Total		
Phenotype	**Number of Cells**	**Phenotype**	**Number of Cells**	**Phenotype**	**Number of Cells**	**Phenotype**	**Number of Cells**	**% total cells**
(A)	0	(A)	0	(A)	0	(A)	0	0%
(B)	0	(B)	1	(B)	0	(B)	1	1%
(C)	0	(C)	3	(C)	1	(C)	4	4%
(D)	1	(D)	0	(D)	0	(D)	1	1%
(E)	2	(E)	9	(E)	3	(E)	14	13%
(F)	4	(F)	9	(F)	8	(F)	21	20%
(G)	13	(G)	12	(G)	28	(G)	53	50%
(H)	0	(H)	0	(H)	0	(H)	0	0%
(I)	0	(I)	0	(I)	0	(I)	0	0%
(J)	1	(J)	5	(J)	6	(J)	12	11%
Total Cells	**21**	**Total Cells**	**39**	**Total Cells**	**46**	**Total Cells**	**106**	

Figure 4.12. Protein line widths do not affect phenotypes observed with heparin in the culture media.

When heparin is added to the media during cell culture, the effect of the heparin on cell body attachment to the laminin stripes does not correlate to the surface area coverage of laminin. Rather, in the presence of heparin, the neurons exhibit a preference for intermolecular zwitterionic SAM over the laminin protein; on average, 4% of cells adhere to the laminin, which is found on 14% of the average surface area. The breakdown of percentages by line width is shown in Figure 4.13. The preference for cell bodies to associate with the zwitterionic monolayer in the presence of heparin clearly underscores the important role that polysaccharides, like heparin, play in neuronal adhesion and neurite extension. This is further highlighted by the fact that 30% of neurites for cell bodies that are found in the zwitterionic region extend into the laminin region in the absence of heparin, while only 9% of the same neurites extend into the laminin region in

the presence of heparin. As a result of the zwitterionic monolayer's ability to absorb polysaccharides from the solution, this assay can be used to evaluate both the role of polysaccharides and proteins in neuronal guidance.

	Percentage of Cell Bodies Located on Laminin Protein Pattern		
Line Width	**Surface Area, Laminin**	**Cells Observed on Laminin, (-) Heparin**	**Cells Observed on Laminin, (+) Heparin**
12 μm	11%	20% (1)	0% (0)
15 μm	13%	39% (13)	8% (3)
20 μm	17%	55% (17)	2% (2)
Average	14%	45% (31)	4% (5)

Figure 4.13. The probability of a cell body attaching to the protein pattern based on the surface area of the pattern is much lower than what is observed for neurons cultured without heparin, and much higher than for neurons cultured with heparin.

The ability of heparin to modify protein and cellular adhesion to the intermolecular zwitterionic surface suggests that cell-surface polysaccharides found on the surface of mammalian cells facilitate the initial interaction of cells with the intermolecular zwitterionic monolayer, as illustrated in Figure 4.14. Following initial attachment, cells can deposit their own ECM proteins onto the substrate, and these proteins will adhere through polysaccharide-mediated binding interactions. Thus, this patterned monolayer system allows for the evaluation of cell-protein interactions in a stripe assay. Additionally, because the cells are creating their own ECM on the zwitterionic monolayer, even subtle adhesive differences, such as the role of high concentrations of laminin or fibronectin can be ascertained.

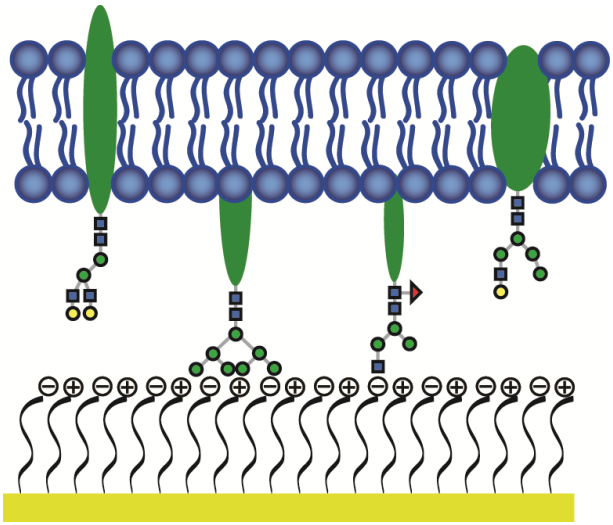

Figure 4.14. Various cell surface sugars are available to interact with the intermolecular zwitterionic surface. We demonstrate that heparin, a member of the glycosaminoglycan family with many repeating disaccharide units of variable sulfation patterns interacts with the intermolecular zwitterionic surface. Sulfated sugars similar to heparin are found on mammalian cells including CHO-K1 and hippocampal neurons.

4.3. Conclusions

In contrast to traditional protein-resistant, ethylene glycol self-assembled monolayers (SAMs), intermolecular zwitterionic SAMs, while protein resistant, are also an excellent substrate for cell culture. We demonstrated that cell attachment on the intermolecular zwitterionic monolayer is mediated by interactions of cell-surface polysaccharides with the monolayer, thus allowing the cell to excrete its own ECM proteins onto the surface. Exploiting these properties, we observed and quantified the interactions between neurons (cell bodies and neurites) and ECM proteins or guidance cues. This system improves upon the traditional stripe-assay platform, by allowing for non-receptor mediated attachment to the background substrate.

We explored neuronal response to laminin as a model protein to demonstrate the utility of this system. When neurons are cultured on patterned substrates with laminin, the neurons show a preference for the laminin-coated region over the zwitterionic background. However, this preference for the laminin region is eliminated when heparin is added to the media during cell culture. In the presence of heparin, the cells prefer to attach and grow neurites in the zwitterionic background region, highlighting the importance of polysaccharides in cell adhesion. As well, we observe that other molecules, such as heparin are capable of modulating cellular responses. This type of response is observed for phenotype (E), which account for 13% of neurons in the presence of heparin, where laminin acts as a repulsive cue. The conversion of laminin from an adhesive or attractive cue, which is observed in the absence of heparin, to a repulsive cue demonstrates how ECM proteins can be modulated.

Taken together, our work has revealed some features of the mechanism of neuronal attachment on intermolecular zwitterionic SAM substrates. We have also utilized this system to develop an *in vitro* platform for studying protein guidance cues. This system goes beyond current technologies, since it is capable of evaluating neuronal response to the extracellular matrix protein, laminin, which was previously considered a control molecule for stripe-assays.

4.4. Materials and Methods

4.4.1. Monomer Synthesis

The amide-linked glycol-terminated alkanethiol, sulfonate-terminated alkanethiol, and trimethyl quaternary amine alkanethiol were synthesized as previously described. [12, 19, 23]

4.4.2. Substrate Patterning /Microcontact Printing

Gold-coated coverslips, master fabrication, and microcontact printing with hexadecanethiol were performed as previously described.[6] Substrates were either backfilled with amide-linked glycol-terminated alkanethiol (previously described)[12, 43] or for intermolecular zwitterionic surfaces, substrates were backfilled in a solution containing 0.5 mM quaternary amine alkanethiol and 0.5 mM sulfonate alkanethiol (final thiol concentration = 1 mM) in 100% ethanol.

4.4.3. Surface Plasmon Resonance Imaging

Surface plasmon resonance imaging (SPRi) was conducted using a SPRimager II (GWC Technologies). Monolayers were prepared on SPRi chips coated with 25 Å titanium metal and 425 Å gold. Dulbecco's Phosphate Buffered Saline (DPBS, Gibco/Life Technologies) was flowed over the surface, followed by either 100 μg mL^{-1} of human plasma fibronectin (Invitrogen) or 96 μg mL^{-1} mouse Laminin I (Trevigen). The surface was rinsed with DPBS to remove excess electrostatically-bound protein. For heparin studies, the sodium salt of porcine-derived heparin (Activity = 197.0 U mg^{-1},

Calbiochem) was dissolved in DPBS to a concentration of 10 μg mL^{-1} and flowed over the surface after the initial DPBS equilibration. Regions of interest or ROIs (760 μm x 600 μm, 456 mm^2) were analyzed and percent change in reflectivity plotted. Change in reflectivity was averaged over 100 s periods (flat/level regions) at each stage of the experiment, including the initial DPBS equilibration. The DPBS background value was subtracted from the final protein adsorption values for each individual ROI trace. Ten ROIs for each substrate (5 hexadecanethiol regions, 5 background regions) were averaged and are reported with standard error. Average traces for each experiment including both hexadecanethiol and intermolecular zwitterionic background (5 ROIs each) are shown.

4.4.4. CHO-K1 Cell Culture

Human Plasma Fibronectin (20 μg, Invitrogen) was labeled with 10 μg AlexaFluor 488 N-hydroxysuccinimide-ester (Invitrogen) at pH=8 and quenched with 0.31 μg hydroxylamine (Sigma) in 1 M NaOH before mixing with and equal amount of unlabeled protein. Patterned monolayers were prepared on metal-coated glass coverslips (No. 1, 25 mm with 50 Å titanium metal and 100 Å gold) and 20 μg mL^{-1} (10 μg labeled, 10 μg unlabeled) fibronectin was absorbed onto the substrates at 37 °C for 1 h in Dulbecco's Phosphate Buffered Saline (DPBS, Gibco/Life Technologies). Excess protein was removed by rinsing with DPBS (3x) and the coverslips were covered with fresh DPBS. CHO-K1 cells (ATCC) were detached using TrypLE Express (Invitrogen), followed by resuspension in Dulbecco's Modified Eagle Medium (DMEM, low glucose 1X, glutamax, 1 g L^{-1} D-glucose, 110 mg L^{-1} sodium pyruvate, 10% FBS, 1% penicillin/streptomycin - 10,000 units mL^{-1} Penicillin G Sodium and 10,000 μg mL^{-1}

Streptomycin Sulfate in 0.85% saline, Invitrogen), and counted using a hemacytometer (Bright-Line, Hausser Scientific). After rinsing the patterned coverslip with DPBS, approximately 30,000 or 90,000 cells were applied in 1 mL of DMEM. Plated cells were grown at 37 °C and 5% CO_2. Cell and fluorescent protein images were visualized using live-cell inverted microscopy with a Nikon TE2000-PFS microscope running NIS-Elements imaging software and equipped with an EXFO X-Cite UV illuminator, Photometrics CoolSNAP camera, and an In Vivo Scientific incubator chamber held at 37˚C, 5% CO_2.

4.4.5. E18 Hippocampal Neuron Culture

CD-1 timed pregnancy mice (Charles River Laboratories) were sacrificed at day E18 and hippocampal pairs were microdissected from the embryonic mouse brains. E18 mouse hippocampi were stored in Hibernate E (BrainBits, LLC) for no longer than 72 hours and dissociated using a GentleMACS system in conjunction with the Neural Tissue Dissociation Kit (P) and Dead Cell Removal Kit (Miltenyi Biotec). Mouse Laminin I (Trevigen) was labeled with AlexaFluor 488 as described above (Invitrogen) and deposited onto patterned substrates at 12 μg mL^{-1} (6 μg labeled, 6 μg unlabeled) for 1 h prior to plating. Following dissociation, neurons were counted using a hemacytometer (Bright-Line, Hausser Scientific) and seeded onto patterned substrates at a 45,000 cells mL^{-1} in Neurobasal medium supplemented with 2% B27 supplement, 1% Glutamax, 1% Penicillin/Streptomycin (Invitrogen). Heparin (sodium salt, porcine-derived heparin (Activity = 197.0 U mg^{-1}, Calbiochem)) was dissolved in DPBS at a concentration of 20 mg mL^{-1}, filter sterilized and diluted in fully-supplemented Neurobasal media (described

above) to a final concentration of 2 μg mL^{-1}. Cells were incubated at 37 °C, 5% CO_2. After two days *in vitro*, cultures were imaged by live-cell inverted microscopy. For the cell-neurite phenotype analysis, cells within the patterned region of the coverslip, with projections greater than 5 μm were counted and the path of their neurites evaluated.

4.5. References

1. Knöll, B.; Weinl, C.; Nordheim, A.; Bonhoeffer, F., Stripe assay to examine axonal guidance and cell migration. *Nat Protoc* 2007, 2, 1216-24.
2. Walter, J.; Henkefahle, S.; Bonhoeffer, F., Avoidance of Posterior Tectal Membranes by Temporal Retinal Axons. *Development* 1987, 101, 909-913.
3. Mecham, R., Laminin Receptors. *Annual Review of Cell Biology* 1991, 7, 71-91.
4. Mecham, R., Receptors for Laminin on Mammalian-Cells. *Faseb Journal* 1991, 5, 2538-2546.
5. Nguyen-Ba-Charvet, K. T.; Brose, K.; Marillat, V.; Sotelo, C.; Tessier-Lavigne, M.; Chédotal, A., Sensory axon response to substrate-bound Slit2 is modulated by laminin and cyclic GMP. *Mol Cell Neurosci* 2001, 17, 1048-58.
6. Johnson, D. M.; LaFranzo, N. A.; Maurer, J. A., Creating two-dimensional patterned substrates for protein and cell confinement. *J Vis Exp* 2011, e3164.
7. Mrksich, M.; Whitesides, G. M., Patterning self-assembled monolayers using microcontact printing: A new technology for biosensors? *Trends in Biotechnology* 1995, 13, 228-235.
8. Quist, A.; Pavlovic, E.; Oscarsson, S., Recent advances in microcontact printing. *Analytical and Bioanalytical Chemistry* 2005, 381, 591-600.
9. Ruiz, S. A. a. C., Christopher S., Microcontact printing: A tool to pattern. *Soft Matter* 2007, 2007, 168-177.
10. Prime, K.; Whitesides, G., Self-assembled organic monolayers: model systems for studying adsorption of proteins at surfaces. *Science* 1991, 252, 1164-7.
11. Mrksich, M.; Dike, L. E.; Tien, J.; Ingber, D. E.; Whitesides, G. M., Using microcontact printing to pattern the attachment of mammalian cells to self-assembled monolayers of alkanethiolates on transparent films of gold and silver. *Exp Cell Res* 1997, 235, 305-13.
12. Strulson, M. K.; Johnson, D. M.; Maurer, J. A., Increased stability of glycol-terminated self-assembled monolayers for long-term patterned cell culture. *Langmuir* 2012, 28, 4318-24.
13. Johnson, D. M.; Abi-Mansour, J. P.; Maurer, J. A., Spatial confinement instigates environmental determination of neuronal polarity. *Integr Biol (Camb)* 2012, 4, 1034-7.
14. Houseman, B. T.; Gawalt, E. S.; Mrksich, M., Maleimide-Functionalized Self-Assembled Monolayers for the Preparation of Peptide and Carbohydrate Biochips†. *Langmuir* 2002, 19, 1522-1531.

15. Roberts, C.; Chen, C. S.; Mrksich, M.; Martichonok, V.; Ingber, D. E.; Whitesides, G. M., Using Mixed Self-Assembled Monolayers Presenting RGD and (EG)3OH Groups To Characterize Long-Term Attachment of Bovine Capillary Endothelial Cells to Surfaces. *Journal of the American Chemical Society* 1998, 120, 6548-6555.
16. Hudalla, G. A.; Murphy, W. L., Using "click" chemistry to prepare SAM substrates to study stem cell adhesion. *Langmuir* 2009, 25, 5737-46.
17. Kiernan, J. A., Formaldehyde, formalin, paraformaldehyde and glutaraldehyde: what they are and what they do. *Microscopy Today* 2000, 2000, 8-10.
18. Hynes, M. J.; Maurer, J. A., Unmasking photolithography: a versatile way to site-selectively pattern gold substrates. *Angew Chem Int Ed Engl* 2012, 51, 2151-4.
19. Liu, X.; Huang, H.; Jin, Q.; Ji, J., Mixed charged zwitterionic self-assembled monolayers as a facile way to stabilize large gold nanoparticles. *Langmuir* 2011, 27, 5242-51.
20. Park, J.; Nam, J.; Won, N.; Jin, H.; Jung, S.; Cho, S.; Kim, S., Compact and Stable Quantum Dots with Positive, Negative, or Zwitterionic Surface: Specific Cell Interactions and Non-Specific Adsorptions by the Surface Charges. *Advanced Functional Materials* 2011, 21, 1558-1566.
21. Liu, X.; Jin, Q.; Ji, Y.; Ji, J., Minimizing nonspecific phagocytic uptake of biocompatible gold nanoparticles with mixed charged zwitterionic surface modification. *Journal of Materials Chemistry* 2012, 22, 1916-1927.
22. Ostuni, E.; Chapman, R.; Liang, M.; Meluleni, G.; Pier, G.; Ingber, D.; Whitesides, G., Self-assembled monolayers that resist the adsorption of proteins and the adhesion of bacterial and mammalian cells. *Langmuir* 2001, 17, 6336-6343.
23. Holmlin, R.; Chen, X.; Chapman, R.; Takayama, S.; Whitesides, G., Zwitterionic SAMs that resist nonspecific adsorption of protein from aqueous buffer. *Langmuir* 2001, 17, 2841-2850.
24. The quaternary amine monomer used in this work was synthesized by undergraduate researcher Amir Munir with the assistance of Matthew Hynes.
25. Hynes, M. J.; Maurer, J. A., Photoinduced monolayer patterning for the creation of complex protein patterns. *Langmuir* 2012, 28, 16237-42.
26. Miyamoto, S.; Kathz, B.-Z.; Lafrenie, R. M.; Yamada, K. M., Fibronectin and Integrins in Cell Adhesion, Signaling, and Morphogenesis.
27. Biasco, A.; Pisignano, D.; Krebs, B.; Pompa, P. P.; Persano, L.; Cingolani, R.; Rinaldi, R., Conformation of microcontact-printed proteins by atomic force microscopy molecular sizing. *Langmuir* 2005, 21, 5154-8.
28. Tashiro, K.; Sephel, G.; Weeks, B.; Sasaki, M.; Martin, G.; Kleinman, H.; Yamada, Y., A synthetic peptide containing the IKVAV sequence from the A chain of laminin mediates cell attachment, migration, and neurite outgrowth. *J Biol Chem* 1989, 264, 16174-82.
29. Tashiro, K.; Sephel, G. C.; Greatorex, D.; Sasaki, M.; Shirashi, N.; Martin, G. R.; Kleinman, H. K.; Yamada, Y., The RGD containing site of the mouse laminin A chain is active for cell attachment, spreading, migration and neurite outgrowth. *J Cell Physiol* 1991, 146, 451-9.

30. Graf, J.; Ogle, R.; Robey, F.; Sasaki, M.; Martin, G.; Yamada, Y.; Kleinman, H., A pentapeptide from the laminin B1 chain mediates cell adhesion and binds the 67,000 laminin receptor. *Biochemistry* 1987, 26, 6896-900.
31. Saneinejad, S.; Shoichet, M., Patterned glass surfaces direct cell adhesion and process outgrowth of primary neurons of the central nervous system. *J Biomed Mater Res* 1998, 42, 13-9.
32. Graf, J.; Iwamoto, Y.; Sasaki, M.; Martin, G.; Kleinman, H.; Robey, F.; Yamada, Y., Identification of an amino acid sequence in laminin mediating cell attachment, chemotaxis, and receptor binding. *Cell* 1987, 48, 989-96.
33. Kleinman, H. K.; Weeks, B. S.; Cannon, F. B.; Sweeney, T. M.; Sephel, G. C.; Clement, B.; Zain, M.; Olson, M. O.; Jucker, M.; Burrous, B. A., Identification of a 110-kDa nonintegrin cell surface laminin-binding protein which recognizes an A chain neurite-promoting peptide. *Arch Biochem Biophys* 1991, 290, 320-5.
34. Lebaron, R.; Hook, A.; Esko, J.; Gay, S.; Hook, M., Binding of Heparan-Sulfate to Type-V Collagen - A Mechanism of Cell-Substrate Adhesion. *Journal of Biological Chemistry* 1989, 264, 7950-7956.
35. Elenius, K.; Salmivirta, M.; Inki, P.; Mali, M.; Jalkanen, M., Binding of Human Syndecan to Extracellular-Matrix Proteins. *Journal of Biological Chemistry* 1990, 265, 17837-17843.
36. Kokenyesi, R., Ovarian carcinoma cells synthesize both chondroitin sulfate and heparan sulfate cell surface proteoglycans that mediate cell adhesion to interstitial matrix. *Journal of Cellular Biochemistry* 2001, 83, 259-270.
37. Kallapur, S.; Akeson, R., The Neural Cell-Adhesion Molecule (NCAM) Heparin Binding Domain Binds to Cell-Surface Heparan-Sulfate Proteoglycans. *Journal of Neuroscience Research* 1992, 33, 538-548.
38. Jalkanen, M., Biology of Cell-Surface Heparan-Sulfate Proteoglycans. *Medical Biology* 1987, 65, 41-47.
39. Gama, C. I.; Hsieh-Wilson, L. C., Chemical approaches to deciphering the glycosaminoglycan code. *Curr Opin Chem Biol* 2005, 9, 609-19.
40. Rhiner, C.; Hengartner, M. O., Sugar antennae for guidance signals: syndecans and glypicans integrate directional cues for navigating neurons. *ScientificWorldJournal* 2006, 6, 1024-36.
41. Lee, J. S.; Chien, C. B., When sugars guide axons: insights from heparan sulphate proteoglycan mutants. *Nat Rev Genet* 2004, 5, 923-35.
42. de Wit, J.; Verhaagen, J., Proteoglycans as modulators of axon guidance cue function. *Adv Exp Med Biol* 2007, 600, 73-89.
43. Johnson, D. M.; Maurer, J. A., Recycling and reusing patterned self-assembled monolayers for cell culture. *Chem Commun (Camb)* 2011, 47, 520-2.

CHAPTER FIVE

CONCLUSIONS AND FUTURE DIRECTIONS

5.1. Conclusions

Self-assembled monolayers (SAMs) have the ability to generate well-defined, functionalized surfaces. SAMs have been explored previously for a number of applications, and in this work we build upon and expand classic SAMs to impact two major areas, surface coatings for MEMS lubrication and *in vitro* cell culture. We have accomplished this by utilizing the modularity of SAMs to tailor both the surface reactive group of the monomers, and the chemical functionality presented on the surface. These surfaces were characterized by a broad array of experimental techniques.

A simple method for the preparation of arsonate SAMs on multiple oxide surfaces was achieved. The increased reactivity of arsonates over phosphonates allowed for the functionalization of ordinary glass substrates. The arsonic acid monolayer provides surface protection against micronewton forces on a variety of substrates. As a wear-protection coating, the arsonate monolayer shows better performance on both titanium oxide and glass substrates than the corresponding phosphonate analog. As mechanical properties are scale-dependent, the nanoscratching measurement utilized here is particularly relevant to the use of arsonate SAMs as coatings for MEMS devices, where the surface area of the device is large, but the volume is small.[1] The surface coating

methodology described here is easily implemented and amenable to large-scale commercial applications for the functionalization of many oxide substrates; thus, it has excellent potential for wear-protection applications within MEMS devices.

We also achieved the goal of preparing protein-resistant, cell-permissive substrates for neuronal cell culture platforms. In this area, we first developed a method for incorporating a low concentration of the laminin-derived adhesive peptide IKVAV into a protein-resistant surface. This is facilitated by introducing a defined percentage of azide-terminated monomers into a glycol-terminated monolayer that presents a bio-orthogonal attachment point on the surface for the alkyne-terminated peptide. QCM characterization of the 1% peptide surface reveals this substrate is not protein resistive, contrary to results presented in the literature where 100% peptide surfaces are incorrectly described as resistive.[2] We found that even at concentrations below 1%, where the substrate has been determined to be protein resistive, the substrate continues to support neuronal attachment and neurite outgrowth. However, standard fixation techniques do not robustly adhere the neurons to the SAM surface, owing to the low number of attachment points associated with the receptor-mediated interaction. Although this limits the use of this mixed-monolayer surface for developmental cell biology studies that require downstream immunohistochemical analysis, the surface is still useful for interrogating receptor-mediated interactions.

Using intermolecular zwitterionic monolayers, we have also developed a patterned substrate that may be used for stripe assays in combination with standard fixation techniques for downstream immunohistochemical analysis. The patterned substrate uses standard hexadecanethiol microcontact printing and backfills with a 50:50 mixture of sulfonate and tetramethylammonium-terminated monomers to create a substrate with regions of protein adsorption (hexadecanethiol) and protein resistance (intermolecular zwitterionic monolayer). However, in contrast to traditional protein-resistant, ethylene glycol self-assembled monolayers (SAMs), intermolecular zwitterionic SAMs, while protein resistant, are also an excellent substrate for cell culture.

We demonstrated that neuronal attachment on the intermolecular zwitterionic monolayer is mediated by interactions of cell-surface polysaccharides with the monolayer, thus allowing the cell to excrete its own ECM proteins onto the surface. Exploiting these properties, we found that the interactions between neurons (cell bodies and neurites) and ECM proteins or guidance cues can be observed and quantified. This system improves upon the traditional stripe-assay platform, by allowing for non-receptor mediated attachment to the background substrate. Impressively, this system is also capable of evaluating neuronal response to cues such as the extracellular matrix protein, laminin, that was previously considered a control molecule for stripe-assays.

Overall, our work in this area is not only a significant contribution to the field of self-assembled monolayer chemistry, but also provides tools for researchers in other fields. We demonstrated applications for these advancements, which have wide-spread utility from materials science to developmental cell biology. While we have explored some of

these applications in the work described here, there is room to expand and apply our contributions as described below.

5.2. Future Directions

5.2.1. Synthesis of Glycol-Terminated Arsonic Acid Monomer for Anti-Fouling and Cell Patterning Applications

As described in Chapter Two, the hexadecylarsonic acid monomer was postulated to be non-toxic due to the high aliphatic nature of the compound.[3, 4] When CHO-K1 cells are cultured on a monolayer of hexadecylarsonic acid on a titanium oxide substrate, the cells attach, spread, and continue to grow over a period of 96 hours, showing no apparent detrimental effects from the monolayer (Figure 5.1.). As well, when hexadecylarsonic acid is added to the media at concentrations up to 100 μm, no toxic effects are observed with cells continuing to proliferate.

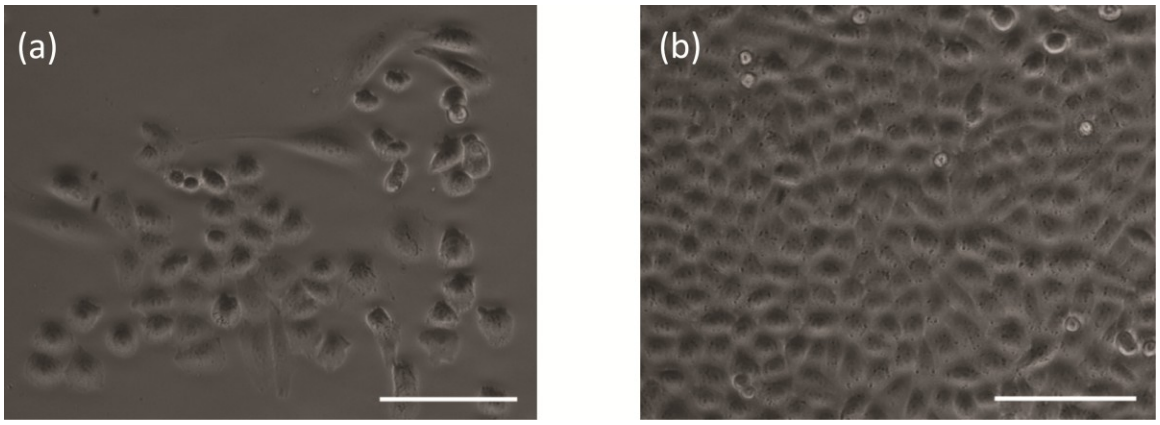

Figure 5.1. CHO-K1 cells cultured on hexadecylarsonic acid monolayers prepared on titanium oxide substrates are alive and spread at 48 hours (a) and have replicated to form a confluent monolayer by 96 hours (b). Scale bar is 100 μm.

Since the arsonic acid monolayer shows excellent stability as a surface coating and can be used to modify glass, silicon oxide, and titanium oxide substrates applications of this system could be extended into biotechnology. In particular, surfaces of medical devices such as implants, which are coated with titanium, require coatings to prevent biofilm formation and improve implant fixation.[5-9] We propose that a protein-resistant arsonate monomer could be prepared by adding a tetra ethylene-glycol moiety to the end of the aliphatic chain before generating the Grignard Reagent, as shown in Figure 5.2.

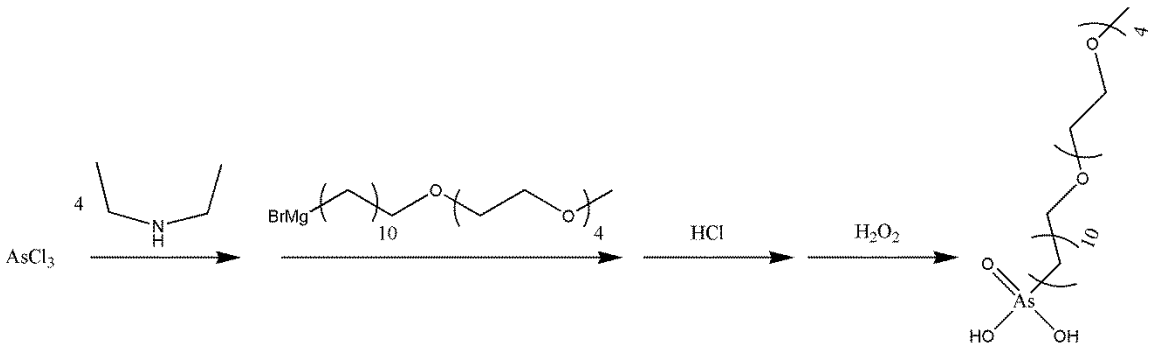

Figure 5.2. The synthetic scheme proposed above would introduce an ethylene-glycol moiety to the tail group of the arsonic acid monomer following the same approach as previously reported for the synthesis of the alkyl arsonic acid.[10]

Ethylene-glycol terminated monolayers have applications ranging from the prevention of biofouling to patterned surfaces for cell culture studies. Once synthesized, the monolayer may be characterized using techniques described previously, with protein resistance evaluated by surface plasmon resonance (SPR) on titanium coated substrates.

5.2.2. Investigating the Attachment of Neuronal Cells to Low-Density Peptide Substrates with Live-Cell Imaging of Focal Adhesion Complexes

While traditional cell fixation methods were unsuccessful on low-density peptide substrates as described in Chapter Three, a method for visualizing focal adhesion (FA) morphology[11] in live cells with GFP-tagged vinculin was developed that has wide-spread application in studying cell-substrate interactions. The focal adhesion complexes are the anchorage points that connect the cellular cytoskeleton to adhesive biomolecules in the extracellular matrix (ECM) *in vivo* and a cell culture substrate *in vitro*. As shown in Figure 5.3., there are multiple proteins included in these complexes.

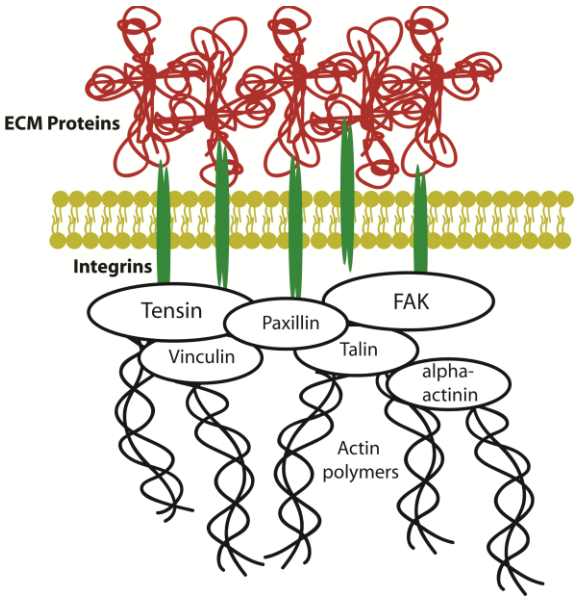

Figure 5.3. A cartoon representation of a focal adhesion complex illustrates some of the many proteins that are present in the complex which anchors the intracellular cytoskeleton to adhesive cues such as extracellular matrix (ECM) proteins or peptides.

Investigation of the morphology of the FA complexes on the low-density peptide substrates will be particularly interesting as focal complexes are thought to occur only in

integrin-receptor mediated cell attachment as shown in Figure 5.2.2.1. Since the IKVAV peptide is believed to have its own non-integrin LBP110 receptor protein[12], it is unclear if the same protein complexes will be present during IKVAV cell attachment.

The focal complex protein vinculin has previously been a target for both immunohistochemical staining and GFP-fusion protein expression for live-cell imaging of focal complexes.[11, 13-15] Using a construct encoding EGFP-Vinculin, we evaluated a number of different transfection methods including chemical reagents and electroporation to deliver the DNA to E18 mouse hippocampal neurons. However, live-cell imaging techniques are rarely utilized in primary cells, such as neurons, due to difficulties in transfecting these cells, and none of these traditional methods were successful. Successful transfection was achieved using a new technique known as Nucleofection (Amaxa/Lonza), which provides gentle electric pulses that are able to deliver the DNA through not only the cellular membrane, but also the nuclear membrane. This maximizes expression of the construct with minimal cell death as compared to traditional electroporation. Representative images of cells transfected with the GFP-vinculin construct and cultured on laminin adsorbed onto hexadecane thiol are shown in Figure 5.4. below. Areas of high vinculin concentration are visible within the neurites, and are seen clearly on the inverted image. By culturing transfected cells prepared in this same way on the low-density peptide substrates, we will be able to investigate whether integrin or non-integrin mediated attachment is at play in cell adhesion.

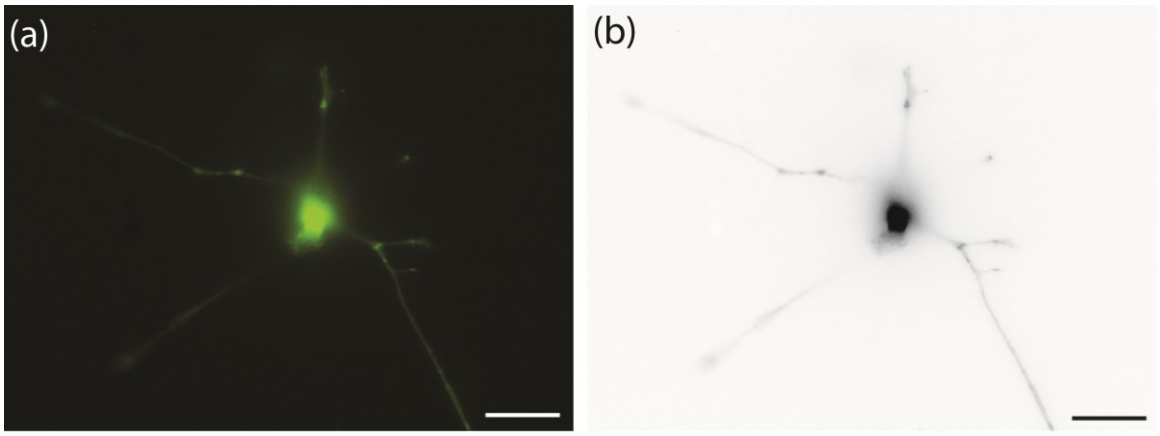

Figure 5.4. Live-cell imaging of GFP-vinculin highlights the locations where vinculin concentration is high, indicating the presence of a focal adhesion complex. Image (a) is the fluorescence microscopy image and image (b) inverts the image and displays it in black and white to make the high-concentration domains more clear. Cells are E18 mouse hippocampal neurons at 2 days *in vitro*.

These experiments could shed new light on how neurons interact with laminin-derived peptide surfaces supplementing the current literature on this topic.[2, 16] Furthermore, this method provides a means of evaluating neuronal interactions with a variety of substrates, including other protein cues and microtopography.[13, 17]

5.2.3. Screening Putative Guidance Cues involved in Enteric Nervous System Development using Patterned Substrates with Intermolecular-Zwitterionic Monolayers

While many axon guidance molecules have been identified for nervous systems such as the central nervous system and peripheral nervous system as discussed in Appendix II, the enteric nervous system, or ENS, is a system where few axon guidance molecules have been identified. Proper function of the ENS, made up of neurons and glial cells involved in intestinal function, requires the development of a complex neural circuit

containing many neuronal subtypes with distinct axon paths.[18-20] Until now, it has been difficult to study this system as no good *in vitro* methods to study individual axon growth, guidance, and protein interactions were available. However, our advancements over existing patterned substrates to develop an *in vitro* platform as described in Chapter Four, facilitates the study of putative guidance cues thought to be involved in enteric axon guidance.

In collaboration between our laboratory and the laboratory of Dr. Robert Heuckeroth, we aim to screen putative guidance cues using these substrates, patterned with hexadecanethiol and backfilled with the intermolecular zwitterionic alkanethiol monolayer, in a manner similar to a traditional stripe assay, with more well-defined control over the system.[21] Current experiments with laminin and glial-derived neurotrophic factor (GDNF) are in progress to optimize the system before exploring cues such as the ephrin/Eph family of proteins, known to be involved in the guidance of axons in other systems but not yet implicated in ENS development.[22-27] Furthermore, initial experiments by the Heuckeroth lab confirm that traditional cell fixation methods may be used on these substrates, for downstream immunohistochemical analysis of neuronal subtypes.

5.3. References

1. Bhushan, B., Nanotribology and nanomechanics in nano/biotechnology. *Philos Transact A Math Phys Eng Sci* 2008, 366, 1499-537.
2. Jans, K.; Van Meerbergen, B.; Reekmans, G.; Bonroy, K.; Annaert, W.; Maes, G.; Engelborghs, Y.; Borghs, G.; Bartic, C., Chemical and biological characterization of thiol SAMs for neuronal cell attachment. *Langmuir* 2009, 25, 4564-70.
3. Sakurai, T.; Kojima, C.; Ochiai, M.; Ohta, T.; Fujiwara, K., Evaluation of in vivo acute immunotoxicity of a major organic arsenic compound arsenobetaine in seafood. *Int Immunopharmacol* 2004, 4, 179-84.
4. Adler, S.; Haskelberg, L.; Bergmann, F., Synthesis of lipophilic chemotherapeuticals. Part II. 4-Alkylaminoazobenzene-4′-arsonic acids. *J. Chem. Soc.* 1940, 576-578.
5. Heijink, A.; Schwartz, J.; Zobitz, M.; Crowder, K.; Lutz, G.; Sibonga, J., Self-assembled monolayer films of phosphonates for bonding RGD to titanium. *Clinical Orthopaedics and Related Research* 2008, 466, 977-984.
6. Mastrangelo, F.; Fioravanti, G.; Quaresima, R.; Vinci, R.; Gherlone, E., Self-Assembled Monolayers (SAMs): Which Perspectives in Implant Dentistry? *Journal of Biomaterials and Nanobiotechnology* 2011, 2, 533-543.
7. Raynor, J.; Capadona, J.; Collard, D.; Petrie, T.; Garcia, A., Polymer brushes and self-assembled monolayers: Versatile platforms to control cell adhesion to biomaterials (Review). *Biointerphases* 2009, 4, FA3-FA16.
8. Zhao, L.; Chu, P.; Zhang, Y.; Wu, Z., Antibacterial Coatings on Titanium Implants. *Journal of Biomedical Materials Research Part B-Applied Biomaterials* 2009, 91B, 470-480.
9. Amalric, J.; Mutin, P.; Guerrero, G.; Ponche, A.; Sotto, A.; Lavigne, J., Phosphonate monolayers functionalized by silver thiolate species as antibacterial nanocoatings on titanium and stainless steel. *Journal of Materials Chemistry* 2009, 19, 141-149.
10. LaFranzo, N. A.; Maurer, J. A., Arsonic Acid Self-Assembled Monolayers Protect Oxide Surfaces from Micronewton Nanomechanical Forces. *Advanced Functional Materials* 2013.
11. Renaudin, A.; Lehmann, M.; Girault, J.; McKerracher, L., Organization of point contacts in neuronal growth cones. *J Neurosci Res* 1999, 55, 458-71.
12. Kleinman, H. K.; Weeks, B. S.; Cannon, F. B.; Sweeney, T. M.; Sephel, G. C.; Clement, B.; Zain, M.; Olson, M. O.; Jucker, M.; Burrous, B. A., Identification of a 110-kDa nonintegrin cell surface laminin-binding protein which recognizes an A chain neurite-promoting peptide. *Arch Biochem Biophys* 1991, 290, 320-5.
13. Brunetti, V.; Maiorano, G.; Rizzello, L.; Sorce, B.; Sabella, S.; Cingolani, R.; Pompa, P., Neurons sense nanoscale roughness with nanometer sensitivity. *Proceedings of the National Academy of Sciences of the United States of America* 2010, 107, 6264-6269.
14. Kolodziej, C. M.; Kim, S. H.; Broyer, R. M.; Saxer, S. S.; Decker, C. G.; Maynard, H. D., Combination of integrin-binding Peptide and growth factor promotes cell adhesion on electron-beam-fabricated patterns. *J Am Chem Soc* 2012, 134, 247-55.

15. Humphries, J.; Wang, P.; Streuli, C.; Geiger, B.; Humphries, M.; Ballestrem, C., Vinculin controls focal adhesion formation by direct interactions with talin and actin. *Journal of Cell Biology* 2007, 179, 1043-1057.
16. Hudalla, G. A.; Murphy, W. L., Using "click" chemistry to prepare SAM substrates to study stem cell adhesion. *Langmuir* 2009, 25, 5737-46.
17. Ferrari, A.; Cecchini, M.; Serresi, M.; Faraci, P.; Pisignano, D.; Beltram, F., Neuronal polarity selection by topography-induced focal adhesion control. *Biomaterials* 2010, 31, 4682-4694.
18. Foong, J. P.; Nguyen, T. V.; Furness, J. B.; Bornstein, J. C.; Young, H. M., Myenteric neurons of the mouse small intestine undergo significant electrophysiological and morphological changes during postnatal development. *J Physiol* 2012, 590, 2375-90.
19. Sang, Q.; Williamson, S.; Young, H. M., Projections of chemically identified myenteric neurons of the small and large intestine of the mouse. *J. Anat.* 1997, 190, 209-222.
20. Sang, Q.; Young, H. M., The identification and chemical coding of cholinergic neurons in the small and large intestine of the mouse. *Anatomical Record* 1998, 251, 185-199.
21. Knöll, B.; Weinl, C.; Nordheim, A.; Bonhoeffer, F., Stripe assay to examine axonal guidance and cell migration. *Nat Protoc* 2007, 2, 1216-24.
22. Bonanomi, D.; Chivatakarn, O.; Bai, G.; Abdesselem, H.; Lettieri, K.; Marquardt, T.; Pierchala, B. A.; Pfaff, S. L., Ret is a multifunctional coreceptor that integrates diffusible- and contact-axon guidance signals. *Cell* 2012, 148, 568-82.
23. Lim, Y. S.; McLaughlin, T.; Sung, T. C.; Santiago, A.; Lee, K. F.; O'Leary, D. D., p75(NTR) mediates ephrin-A reverse signaling required for axon repulsion and mapping. *Neuron* 2008, 59, 746-58.
24. Marler, K. J.; Becker-Barroso, E.; Martinez, A.; Llovera, M.; Wentzel, C.; Poopalasundaram, S.; Hindges, R.; Soriano, E.; Comella, J.; Drescher, U., A TrkB/EphrinA interaction controls retinal axon branching and synaptogenesis. *J Neurosci* 2008, 28, 12700-12.
25. Gierer, A., Model for the retino-tectal projection. *Proc R Soc Lond B Biol Sci* 1983, 218, 77-93.
26. Yates, P. A.; Roskies, A. L.; McLaughlin, T.; O'Leary, D. D., Topographic-specific axon branching controlled by ephrin-As is the critical event in retinotectal map development. *J Neurosci* 2001, 21, 8548-63.
27. McLaughlin, T.; Hindges, R.; O'Leary, D. D., Regulation of axial patterning of the retina and its topographic mapping in the brain. *Curr Opin Neurobiol* 2003, 13, 57-69.

APPENDIX ONE

QUATERNARY AMINES AND IMIDE MONOMERS FOR THE FUNCTIONALIZATION OF GLASS SUBSTRATES

A1.1. Introduction

Surface properties may have large effects on the performance or function of a material in applications from biofouling to prevention of friction and wear. Self-assembled monolayers (SAMs) have been utilized for the functionalization of a variety of substrates including both metal and oxide surfaces. In particular, the functionalization of silicon oxide, or glass is desired because glass substrates are inexpensive, non-conductive, and are found in many commercial products. The functionalization of glass substrates using SAMs has centered on long-chain silanes. However, the propensity of silanes to react quickly with both water and silicon oxide complicates monomer synthesis and purification. Furthermore, silane monomers crosslink on the surface, resulting in a monolayer that lacks robust attachment to the surface, thereby limiting stability. In this work, we synthesized new monomers for the functionalization of glass substrates.

Inspired by the ability of long-chain phosphonic acid monolayers to assemble onto metal oxides and glass, as well as the chemical similarities between arsenic and phosphorus, we attempted to synthesize an alkyl arsonic acid monomer using the method reported by Quick and Adams, Figure A1.1.[1] While this method was unsuccessful, a modified

method as described in Chapter Two, successfully produced the desired molecule and the arsonic acid monolayers have been assembled and characterized.[2]

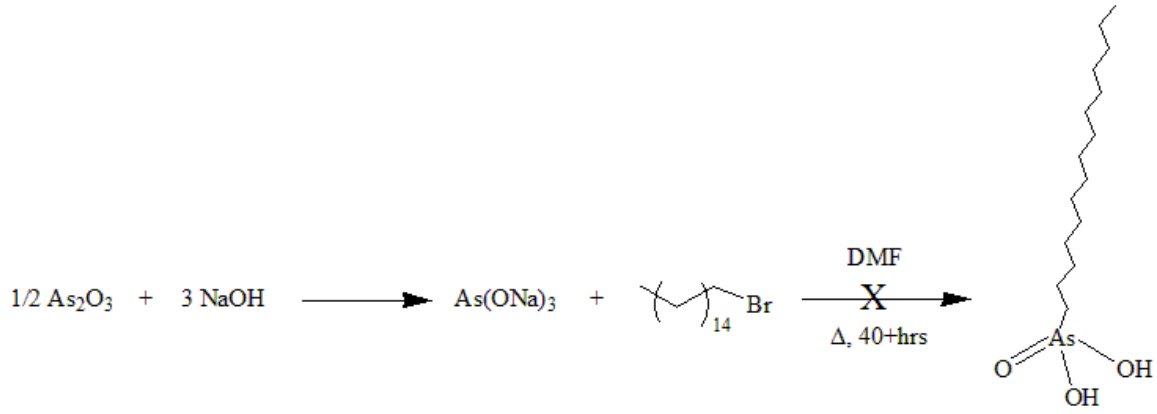

Figure A1.1. Initial method attempted to synthesize arsonic acid monomers was unsuccessful.

Serendipitously, while working to synthesize alkyl arsonic acid species and characterize the resulting product, two different molecules were synthesized that also showed reactivity towards glass substrates. One has a quaternary amine head group, and the other an imide head group.

Quaternary amine cations have been shown to react with glass[3], metal films[3], clay[4], and mica[5-7] in a cation-exchange reaction, replacing potassium and other positive ions on the surface. Reports indicate either monolayers or bilayers of the molecules may be formed on the surface.[5] Once exchanged on the surface, the quaternary amine molecules are strongly bound, with little desorption observed in water over a period of 180 days.[4] While these surfaces have been examined as a means of sequestering and eliminating organic pollutants, they have not been explored as a substrate for cell culture or further functionalized for other applications.[4] We have assembled and characterized

dihexadecylquaternary amine monolayers on glass, and demonstrated that the surfaces are non-toxic as cell-culture substrates.

The other class of glass-reactive species investigated in this work was a dialkyl imide monomer. While imides have not been explored previously as surface coatings, reports of ureas[8], amides[8, 9] and other functional groups[10] assembling in a two-dimensional lattice have allowed us to postulate how an imide molecule might assemble in a similar manner. We have also successfully assembled and characterized imide monolayers on glass substrates.

A1.2. Results and Discussion

A1.2.1. Synthesis and Characterization

While the reaction shown above in Figure A1.1. had previously been reported with shorter-chain alkyl halides, we required longer-chain alkyl halides for our downstream application of preparing well-ordered SAM surfaces. To achieve this, a more organic solvent than reported was required to solubilize the long-chain alkyl halides. This was the only variation from the synthesis reported. The product that resulted was not the arsonic acid, but instead the quaternary ammonium molecule shown in Figure A1.2. Formation results from decomposition of DMF at elevated temperatures of the reaction, followed by subsequent reaction with two alkyl bromide molecules.

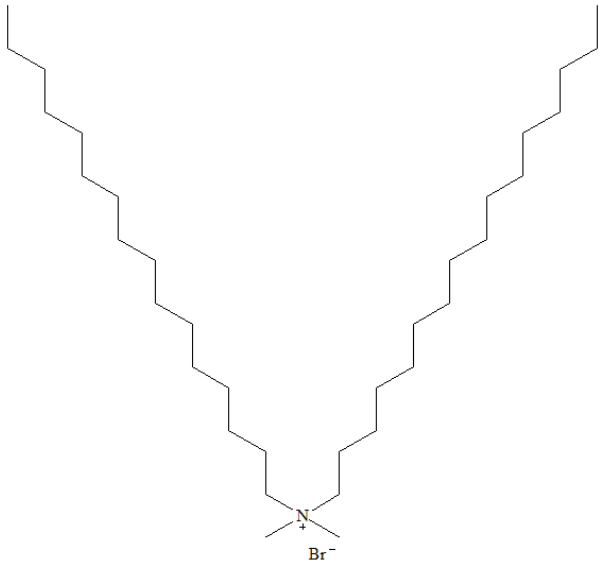

Figure A1.2. Structure of quaternary amine monomer

During our characterization of the quaternary amine salt, we initially postulated that the product was the imide molecule shown below in Figure A1.3., which has the identical mass/charge ratio, *m/z*.

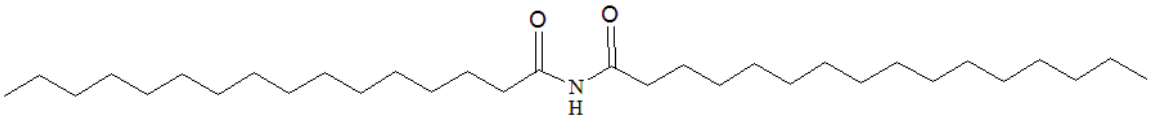

Figure A1.3. Structure of imide monomer

Since other spectral data did not agree with this hypothesis, independent synthesis of the imide molecule was carried out as shown below, Figure A1.4.

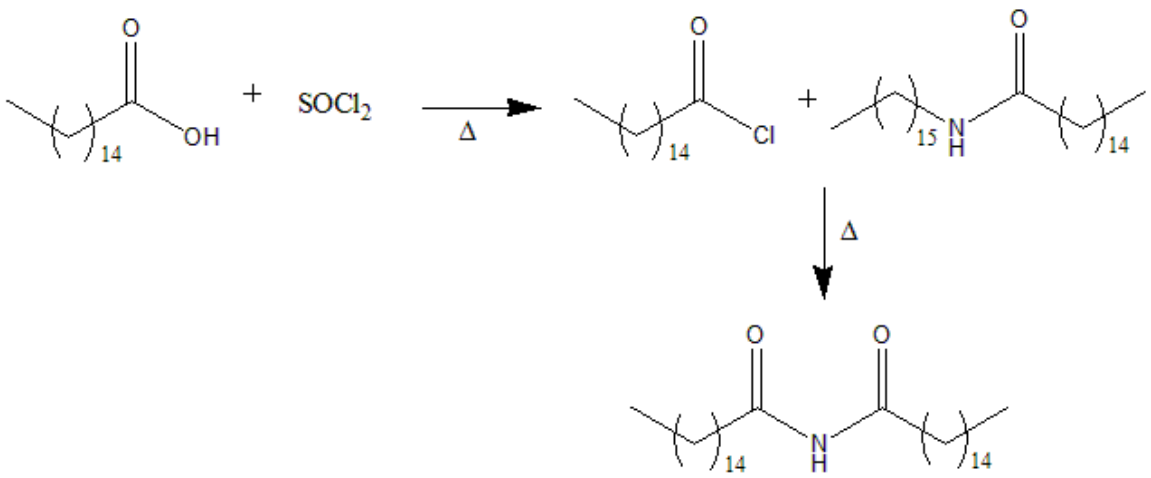

Figure A1.4. Synthesis of the alkyl imide monomer was performed neat.

Both the quaternary amine and imide molecules were examined as monomers for assembly on glass substrates.

A1.2.2. Quaternary Amine Assembly on Glass

The type of substrate, method of substrate cleaning, and monomer setting time were evaluated to determine the ideal conditions for assembly of the quaternary amine monomer. Borosilicate glass was found to be a better substrate than float glass, quartz, titanium dioxide, aluminum (III) oxide, or indium-tin oxide, based on screening by water contact angle and infrared spectroscopy. The monomer was also found to interact strongly with titanium oxide, but this was not further explored. It was also determined that for the borosilicate substrate, cleaning with a basic solution of boiling 1:1 solution of 30 % hydrogen peroxide: ammonium hydroxide generates a deprotonated surface ideal for reaction with the quaternary amine head group, as illustrated in Figure A1.5.

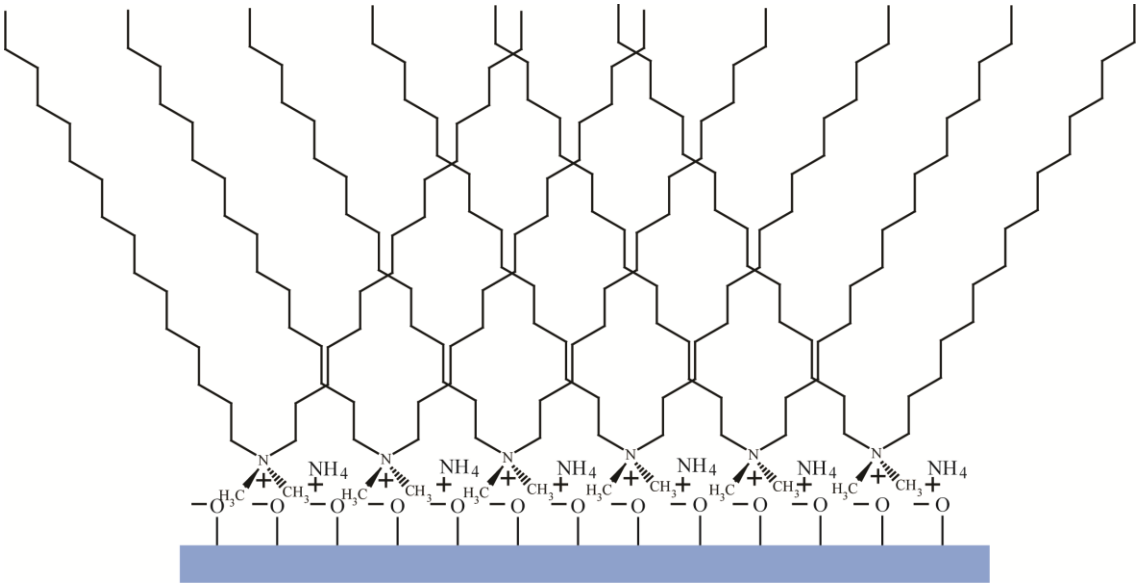

Figure A1.5. The positively charged nitrogen of the quaternary amine head group interacts with deprotonated oxygen atoms on glass.

Two methods to characterize monolayer formation were employed including water contact angle (CA) measurements, and infrared spectroscopy. Water CA values indicate that one hour is not sufficient time for the monolayer to assemble, but soak times of two and three hours generate surfaces with similar hydrophobicity (CA = 50.0˚, 76.4˚, and 77.1˚, respectively). Representative images from these experiments are shown in Figure A1.6.

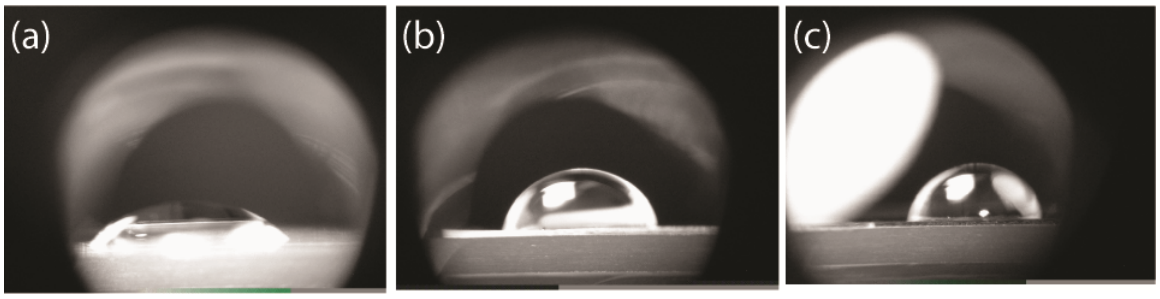

Figure A1.6. Images for water CA on quaternary amine surfaces prepared on borosilicate glass with one hour soak time (a) 50.0˚, two hour soak time (b) 76.4˚, and three hour soak time (c) 77.1˚.

To evaluate the ordering of the monomers on the surface, transmission infrared spectroscopy (IR) was employed. The positions of the asymmetric and symmetric methylene stretches of the alkyl chains is an indication of the ordering of the monolayer. For our analysis, we define "ordered" monolayers as having asymmetric methylene stretching frequencies below 2920 cm^{-1} and symmetric methylene stretching frequencies below 2850 cm^{-1}. These definitions are based on peak positions for crystalline alkane chains in the extended *trans* conformation.[11] For the quaternary amine monolayer assembled using the ideal conditions (base-cleaned substrate, two hour assembly time) on borosilicate glass, the resulting monolayer is not ordered by these standards. However, the % transmission peak intensities observed (values < 1%) are an indication that the surface formed is a monolayer, and not multi-layers of adsorbed molecules on the substrate. Figure A1.7.

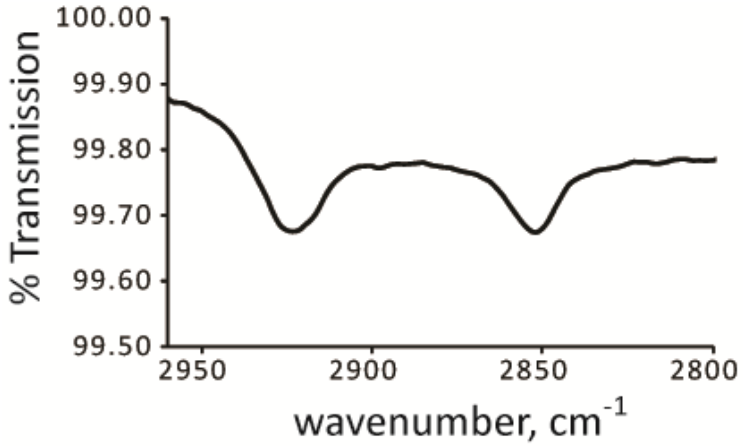

Figure A1.7. Transmission IR for dihexadecyl quaternary amine monolayer prepared on borosilicate glass with a two-hour assembly time shows asymmetric and symmetric methylene stretches at 2923 cm^{-1}, 2852 cm^{-1}, respectively.

CHO-K1 cells were cultured on a quaternary amine monolayer prepared via a two hour assembly time as described above. When the cells are allowed to grow on the surface for a period of 1 week as shown in Figure A1.8., they continue to replicate and grow with no detrimental affects observed from desorption of the monomers, if it is occurring.

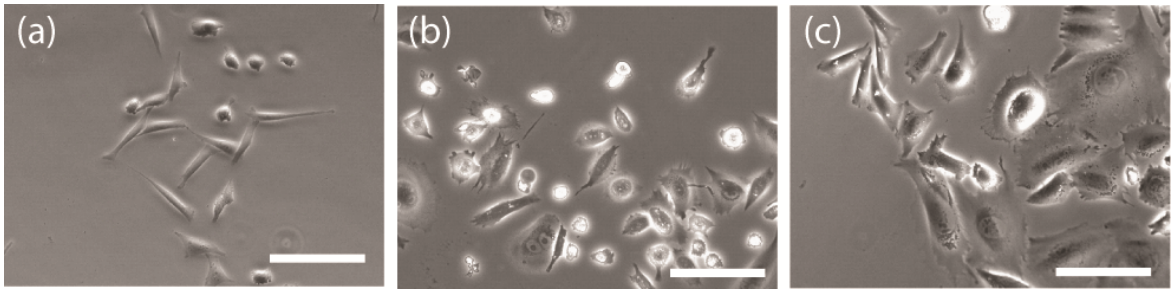

Figure A1.8. CHO-K1 cells cultured on quaternary amine substrates prepared with two hour assembly time survive and replicate over a period of time from 24 hours (a), to 4 days (b), to 1 week (c). Scale bars are 50 μm.

A1.2.3. Imide Assembly on Glass

The preparation of imide-functionalized substrates was found to be more difficult than describe above for the quaternary amine molecule. Again, cleaning borosilicate glass using hydrogen peroxide and ammonium hydroxide worked best for substrate functionalization. However, in order to achieve reactivity with the surface, it was found that the addition of the organic base, ethyl magnesium bromide, in the assembly solution was necessary. The mechanism and effects of this base are not known, however, we believe that the resulting surface is not a three-dimensional assembly as is seen with other monolayer head-groups. Rather, as demonstrated by other groups with urea and amide headgroups, we believe the monolayer assembles as a two-dimensional surface coating as shown in Figure A1.9.

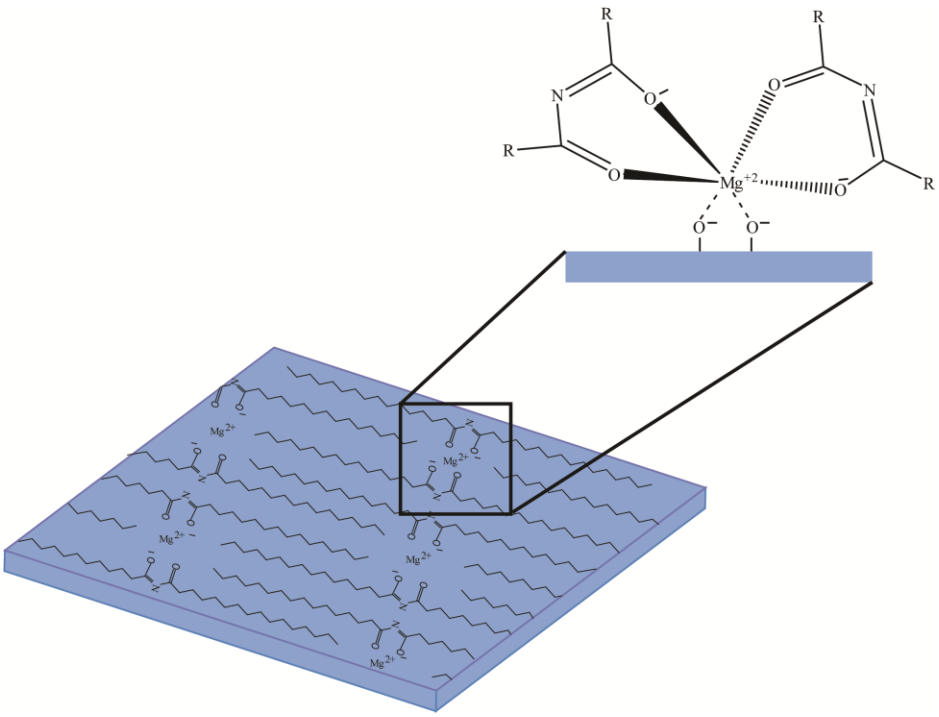

Figure A1.9. Imide molecules assemble in a two-dimensional manner on glass facilitated by interactions between head groups and Mg^{2+} ions and van der Waals interactions between chains.

When characterized by infrared spectroscopy, an asymmetric methylene stretching frequency of 2916 cm^{-1} and symmetric methylene stretching frequency of 2849 cm^{-1} were observed. These peak positions and intensities are indicative of a well-ordered monolayer as described above.

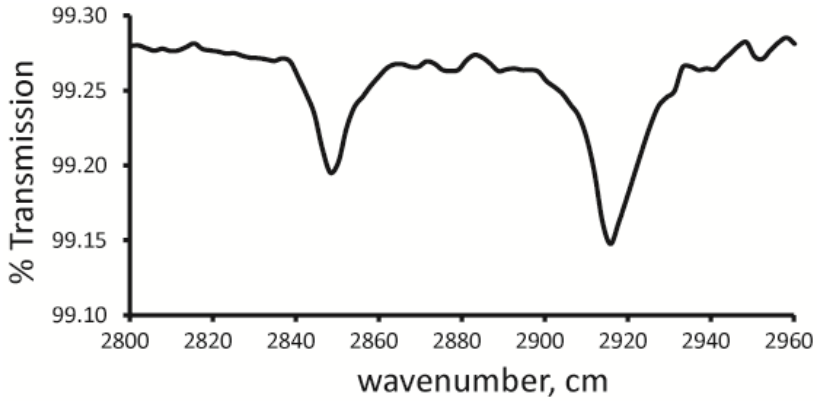

Figure A1.10. Transmission IR of imide monolayers shows peaks representative of well-ordered monolayer on the surface.

When the water contact angle for the surface prepared as described above was measured, the average contact angle measured was 32.7 ˚, indicating that the hydrophobicity of the surface is quite low, as compared to hydrophobic SAM surfaces with water CAs greater than 100 ˚. This suggests that the SAM is assembled in a non-conventional way, and is not only presenting the hydrophobic tail groups on the surface.

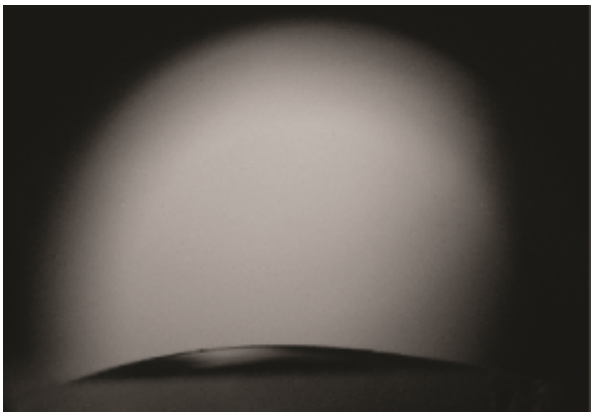

Figure A1.11. Representative image for water contact angle measurement on imide surface.

Due to the results of the water CA measurements, we postulated that the imide-functionalized surface might have protein-resistance similar to ethylene-glycol terminated monolayers, which are also hydrophilic in nature. To evaluate this, a borosilicate glass coverslip was patterned using microcontact printing as described in Chapter One. However, because the surface is glass rather than gold, octadecyltrichlorosilane (OTS) was used as the molecule for inking and stamping. Following stamping, the remaining substrate was backfilled with the imide molecule as described. Fluorescently labeled fibronectin protein was adsorbed to the surface, and then imaged using fluorescent

microscopy. As seen in Figure A1.12., there is a visible pattern on the surface, with the areas corresponding to the OTS showing much higher adsorption of the protein.

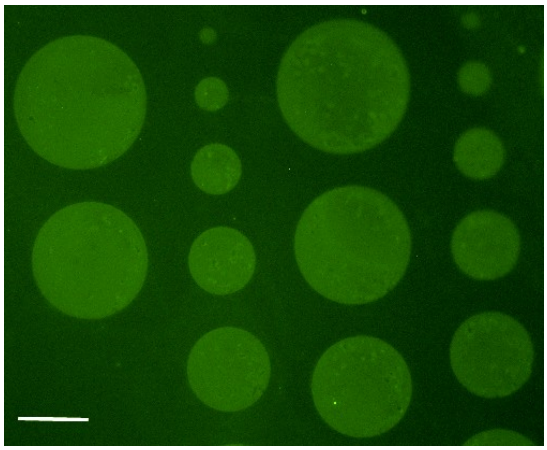

Figure A1.12. Surfaces patterned with octadecyltrichlorosilane (OTS) and backfilled with imide monomer shows a difference in protein-resistance between the two molecules. Scale bar is 200 μm.

While this result does indeed show that there is a difference in protein adsorption between the two molecules on the substrate, it is important to evaluate this further by examining the cell resistance of the imide surface as previously described.[12]

A1.3. Conclusions and Future Directions

The quaternary amine system explored in this work shows promise as a highly-stable surface coating, as desorption of quaternary amines has been shown to be very slow, with little desorption occurring over 180 days.[4] However, this system will require additional method development to obtain well-ordered, well-characterized monolayers. Stability and attachment could be evaluated using the Scotch-tape peel test as described in Chapter Two.[2] In considering applications in biofouling or cell culture substrates as described in

Chapter One, introduction of an ethylene glycol moiety at the end of the chains could yield a protein and cell-resistant surface. As such, a future direction of this work is the development of a synthetic method to attach an ethylene-glycol terminated chain to the amine head group to generate a highly stable monolayer system.

The imide monomer system developed here is a new surface coating that has not been previously reported. While molecules containing similar functional groups such as amides and ureas have been shown to assemble in a two-dimensional fashion on flat, homogenous surfaces such as highly ordered pyrolytic graphite (HOPG), they have not been reported to assemble on glass, which is rougher and more heterogeneous. Characterization of the monolayers on a substrate such as HOPG using scanning tunneling microscopy (STM) as described by other groups who have investigated similar systems, would provide insight into the mode of assembly.[8] Additionally, matrix assisted laser desorption/ionization mass spectrometry (MALDI-MS) of the monolayer reacted with glass substrates will confirm if unanticipated reaction with ethyl magnesium bromide occurs during surface assembly. Preliminary contact angle and protein-resistance studies indicate that there is the potential for the system to show anti-fouling properties, however, this needs to be further explored. While the imide monomer affords an ordered, hydrophobic surface coating the monomers are likely not covalently, nor robustly attached to the surface. Therefore, the stability of the monolayers may be a limitation.

A1.4. Materials and Methods

A1.4.1. Synthesis of Quaternary Amine Monomer

2.02 g (5.11 mmol) of arsenic trioxide (Sigma, St. Louis, MO) was placed in a 250 mL round bottom flask with a stir bar. 5 mL (95.5 mmol) of 50% sodium hydroxide (VWR) was added to the flask at room temperature slowly with stirring. 3.36 mL (31.26 mmol) of hexadecyl bromide (Sigma, St.Louis, MO) in ethanol (Pharmco-AAPER) was added to the flask slowly. The reaction was allowed to reflux in an oil bath for 46.5 hours. Crude product was extracted with chloroform, and solvent removed by rotary evaporation before recrystallization from hexanes to yield a white solid. Yield: 1.29 g (1.68%). ^{1}H NMR in $CDCl_3$ (300 mHz Varian) – 3.52 ppm (t), 3.39 (s), 1.71 (m), 1.37 (m), 1.26 (m), 0.89 (t). LR-ESI (positive mode) Mass Spectrometry (Washington University Mass Spectrometry Facility, St. Louis, MO) analysis – $C_{34}H_{72}N^{+}$; expected: 494.57 m/z, obtained: 494.56 m/z. Elemental analysis by C,H,N combustion analysis was performed for $C_{34}H_{72}NBr$ salt; Theoretical: C, 71.04; H, 12.62; N, 2.44, Actual: C,71.48; H, 13.08; N,2.67. Arsenic composition was obtained by inductively-coupled plasma analysis (ICP-MS) – Found 0.031%, or negligible amount (EA and ICP-MS by University of Illinois, Urbana-Champaign Analytical Laboratory).

A1.4.2. Surface Preparation and Assembly of Quaternary Amine Monolayers

Soda lime glass microscope slides (VWR) for metal oxide deposition were cleaned with plasma oxygen with a Femto plasma oxidizer (Diener Electronic) for 10 minutes on each side. The slides were subsequently rinsed with ethanol, deionized water, and ethanol, drying with nitrogen gas following each rinse. Titanium (50 Å) and metal dioxide (100

Å) were deposited using an electron beam evaporator at a rate of 0.1 Å/s Oxide surfaces of titanium dioxide, aluminum (III) oxide, and indium-tin oxide were utilized in this study. Glass substrates including soda lime glass microscope slides (VWR), borosilicate glass coverslips (No. 1, 25 mm, VWR), borosilicate glass microscope slides (Pearl), quartz microscope slides (Alfa Aesar) and float glass were cleaned by soaking in piranha solution (4:7 30% hydrogen peroxide : concentrated sulfuric acid) or a solution of boiling 1:1 30% hydrogen peroxide: ammonium hydroxide for 2 hours followed by a thorough rinse in deionized water, rinse with ethanol and a final rinse with deionized water before drying with nitrogen gas. Substrates were soaked in a 7 mM solution of quaternary amine monomer in chloroform from 1-3 hours, removed and rinsed with ethanol, deionized water, and ethanol, drying with nitrogen gas following each rinse.

A1.4.3. Synthesis of Imide Monomer

0.517 g (2.02 mmol) palmitic acid was added to a 10 mL round bottom flask. The flask was warmed to 35 ºC in an oil bath. 0.14 mL (1.92 mmol) thionyl chloride was added slowly while stirring. A short reflux condenser was attached and the reaction was allowed to proceed for 6.5 hours at 100ºC. Flask was cooled to room temperature and 0.510 g (2.00 mmol) hexadecanamide was added to the flask. A vacuum adapter was placed on the flask and attached to house vacuum. The reaction was heated at 130 ºC in an oil bath for 6.5 hours under vacuum (to remove hydrogen chloride gas as generated). Product was purified by silica plug chromatography in 10:1 chloroform: hexanes. Solvent was removed from product by rotary evaporation to yield a white solid. Product was analyzed by ^{1}H NMR in $CDCl_3$ (300 mHz Varian) - 7.90 ppm (s); 2.60 ppm (t); 2.35 ppm

(q); 1.29 ppm (m); 0.88 ppm (t). LR-ESI (positive mode) Mass Spectrometry (Washington University Mass Spectrometry Facility, St. Louis, MO) analysis – $C_{32}H_{63}NO_2+H^+$; expected: 494.49 m/z, obtained: 494.49 m/z.

A1.4.4. Surface Preparation and Assembly of Imide Monolayers

Dihexadecyl imide synthesized as described above was added to a jar with a septa and stir bar, sealed, and purged with argon. The molecule was dissolved in 5 mL dry methylene chloride to a final concentration of 1.1 mM and 1 drop of 1 M ethyl magnesium bromide in tetrahydrofuran was added to the jar with stirring. The jar was opened to air and borosilicate glass slides (prepared by boiling in a 1:1 solution of 30% hydrogen peroxide: ammonium hydroxide as described above) were added to the solution. Multiple assembly/soak times were evaluated from two hours to five hours. After soaking, slides were thoroughly rinsed in deionized water, rinsed with ethanol and a finally rinsed with deionized water before drying with nitrogen gas. Transmission infrared spectra and water contact angles were collected as described above.

A1.4.5. Characterization of Monolayers

FT-IR spectra were collected on a 670 Nicolet Fourier-Transform Infrared Spectrometer with Smart SAGA (spectral apertured grazing angle) reflectance accessory (Thermo Scientific). Water contact angle (CA) measurements were made at room temperature using a home-built apparatus consisting of a stage, microscope objective and digital camera. Images were taken with a digital camera and analyzed using the BIGDrop

Analysis plugin for ImageJ with the Low Bond Axisymmetric Drop Shape Analysis model.[13]

For cell culture experiments, surfaces were prepared on glass coverslips as described above with a two hour assembly time. 20 μg/mL of human plasma fibronectin solution in Dulbecco's Phosphate Buffered Saline (DPBS, Gibco/Life Technologies) at 37 °C for 1 h. Excess protein was removed by rinsing with DPBS (3x) and the coverslip was covered with fresh DPBS. CHO-K1 cells (ATCC) were detached using TrypLE Express (Invitrogen), followed by resuspension in Dulbecco's Modified Eagle Medium (DMEM, low glucose 1X, glutamax, 1 g L^{-1} D-glucose, 110 mg L^{-1} sodium pyruvate, 10% FBS, 1% penicillin/streptomycin -10,000 units mL^{-1} Penicillin G Sodium and 10,000 μg mL^{-1} Streptomycin Sulfate in 0.85% saline, Invitrogen), and counted using a hemacytometer (Bright-Line, Hausser Scientific). After rinsing the surface with DPBS, approximately 30,000 cells were applied in 1 mL of DMEM. Cells were grown at 37 °C and 5% CO_2. Cultures were visualized using live-cell inverted microscopy at 24h, 96h, and 1 week on a Nikon TE2000-PFS microscope running NIS-Elements imaging software and equipped with a Photometrics CoolSNAP camera, and an In Vivo Scientific incubator chamber held at 37 ˚C, 5% CO_2.

For patterned surfaces, a 10 mM solution of octadecyltrichlorosilane (OTS, Sigma) in toluene was stamped by micro-contact printing onto glass coverslips as previously described.[12] The background of the surface was backfilled with 1.1 mM imide monomer solution for five hours as described above. Patterned coverslips were coated with Oregon-green 488 labeled fibronectin (20 μg /mL, Invitrogen) in Dulbecco's Phosphate Buffered Saline (DPBS, Gibco/Life Technologies) at 37 °C for 1 h. Excess protein was

removed by rinsing with DPBS (3x) and the coverslip was covered with fresh DPBS. Fluorescent protein images were obtained using a Nikon TE2000-PFS microscope running NIS-Elements imaging software and equipped with an EXFO X-Cite UV illuminator and Photometrics CoolSNAP camera.

A1.5. References

1. Quick, A. J.; Adams, R., Aliphatic Arsonic and Arsinic Acids, and Aliphatic-aromatic Arsinic Acids. *J. Am. Chem. Soc* 1922, 44, 805-816.
2. LaFranzo, N. A.; Maurer, J. A., Arsonic Acid Self-Assembled Monolayers Protect Oxide Surfaces from Micronewton Nanomechanical Forces. *Advanced Functional Materials* 2012, n/a-n/a.
3. Kivel, J.; Albers, F. C.; Olsen, D. A.; Johnson, R. E., Surface Areas by Adsorption of a Quaternary Ammonium Halide from Aquesous Solution. *The Journal of Physical Chemistry* 1963, 67, 1235-1238.
4. Zhang, Z. Z.; Sparks, D. L.; Scrivner, N. C., Sorption and desorption of quaternary amine cations on clays. *Environmental Science & Technology* 1993, 27, 1625-1631.
5. Blom, A.; Warr, G.; Wanless, E., Growth of double-chained cationic surfactant films on mica. *Australian Journal of Chemistry* 2006, 59, 381-385.
6. Li, B.; Fujii, M.; Fukada, K.; Kato, T.; Seimiya, T., Time dependent anchoring of adsorbed cationic surfactant molecules at mice/solution interface. *Journal of Colloid and Interface Science* 1999, 209, 25-30.
7. Fujii, M.; Li, B.; Fukada, K.; Kato, T.; Seimiya, T., Two-dimensional arrangements of adsorbed alkylammonium halides on cleaved mica surface. *Langmuir* 2001, 17, 1138-1142.
8. Dreger, K.; Zou, B.; Mu, Z.; Galla, H.; Chi, L.; Fuchs, H.; Schafer, H., Synthesis and surface properties of new ureas and amides at different interfaces. *Langmuir* 2006, 22, 1619-1625.
9. Zou, B.; Dreger, K.; Muck-Lichtenfeld, C.; Grimme, S.; Schafer, H.; Fuchs, H.; Chi, L., Simple and complex lattices of N-alkyl fatty acid amides on a highly oriented pyrolytic graphite surface. *Langmuir* 2005, 21, 1364-1370.
10. Jester, S.; Idelson, A.; Schmitz, D.; Eberhagen, F.; Hoger, S., Shape-Persistent Linear, Kinked, and Cyclic Oligo(phenylene-ethynylene-butadiynylene)s: Self-Assembled Monolayers. *Langmuir* 2011, 27, 8205-8215.
11. Snyder, R. G.; Schachtschneider, J. H., Vibrational analysis of the n-paraffins—I: Assignments of infrared bands in the spectra of C3H8 through n-C19H40. *Spectrochimica Acta* 1963, 19, 85-116.

12. Yanker, D.; Maurer, J., Direct printing of trichlorosilanes on glass for selective protein adsorption and cell growth. *Molecular Biosystems* 2008, 4, 502-504.
13. Stalder, A.; Kulik, G.; Sage, D.; Barbieri, L.; Hoffmann, P., A snake-based approach to accurate determination of both contact points and contact angles. *Colloids and Surfaces a-Physicochemical and Engineering Aspects* 2006, 286, 92-103.

APPENDIX TWO

DNA MANIPULATION AND EXPRESSION OF MOUSE SLIT 2 GENE AND PROTEIN DOMAINS

A2.1. Introduction

During development, axons and dendrites of neurons are guided to their synaptic partners by a complex map of cues. The cues, including both proteins and small molecules, interact with receptors on the growth cone, located on the tip of the growing edge of the neurite. Generally, the cues are thought to operate by the following mechanisms: contact attraction, contact repulsion, diffusible chemoattraction, and diffusible chemorepulsion as illustrated in Figure A2.1.[1] In contact attraction or repulsion, the growth cone interacts directly with a stationary guidance cue. This cue can be in the form of a protein that is anchored to surrounding cells or tissue, or it may be a physical cue such as a change in the modulus of the surrounding tissue or a physical barrier preventing growth.[2] In diffusible chemoattraction or diffusible chemorepulsion, the growth cone interacts with diffusible cues that are excreted by the surrounding cells. These are often found in concentration gradients sensed by the growth cone.[3]

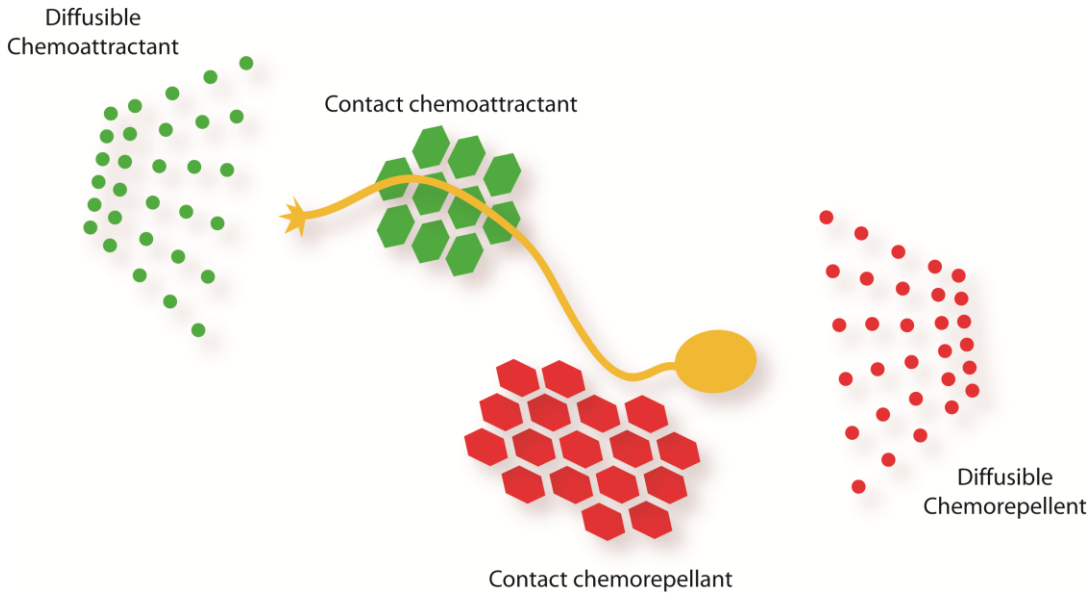

Figure A2.1. Guidance cues are believed to act via four basic mechanisms: diffusible chemoattraction, diffusible chemorepulsion, contact attraction and contact repulsion.

The neurites follow these cues along distinct, stereotypical pathways to their target and make few navigational errors.[1] Multiple families of proteins involved in this process have been identified, and some may exist that have not yet been identified.[4] There is still much to be learned about the mechanism of axon guidance, particularly at midline crossing points such as within the spinal cord or optic chiasm.[1] At these junctions, axons must follow attractive cues up to the crossing point, and subsequently be repelled away from the same region to avoid undesired re-crossing of the midline as demonstrated in Figure A2.2.[5]

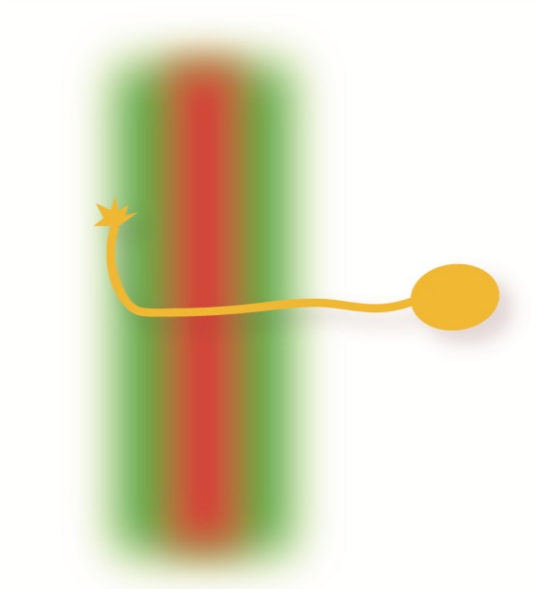

Figure A2.2. At the midline, growth cones encounter overlaid gradients of Slit (red) and Netrin (green) proteins. The Netrin proteins encourage growth of the neuron towards the midline, and after crossing, the Slit proteins repel the neuron away and prevent re-crossing.

The Slit family of proteins, and their complementary Robo receptors, have been found to play an integral role in the repulsion process that directs axons away from the midline.[6-8] Slits are large, secreted proteins that are highly charged, and often associate with proteoglycans such as the heparin sulfate proteoglycan, syndecan.[9-12] In zebrafish, alternative splice variants diversify the proteins that are observed *in vivo*.[13-16] In mice as well as humans, the family includes 3 highly homologous proteins, known as Slit 1, Slit 2 and Slit 3. Slit 2 is the most well-studied of the group. Some domains seen in Slit proteins, as illustrated for Slit 2 in Figure A2.3., such as the epidermal-growth factor like (EGF) domain are common to other guidance cues as well.[17]

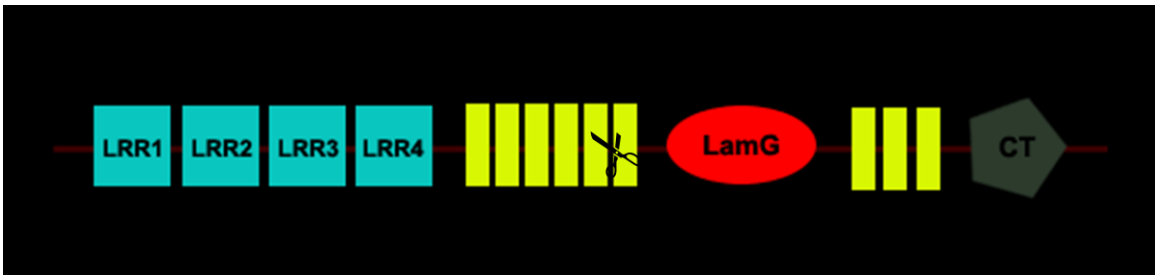

Figure A2.3. The protein motifs observed in the Slit 2 protein include four leucine-rich repeats (LRR), two epidermal-growth factor like (EGF) domains with multiple repeats in each, a laminin-G (LamG) domain and a cystein knot at the c-terminus of the protein. The proteolytic cleavage site within the first EGF domain is indicated by a scissor icon.

Mutagenesis and crystallographic data suggest that the binding site for Slit 2 to its receptor, Robo, is found within the 2nd leucine-rich repeat domain, LRR2.[18, 19] The protein is known to have a proteolytic cleavage point located in the first EGF domain.[20] The N-terminal half of the protein, containing the putative receptor binding domain is generally regarded as the active half of the protein.[20] However, it is possible that the domains on the C-terminal half of the protein have activity, but they have not been explored in detail.

The response of neurons to the guidance cue Slit 2 is highly dynamic. Variations between neuronal populations, along with variations of response depending on the time-point during development are observed.[12, 21] When neurons are exposed to Slit proteins in combination with other guidance cues and small molecules, some have been shown to modulate neuronal responses. Notably, the extracellular proteins netrin, laminin, and stromal-cell derived factor-1 have been shown to modulate the axonal response to Slit.[12, 22, 23] Heparin sulfate proteoglycans and heparan sulfates are also known to be required for and modulators of Slit signaling.[9-11, 24, 25] Intracellular cGMP levels and calcium

signaling, along with other downstream signaling molecules, direct axon growth by initiating cytoskeletal rearrangement and growth.[12, 26]

Each of the Slit proteins has a specific expression map in the brain that changes as development progresses. Notably, neurons do not often encounter a single concentration of proteins on the surface, but rather encounter a gradient of proteins.[15, 21, 27] The concentration and spatial pattern of the protein, along with overlaid patterns of other guidance cues direct neurons to develop proper connections. Due to additional roles outside of axon guidance including cell migration and a role in cancer, preparation of an animal model to study this family of cues is not trivial.[22, 28] Single knockout and knockdown animal models, where protein expression is halted or decreased, results in mis-wiring of neurons.[13, 15] Animal models where multiple proteins are knocked-out are not viable, and do not survive.

This complex guidance map therefore, is an ideal system to study using *in vitro* techniques. As such, development of an *in vitro* platform for examining these cues allows for simple screening and manipulation of experimental conditions. For these studies, it is important to utilize DNA manipulation and protein expression techniques to obtain recombinant, purified proteins. Moreover, using recombinant techniques, we are able to clone cDNA encoding individual protein domains, and express these separate from the full-length protein. In this way, we are able to probe the activity of the individual domains. As well, DNA manipulation allows for the incorporation of affinity tags, facilitating purification of the proteins and identification during western blotting

analysis. The experiments described here have generated individual constructs for expression and purification of multiple mouse Slit 2 protein domains, which may be utilized for *in vitro* studies of their activity. From the ClustalW2 sequence alignment of the human, mouse, and rat Slit 2 homologues of the Drosophila Slit 2 protein, the percent identity of the proteins are compared. The results of this alignment are tabulated in Figure A2.4.

Sequence 1	Sequence 2	Identity
humanSlit2	mouseSlit2	96%
humanSlit2	ratSlit2	96%
mouseSlit2	ratSlit2	98%

Figure A2.4. The % identity generated by pairwise alignment of the human, mouse and rat Slit 2 protein homologues demonstrates the high sequence homology observed between organisms.

The high sequence identity between these organisms demonstrates that the Slit 2 protein has been conserved across organisms. We have chosen to utilize the mouse model for harvesting of neurons, along with cDNA encoding the mouse protein for DNA manipulation and protein expression.

A2.2. Results and Discussion

A1.2.1. DNA Manipulation

cDNA constructs encoding isolated protein domains including LRR1, LRR2, LRR3, LRR4, EGF1, EGF2 were generated in the pTriEx-4 Neo expression vector. Final

constructs in pTriEx-4 Neo contained N-terminal His and S-tags as well as C-terminal HSV and His-tags.

A2.2.2. Protein Expression

To optimize experimental conditions to produce the highest yield of soluble protein, a series of small-scale (50 mL) test expressions for the constructs encoding LRR2 and LRR4 in pTriEx-4 Neo were performed in the Rosetta 2 (DE3) cell strain. Following induction, bacterial cells were allowed to grow for either three or six hours at either 30 ºC or 37 ºC. The supernatant from the whole-cell lysate was probed via anti-HSV Western blot, and the results are shown in Figure A2.5. below. Unfortunately, ideal conditions for protein expression cannot be concluded from this experiment, nor is the expression shown here reproducible.

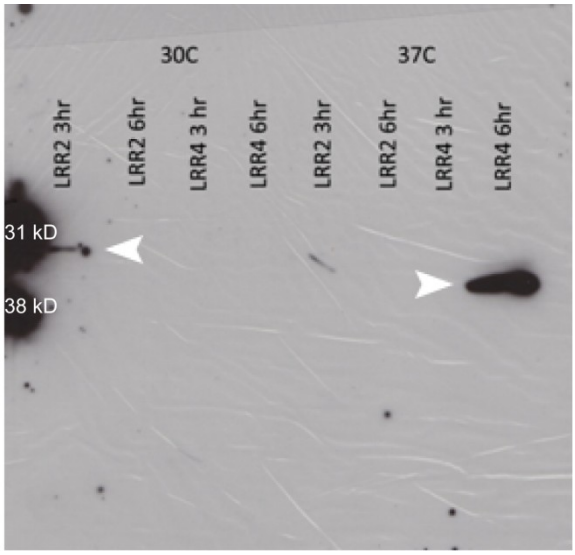

Figure A2.5. Rosetta 2 (DE3) test expressions of LRR2 and LRR4 in pTriEx-4 Neo yield some soluble protein as indicated by the white arrow heads in the anti-HSV Western blot. Molecular weight markers were marked by glow marker on the membrane and are visible on the film. Predicted molecular weights for these protein (including tags) are LRR2: 33.7 kD; LRR4: 30.5 kD

The cell strain BL21 was also evaluated in an attempt to optimize protein expression of the mouse Slit 2 domains. While the reliable expression of the leucine-rich regions (LRR) domains was unsuccessful in this cell strain, the EGF1 domain showed high expression levels, and was successfully purified by metal-affinity chromatography with the 6-His tags on the protein.

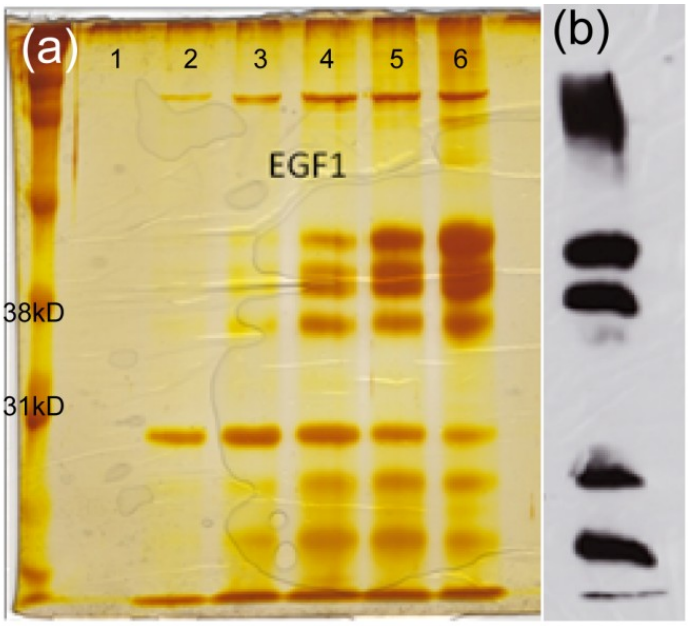

Figure A2.6. (a) The construct encoding the EGF1 domain in pTriEx-4 Neo vector was expressed in BL21 bacterial cells and purified via nickle-affinity chromatography. Samples from collected 1 mL fractions were separated by SDS-PAGE and silver stained to visualize protein. The predicted molecular weight for the EGF1 monomer including tags is 35.9 kD. (b) Purified EGF1 protein is probed by Anti-HSV Western blot. Various putative multimerization states for the protein are observed, as are seen in the silver stained gel in (a).

A band at the expected 35.9 kD region is not observed in the silver stained SDS-PAGE gel above, Figure A2.6.(a). However, EGF-like domains in other proteins have been shown to mediate multimerization.[29, 30] Therefore, the bands observed may be various multimerization states of the EGF1 protein domain. Probing the sample in Lane 6 via

anti-HSV Western blot, Figure A2.6.(b), confirms that the protein purified in this experiment contains the HSV-tag. Since the protein is a mammalian protein, expression in mammalian cells is also desirable to ensure proper post-translational modifications. Trojene transfection and Nucleofector transfection of CHO-K1 cells were evaluated. Using Trojene, a lipid transfection reagent, CHO-K1 cells were transfected with both the LRR2 and LRR4 domains in the pTriEx-4 Neo expression vector for 48 hours. Media was replaced and cells were selected with 1 mg/mL G418 antibiotic for 1 week, or harvested as transiently transfected cells after Trojene treatment. Cell lysates including both soluble and insoluble fractions from these experiments were separated by SDS-PAGE and probed by anti-HSV Western blot. From this analysis, no protein expression was observed in either the soluble or insoluble fraction.

Nucleofector technology, which delivers DNA to the nucleus of the cells via mild electric pulses, is thought to allow for expression of higher yields of protein. Transient expression of the LRR2, LRR4, and EGF1 domains in the pTriEx-4 Neo vector in CHO-K1 cells was performed, and the cell lysate evaluated for protein expression. Following separation by SDS-PAGE, anti-HSV Western blot reveals that only the EGF1 domain is found in the soluble fraction as shown in Figure A2.7. Interestingly, the EGF1 domain does not show the same multimerization as is observed when the protein is expressed in bacterial cells. Unfortunately, using these experimental conditions there is still no visible protein observed for the LRR2 and LRR4 domains in the soluble lysate. In the insoluble fraction, some LRR2 protein is observed with apparent multimerization. However,

following expression, this protein was likely not packaged in its native structure. Therefore, little can be interpreted about the multimerization state of this protein.

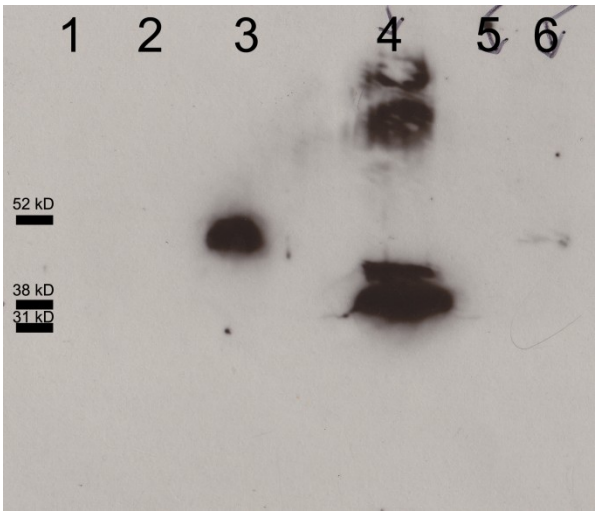

Figure A2.7. Only EGF1 is found in the soluble fraction of the cell lysate following expression in CHO-K1 cells transfected with pTriEx-4 Neo constructs using Nucleofector method. LRR2 is expressed but is found in the insoluble cell pellet following cell lysis. This anti-HSV Western blot of cell lysate and pellets shown here includes Lane 1: LRR2 soluble: Lane 2: LRR4 soluble; Lane 3: EGF1 soluble; Lane 4: LRR2 insoluble; Lane 5: LRR4 insoluble; Lane 6: EGF1 insoluble.

A2.3. Conclusions and Future Directions

We have generated multiple expression constructs containing cDNA for various domains of the mouse Slit 2 protein. It will be important to optimize expression and purification conditions for each domain. As discussed in this work, finding appropriate expression conditions of these domains is not trivial. Furthermore, if protein expression levels are low, purification will be difficult as well. In particular, expression in mammalian cells, where post-translational modifications are performed but protein yields are lower, is desirable.

Alternatively, use of the pTYB2 vector, which allows for incorporation of a bio-orthogonal moiety at the C-terminus of the protein, eliminates the need to optimize purification methodologies for our applications.[31] As described in Chapter One, substrates may be functionalized with mixed self-assembled monolayers terminated with a reactive group that can covalently attach the labeled protein to the substrate, but prevents the non-specific adsorption of other proteins. With this technique, when the complex mixture of proteins contained in the cell lysate is applied to the monolayer substrate, only the target protein expressed with the C-terminal tag from the pTYB2 vector will attach to the surface, and the remaining proteins may be rinsed away. Unfortunately, however, this system is currently designed for bacterial expression of proteins and as such, DNA manipulation to insert mammalian promoters into the expression vector is required.

Once these parameters have been optimized, the recombinant protein may be used for *in vitro* experiments where the activity of an individual protein domain, or combinations of these domains may be studied. It will be important to consider the effects of protein concentration on the activity, which may be achieved by the creation of punctuate protein gradients using soft-lithography (described previously in Chapter One) or smooth protein gradients using monolayer photo-ablation.[32]

A2.4. Materials and Methods

A2.4.1. Sequence Alignment

The National Center for Biotechnology Information database[33] was mined to identify the protein sequences for mouse, rat and human homologues of Drosophila Slit 1, Slit 2 and Slit 3 proteins. Accession numbers for slit homolog 1 [*Mus musculus*], slit homolog 2 [*Mus musculus*], and slit homolog 3 [*Mus musculus*] are NP_056563, NP_848919 and NP_035542, respectively. Accession numbers for slit homolog 1 [*Homo sapiens*], slit homolog 2 [*Homo sapiens*], and slit homolog 3 [*Homo sapiens*] are NP_003052, NP_004778 and NP_003053, respectively. Accession numbers for slit homolog 1 [*Rattus norvegicus*], slit homolog 2 (predicted) [*Rattus norvegicus*], and slit homolog 3 [*Rattus norvegicus*] are NP_075242, XP_346465 and NP_112611, respectively.

Slit 2 protein sequences from each organism were aligned pairwise using standard parameters of ClustalW2 multiple sequence alignment.[34]

A2.4.2. DNA Template Preparation

Slit 1 (Clone ID: 6827560, Accession: BC062091, vector: pYX-ASC), Slit 2 (Clone ID: 9087690, Accession: BC150779, vector: pCR-XL-TOPO), and Slit 3 (Clone ID: 9087691, Accession: BC150780, vector: pCR-XL-TOPO) clones were obtained from OpenBioSystems (Thermo Fisher Scientific) through the I.M.A.G.E. consortium.

A2.4.3. Protein Domain Prediction

The SMART (Simple, Modular, Architecture, Research Tool) program[35, 36] was utilized to predict common protein domains within Slit 2 protein (Figure A2.3). The amino acids corresponding to each domain are as follows: LRR1 27-197; LRR2 209-417; LRR3 434-717; LRR4 730-912; EGF1 925-1159; and EGF2 1348-1461.

A2.4.4. DNA Manipulation

The following primers were designed to amplify the regions predicted by the SMART program as described above:

LRR1: 5'–TTAAGGATCCTGCGTGCCCGGCCC–3' and 5'–AATTGCGGCCGCATGGTTGAAACTTGCC–3'

LRR2: 5'–TTAAGGATCCTAACAACTTGTACTGCG–3' and 5'–AATTGCGGCCGCCTTGGCAACCGTCTGAAGC–3'

LRR3: 5'–TTAAGGATCCTAATCCTTTCATTTGTG–3' and 5'–AATTGCGGCCGCATCACAGGTGAAGTCC–3'

LRR4: 5 –TTAAGGATCCTCGTTGTCCTTCTGAATGTACCTGC–3' and 5'–AATTGCGGCCGCTTGACATGTAAATTTTTTGGAGGG –3'

EGF1: 5'–TTAAGGATCCTCCCTGCTTATCAAATCC–3' and 5'–AATTGCGGCCGCCTGGCATATTGGTTC–3'

EGF2: 5'–TTAAGGATCCTCCATGCCACAAGAAAGTATGTGC–3' and 5'–GCGGCCGCAATTATCACAGCTGTCCCCGG–3'

Polymerase chain reaction (PCR) was performed with template cDNA using the primers described above. *PfuUltra* High-Fidelity DNA Polymerase AD (Stratagene – Agilent Technologies) was utilized under the conditions described by the supplier. PCR fragments were purified using QIAquick Gel Extraction Kit (Qiagen Inc.) after separation

on 1% agarose (GenePure, LE/ISC Bioexpress) gel in TAE buffer. The purified PCR fragments and pTriEx-4 Neo template vector were digested with BamHI (Promega Corp.) and NotI (New England Biolabs) restriction enzymes at 37ºC for 4 hours. Digested DNA was purified following the Nucleotide Removal protocol of the QIAquick Kit (Qiagen Inc.) to remove enzymes and salts. Target vector and inserts were ligated with T4 DNA ligase (New England Biolabs) at 19 ºC for 72 hours. Ligation reactions were transformed into electro-competent *E. coli* XL10-Gold Ultracompetent Cells (Stratagene – Agilent Technologies). Clones were screened by restriction enzyme digest using ApaI (Promega Corp.), and constructs were confirmed by automated sequencing with ABI Prism BigDye Terminator v3.1 (Applied Biosystems) and the T7 primer. Sequence data was aligned with predicted sequence information in the ClustalW2 program.[34]

A2.4.5. Bacterial Protein Expression

Clones previously confirmed by sequencing were transformed into electro-competent Rosetta 2 (DE3) *E.coli* cells (Novagen - EMD Chemicals) or electro-competent BL21 (DE3) *E.coli* cells (Novagen - EMD Chemicals) and plated on LB/Agar media containing Ampicillin. A single colony was selected and a 5 mL culture was grown at 37 ˚C, 250 rpm in Terrific Broth (TB) media (EMD Chemicals) containing Ampicillin, and diluted into 50 mL after 8 hours. This 50 mL starter culture was grown for 14 hours at 37 ºC, 250 rpm and then diluted into 500 mL TB media containing Ampicillin. For small-scale test expressions, the 50 mL starter culture was used for protein expression. In both cases, the cultures were grown to OD_{600} = 0.600. In both culture scales, when OD_{600}=0.600

cells were induced with Isopropyl-β-D-thio-galactoside (IPTG) at a final concentration of 1 mM and grown at either 30 ºC or 37 ºC for a period between 3-8 hours.

A2.4.6. Mammalian Protein Expression

A2.4.6.1. Trojene Transfection

CHO-K1 cells (ATCC) were grown to confluence in a humidified incubator at 37˚C, 5% CO_2 in fully-supplemented low-glucose Dulbecco's Modified Eagle Medium (DMEM) containing DMEM, low glucose 1X, glutamax, 1 g/L D-glucose, 110 mg/L sodium pyruvate, 10% FBS, 1% penicillin/streptomycin (10,000 units/mL Penicillin G Sodium and 10,000 μg/mL Streptomycin Sulfate in 0.85% saline, Invitrogen, Corp.). Media was replaced immediately before the transfection. Trojene (Avanti Polar Lipids) Transfection Procedure was followed according to the manufacturer's recommendations. Transfection solution was added to the cell culture dish and allowed to incubate for 48 hours in a humified incubator at 37˚C, 5% CO_2. Transfected CHO-K1 cells were selected in media containing 1mg/mL G418 (GIBCO/Invitrogen Corp.) antibiotic. Cells were grown to confluence and passaged as appropriate to form stable expression lines over a 1 week period. Transient transfects where no selection media was applied were also prepared.

A2.4.6.2. Nucleofection

Manufacturer's protocol from "Amaxa Mouse Neuron Nucleofector Kit" (Lonza/Amaxa) was followed using homemade buffer solutions (J. Weber Lab – Washington University in St. Louis) consisting of: Solution 1: 2 g ATP-disodium salt, 1.2 g magnesium chloride

hexahydrate, 10 mL water – filter sterilized and stored as 80µL aliquots at -20 ˚C. Solution 2: 6 g potassium hydrogen phosphate, 0.6 g sodium bicarbonate, 0.2 g glucose in 500 mL water pH=7.4, filter sterilized and stored as 4 mL aliquots at -20 ˚C. Before use, 1 aliquot of each solution was mixed to produce the "nucleofector solution". CHO-K1 cells were treated with TrypLE Express (Invitrogen, Crop.) for 5 minutes and centrifuged at 300 x g for 10 minutes. Media was discarded and cells were resuspended in 100 µL of nucleofector solution at room temperature containing 6 µg of desired construct. Cell suspension containing 1.0 x 10^6 cells was immediately placed into a 2 mm electroporation cuvette, tapped to remove bubbles and then pulsed using the U-023 program on the nucleofector.

Immediately following nucleofection, 500 µL pre-warmed fully-supplemented DMEM was added to the cuvette. Solution was removed with a thin, sterile plastic pipet and cells plated on tissue culture dishes.

A2.4.6.3. Cell Lysis

Transfected cells were harvested with TrypLE Express as described above, spun down, and resuspended in an equal volume of resuspension buffer (25 mM imidazole, 100 mM NaCl pH=7.0) containing 1 protease complete mini tablet (Roche Diagnostics). Suspension was sonicated on ice for 7 intervals of 30 seconds on, 30 seconds off. Lysed cell suspension was centrifuged and supernatant containing protein was retained for SDS-PAGE/Western Blot analysis (small scale test expression) or High Performance Liquid

Chromatography (HPLC) purification (large scale expression). Cell pellet was also retained for analysis.

A2.4.7. Protein Purification

A Shimadzu HPLC (Kyoto, Japan) with the following components was utilized for protein purification: LC-10AT (LC component), CBM10-AW (fraction collector), and SPD-M10A (PDA detector). Metal-chelate column (1.7 mL column volume) packed with POROS 50 MC (Applied Biosystems) was stripped with 20 column volumes of 50 mM EDTA in 1 M NaCl. After rinsing with 10 column volumes of water, 10 mL 0.5M $NiCl_2$ was loaded onto the column and rinsed with 10 column volumes water, 10 column volumes 0.5 M NaCl, 10 column volumes of 0.5 M imidazole and 100 mM NaCl, and 10 column volumes 25 mM imidazole and 100 mM NaCl. Supernatant containing protein was filtered through a 0.22 μm syringe-filter and was loaded onto column. Column was rinsed with 25 mM imidazole and 100 mM NaCl to remove non-specifically bound proteins. Bound protein was eluted with an imidazole gradient beginning at 25 mM and ending at 500 mM over a period of 12 minutes. 1 mL fractions were collected throughout the gradient.

A2.4.8. SDS-PAGE and Western Blot Analysis

Samples consisting of HPLC fractions, cellular pellets or supernatant (as appropriate) were denatured by boiling in SDS loading dye with 2-5% beta-mercaptoethanol. These

samples were separated on two identical 12.5% polyacrylamide gels. One gel was stained following silver stain protocol.[37] Protein from second gel was transferred to a nitrocellulose membrane by wet-transfer in Towbin Transfer Buffer (30 minutes at 34 V followed by 100 V for 1.5 hours) at 4˚C. Membrane was probed by Western blotting with Rabbit Anti-HSV polyclonal antibody (GeneScript, Corp.) and horseradish Peroxidase-conjugated AffiniPure Goat Anti-Rabbit IgG secondary antibody (Jackson ImmunoResearch, Inc.). PicoMax Sensitive Chemiluminescent HRP Substrate (Rockland Immunochemicals**)** was mixed and applied to membranes for 5 minutes before exposing to x-ray film.

A2.5. References

1. Tessier-Lavigne, M.; Goodman, C. S., The molecular biology of axon guidance. *Science* 1996, 274, 1123-33.
2. Lu, Y.; Franze, K.; Seifert, G.; Steinhauser, C.; Kirchhoff, F.; Wolburg, H.; Guck, J.; Janmey, P.; Wei, E.; Kas, J.; Reichenbach, A., Viscoelastic properties of individual glial cells and neurons in the CNS. *Proceedings of the National Academy of Sciences of the United States of America* 2006, 103, 17759-17764.
3. Kennedy, T.; Wang, H.; Marshall, W.; Tessier-Lavigne, M., Axon guidance by diffusible chemoattractants: A gradient of netrin protein in the developing spinal cord. *Journal of Neuroscience* 2006, 26, 8866-8874.
4. Yu, T. W.; Bargmann, C. I., Dynamic regulation of axon guidance. *Nat Neurosci* 2001, 4 Suppl, 1169-76.
5. Morlot, C.; Thielens, N.; Ravelli, R.; Hemrika, W.; Romijn, R.; Gros, P.; Cusack, S.; McCarthy, A., Structural insights into the Slit-Robo complex. *Proc Natl Acad Sci U S A* 2007, 104, 14923-8.
6. Dickson, B. J.; Gilestro, G. F., Regulation of commissural axon pathfinding by slit and its Robo receptors. *Annu Rev Cell Dev Biol* 2006, 22, 651-75.
7. Erskine, L.; Williams, S. E.; Brose, K.; Kidd, T.; Rachel, R. A.; Goodman, C. S.; Tessier-Lavigne, M.; Mason, C. A., Retinal ganglion cell axon guidance in the mouse optic chiasm: expression and function of robos and slits. *J Neurosci* 2000, 20, 4975-82.
8. Plump, A. S.; Erskine, L.; Sabatier, C.; Brose, K.; Epstein, C. J.; Goodman, C. S.; Mason, C. A.; Tessier-Lavigne, M., Slit1 and Slit2 cooperate to prevent premature midline crossing of retinal axons in the mouse visual system. *Neuron* 2002, 33, 219-32.

9. Johnson, K. G.; Ghose, A.; Epstein, E.; Lincecum, J.; O'Connor, M. B.; Van Vactor, D., Axonal heparan sulfate proteoglycans regulate the distribution and efficiency of the repellent slit during midline axon guidance. *Curr Biol* 2004, 14, 499-504.
10. Steigemann, P.; Molitor, A.; Fellert, S.; Jäckle, H.; Vorbrüggen, G., Heparan sulfate proteoglycan syndecan promotes axonal and myotube guidance by slit/robo signaling. *Curr Biol* 2004, 14, 225-30.
11. Chanana, B.; Steigemann, P.; Jäckle, H.; Vorbrüggen, G., Reception of Slit requires only the chondroitin-sulphate-modified extracellular domain of Syndecan at the target cell surface. *Proc Natl Acad Sci U S A* 2009, 106, 11984-8.
12. Nguyen-Ba-Charvet, K. T.; Brose, K.; Marillat, V.; Sotelo, C.; Tessier-Lavigne, M.; Chédotal, A., Sensory axon response to substrate-bound Slit2 is modulated by laminin and cyclic GMP. *Mol Cell Neurosci* 2001, 17, 1048-58.
13. Fricke, C.; Lee, J. S.; Geiger-Rudolph, S.; Bonhoeffer, F.; Chien, C. B., astray, a zebrafish roundabout homolog required for retinal axon guidance. *Science* 2001, 292, 507-10.
14. Lee, J. S.; Ray, R.; Chien, C. B., Cloning and expression of three zebrafish roundabout homologs suggest roles in axon guidance and cell migration. *Dev Dyn* 2001, 221, 216-30.
15. Hutson, L. D.; Chien, C. B., Pathfinding and error correction by retinal axons: the role of astray/robo2. *Neuron* 2002, 33, 205-17.
16. Hutson, L.; Jurynec, M.; Yeo, S.; Okamoto, H.; Chien, C., Two divergent slit1 genes in zebrafish. *Dev Dyn* 2003, 228, 358-69.
17. Adams, R.; Alitalo, K., Molecular regulation of angiogenesis and lymphangiogenesis. *Nature Reviews Molecular Cell Biology* 2007, 8, 464-478.
18. Fukuhara, N.; Howitt, J. A.; Hussain, S. A.; Hohenester, E., Structural and functional analysis of slit and heparin binding to immunoglobulin-like domains 1 and 2 of Drosophila Robo. *J Biol Chem* 2008, 283, 16226-34.
19. Seiradake, E.; von Philipsborn, A. C.; Henry, M.; Fritz, M.; Lortat-Jacob, H.; Jamin, M.; Hemrika, W.; Bastmeyer, M.; Cusack, S.; McCarthy, A. A., Structure and functional relevance of the Slit2 homodimerization domain. *EMBO Rep* 2009, 10, 736-41.
20. Wang, K. H.; Brose, K.; Arnott, D.; Kidd, T.; Goodman, C. S.; Henzel, W.; Tessier-Lavigne, M., Biochemical purification of a mammalian slit protein as a positive regulator of sensory axon elongation and branching. *Cell* 1999, 96, 771-84.
21. Ringstedt, T.; Braisted, J. E.; Brose, K.; Kidd, T.; Goodman, C.; Tessier-Lavigne, M.; O'Leary, D. D., Slit inhibition of retinal axon growth and its role in retinal axon pathfinding and innervation patterns in the diencephalon. *J Neurosci* 2000, 20, 4983-91.
22. Ypsilanti, A. R.; Zagar, Y.; Chédotal, A., Moving away from the midline: new developments for Slit and Robo. *Development* 2010, 137, 1939-52.
23. Chalasani, S. H.; Sabol, A.; Xu, H.; Gyda, M. A.; Rasband, K.; Granato, M.; Chien, C. B.; Raper, J. A., Stromal cell-derived factor-1 antagonizes slit/robo signaling in vivo. *J Neurosci* 2007, 27, 973-80.
24. Inatani, M.; Irie, F.; Plump, A. S.; Tessier-Lavigne, M.; Yamaguchi, Y., Mammalian brain morphogenesis and midline axon guidance require heparan sulfate. *Science* 2003, 302, 1044-6.

25. Kastenhuber, E.; Kern, U.; Bonkowsky, J. L.; Chien, C. B.; Driever, W.; Schweitzer, J., Netrin-DCC, Robo-Slit, and heparan sulfate proteoglycans coordinate lateral positioning of longitudinal dopaminergic diencephalospinal axons. *J Neurosci* 2009, 29, 8914-26.
26. Guan, C. B.; Xu, H. T.; Jin, M.; Yuan, X. B.; Poo, M. M., Long-range Ca2+ signaling from growth cone to soma mediates reversal of neuronal migration induced by slit-2. *Cell* 2007, 129, 385-95.
27. Erskine, L.; Williams, S. E.; Brose, K.; Kidd, T.; Rachel, R. A.; Goodman, C. S.; Tessier-Lavigne, M.; Mason, C. A., Retinal ganglion cell axon guidance in the mouse optic chiasm: expression and function of robos and slits. *J Neurosci* 2000, 20, 4975-82.
28. Dallol, A.; Da Silva, N. F.; Viacava, P.; Minna, J. D.; Bieche, I.; Maher, E. R.; Latif, F., SLIT2, a Human Homologue of the Drosophila Slit2 Gene, Has Tumor Suppressor Activity and Is Frequently Inactivated in Lung and Breast Cancers. *Cancer Research* 2002, 62, 5874-5880.
29. Blazar, M.; Briaire-De Bruijn, I.; Rees-Bakker, H.; Prins, F.; Helfrich, W.; de Leij, L.; Riethmuller, G.; Alberti, S.; Warnaar, S.; Fleuren, G.; Litvinov, S., Epidermal growth factor-like repeats mediate lateral and reciprocal interactions of Ep-CAM molecules in homophilic adhesions. *Molecular and Cellular Biology* 2001, 21, 2570-2580.
30. Lorenzen, I.; Trad, A.; Grotzinger, J., Multimerisation of A disintegrin and metalloprotease protein-17 (ADAM17) is mediated by its EGF-like domain. *Biochemical and Biophysical Research Communications* 2011, 415, 330-336.
31. Peng Yang, S. M. M., and Ashutosh Chilkoti, Spatially Addressable Chemoselective C-Terminal Ligation of an Intein Fusion Protein from a Complex Mixture to a Hydrazine-Terminated Surface†.
32. Hynes, M. J.; Maurer, J. A., Photoinduced monolayer patterning for the creation of complex protein patterns. *Langmuir* 2012, 28, 16237-42.
33. PubMed Central/National Center for Biotechnology Information. http://www.ncbi.nlm.nih.gov/
34. Larkin, M.; Blackshields, G.; Brown, N.; Chenna, R.; McGettigan, P.; McWilliam, H.; Valentin, F.; Wallace, I.; Wilm, A.; Lopez, R.; Thompson, J.; Gibson, T.; Higgins, D., Clustal W and Clustal X version 2.0. *Bioinformatics* 2007, 23, 2947-8.
35. Schultz, J.; Milpetz, F.; Bork, P.; Ponting, C., SMART, a simple modular architecture research tool: identification of signaling domains. *Proc Natl Acad Sci U S A* 1998, 95, 5857-64.
36. Letunic, I.; Doerks, T.; Bork, P., SMART 6: recent updates and new developments. *Nucleic Acids Res* 2009, 37, D229-32.
37. Ausubel, F. M.; Brent, R.; Kingston, R. E.; Moore, D. D.; Seidman, J. G.; Smith, J. A.; Struhl, K., *Short Protcols in Molecular Biology*. 5th Edition ed.; John Wiley and Sons, Inc.: 2002; p Pages 10-38 - 10-40.